JPL-IN-35-CR

FINAL REPORT ON HOLOGRAPHIC TESTS AT S-BAND AND K-BAND ON THE DSS-63 64 METRE ANTENNA

Test dates : 18 to 29 May 1985

Prepared for the Jet Propulsion Laboratory
under contract No. 956984

February 1986 80605

Authors:

M.P. Godwin

E.P. Schoessow

P.J. Richards

This work was performed for the Jet Propulsion Laboratory, California Institute of Technology, sponsored by the National Aeronautics and Space Administration.

Eikontech Limited
Minalloy House
18-22 Regent Street
Sheffield S1 4DA
England

ABSTRACT

High resolution holographic tests were carried out on DSS-63 at S-band and K-band during May 1985. These tests followed a mechanical retrofit which involved the addition of structural bracing to the backing stucture.

Geosynchronous satellite beacons were used as sources for the tests. At a resolution of 0.4m the S-band and K-band tests revealed r.m.s. deviations of the surface to be 2.73mm and 1.53mm respectively. The difference between these two results is thought to be due mainly to contamination of the S-band surface error map by expected and generally predictable subreflector diffraction effects. The S-band map is also known to be contaminated by diffraction from the subreflector support struts and has a higher noise level than the K-band map.

A list of corrections to be applied to the reflector panels is derived from the K-band map. These corrections are predicted to reduce the r.m.s. deviation from 1.53mm to 0.86mm at 0.4m resolution.

Comparison with results obtained before the mechanical retrofit suggests the major effect of the added structural bracing to be reduction of a third order deformation of the reflector about its axis.

CONTENTS

1. INTRODUCTION

This report describes high resolution holographic tests carried out on the DSS-63 64 metre antenna at S-band and K-band. The tests were made in May 1985, shortly after a mechanical retrofit to the antenna, involving the addition of structural bracing to the backing structure. Holographic tests were also carried out on the DSS-63 antenna in November 1984, before the mechanical retrofit, and these are described in a seperate report[1].

The holographic tests were made using sources provided by geosynchronous satellite beacons. At S-band the reflex dichroic feed system of DSS-63 was utilised whilst at K-band a specially constructed horn feed was used.

Two scans were made at S-band and these are referred to, here, as scans 1 and 2. Two scans were made at K-band also and these are referred to as scans 3 and 4. Measurements were made overnight, to obtain the most stable conditions, using the automatic data acquisition system developed for tests on the DSS-43 and DSS-45 antennas in Australia in January/February 1985[2][3]. Unlike the earlier measurements on DSS-63, the antenna pointing data required by the Eikontech data acquisiton system were obtained from the new NPL encoders. Thus there was no repetition of the considerable interfacing problems and loss of data which occurred when the old DATEX encoders were used in November 1984.

Since the principles of the holographic antenna testing technique are generally well understood, a detailed description is not given here. However, in order to aid interpretation of the results, the reader is referred to the seperately indexed explanatory notes at the back of the report.

2. DESCRIPTION OF TESTS

2.1 Equipment

Figure 2.1 shows a sketch of the equipment used to carry out the holographic tests on DSS-63.

The outputs from the 2.8 metre trailer mounted reference antenna and from DSS-63 were coherently down-converted to produce i.f. signals in the range 200 to 800 MHz for transmission to the receiver mainframe which was located in the antenna pedestal. The Eikontech computer system, which was used to control data acquisition and for preliminary on-site data processing, was also situated in the antenna pedestal.

Antenna pointing information was obtained from the NPL encoders fitted to the elevation and azimuth axes of the antenna†. Data were obtained by performing a succession of elevation cuts, between which the azimuth was incremented. Scanning instructions were generated by the Eikontech computer and sent to the antenna drive system via a JPL INTEL computer. The Eikontech computer continuously monitored the antenna pointing and initiated sampling of the phase and amplitude pattern data at the appropriate angles. Thus the data acquisition system was completely automatic and required no operator action once scanning had commenced.

† For the earlier tests on DSS-63, pointing information was obtained from the DATEX encoders which formed part of the the Master Equatorial system at that time. These were used in prefernce to the encoders on the elevation and azimuth axis for reasons of accuracy, despite certain complexities which arose due to use of an hour angle/declination encoder system on an elevation/azimuth mounted antenna. During the mechanical retrofit the accuracy of the elevation and azimuth encoder system was improved by installation of the NPL devices and hence these were used for the tests described here.

2.2 Satellite Sources

The signal used for the S-band tests was the 2.2775 GHz beacon radiated by the geosynchronous DSCS-II satellite, NORAD No. 11622. Permission to use this beacon for the tests was kindly granted via the Air Force Satellite Command Facility (AFSCF), Sunnyvale, California. In addition to technical data about the beacon and its operational status, AFSCF also supplied the orbital elements of the satellite on a daily basis for the duration of the tests.

The orbital data were transmitted to the Royal Aircraft Establishment, Farnborough, U.K., who derived the look angles of the satellite appropriate to DSS-63. This information was then transmitted to the site and fed into the Eikontech computer in order for the diurnal motion of the satellite to be superimposed on the antenna scanning.

At DSS-63 the DSCS-II satellite appears at a nominal position of Azimuth 191°, Elevation 41°. However the diurnal motion of this satellite is a few degrees in elevation and azimuth and the S-band scans were recorded when the satellite was almost at the limit of its daily travel. Thus the satellite elevation angles for the scans are a few degrees higher than the nominal value. Such is the movement of this satellite that tracking of the 2.8m reference antenna was required.

The e.i.r.p. of the right hand circularly polarised, S-band beacon was -8 dBW. With the receiver noise bandwidth of 2.5 Hz, used for the tests, the signal to noise ratio on the beam peak of the DSS-63 antenna was 64 dB.

For the K-band tests the 11.451 GHz, linearly polarised beacon from the satellite ECS-1 was used. This satellite is positioned 13° East of Greenwich. Permission to receive signals from ECS-1 was kindly granted by the Spanish PTT and by EUTELSAT, who also provided the look angle data. At DSS-63, this satellite appears at elevation 40.2°, azimuth 154.4°. Its diurnal motion is considerably less than that of DSCS-II and was less than ± 0.1° in elevation and azimuth at the time of the tests.

The e.i.r.p. of the linearly polarised ECS-1 beacon is 11 dBW. With the receiver bandwidth of 2.5 Hz, this provided a beam peak signal to noise ratio of 73 dB in K-band.

2.3 Scan parameters

(See also explanatory notes section A)

Summaries of the scan parameters for the S-band and K-band tests are given in tables 1 and 2 respectively.

The panels of the DSS-63 antenna typically measure about 3.5m x 1.5m. In order to determine the mean position and tilt of the panels it is necessary for the microwave image of the reflector to be formed with a resolution at least as small as half the smallest panel dimension. All the scans recorded provide resolutions which satisfy this condition. However at both S-band and K-band the second scans (2 and 4) are larger than the first (1 and 3) and hence provide better resolution. The highest resolutions obtained at S-band and K-band are 0.406m and 0.400m respectively.

The duration of the longest scan was almost 11 hours. This includes the time required periodically to remeasure the beam peak sample during the scan, in order to monitor equipment drift and propagation changes, and to perform several calibration scans at the end of the main scan. Had the semi-automatic scanning system been used, as for the earlier measurements on this antenna, the scan durations would have been greater by several hours and would have required a number of skilled antenna operators working in rotation.

Scan	1	2
Start date	20 May 1985	23 May 1985
Start time	1814 GMT	1811 GMT
Duration	361 mins	717 mins
Frequency	2.2775 GHz	2.2775 GHz
Polarisation	RHCP	RHCP
Source type	Satellite	Satellite
Approx. source el.	45.2°	44.1°
Approx. source az.	193.0°	193.0°
Scan type	Zig-zag	Zig-zag
Subscan co-ord.	Elevation	Elevation
Data size (az. x el.)	127 x 127	187 x 187
Angular limits, el.	± 6.29°	± 9.29°
Angular limits, az.	± 8.52°	± 12.58°
Resolution *	0.599m	0.406m
Calibration scan	Yes	Yes
Beam-peak mon.	Yes	Yes
Beam-peak SNR	64 dB	64 dB

---

* The resolution parameter is a measure of the definition available in the microwave image of the antenna. Resolution is explained in more detail in section A of the explanatory notes.

Table 1. Summary of S-band scan parameters

Scan	3	4
Start date	25 May 1985	28 May 1985
Start time	2245 GMT	1835 GMT
Duration	441 mins	682 mins
Frequency	11.451 GHz	11.451 GHz
Polarisation	Linear	Linear
Source type	Satellite	Satellite
Approx. source el.	40.2°	40.2°
Approx. source az.	154.4°	154.4°
Scan type	Zig-zag	Zig-zag
Subscan co-ord.	Elevation	Elevation
Data size	151 x151	189 x 189
Angular limits el.	± 1.49°	± 1.87°
Angular limits az.	± 1.96°	± 2.45°
Resolution *	0.502m	0.400m
Calibration scan	Yes	Yes
Beam-peak mon.	Yes	Yes
Beam peak SNR	73 dB	73 dB

---

* The resolution parameter is a measure of the definition available in the microwave image of the antenna. Resolution is explained in more detail in section A of the explanatory notes.

Table 2. Summary of K-band scan parameters

3. REFLECTOR SURFACE CURRENT DISTRIBUTION

(See explanatory notes Section B)

3.1 S-band surface current distribution

Plate 1 S-band reflector surface current distribution from scan 1 shown in red/blue colour table

Plate 2 S-band reflector surface current distribution from scan 2 shown in red/blue colour table

Plate 5 S-band reflector surface current distribution from scan 2 shown in white/red/orange/blue colour table

Plate 7 S-band reflector surface current distribution from scan 2 shown in monochrome

Note that a mask, which appears black in the photographs, has been superimposed on the image to delineate the blockage due to the subreflector and its supports.

Considering firstly plates 1 and 2, both S-band scans show well formed shadow regions at the bases of the four subreflector support struts. In comparing these two displays it should be remembered that the resolutions for scans 1 and 2 are different, at 0.599m and 0.406m respectively. Nevertheless the same features are observed in both, confirming the repeatibility of the tests.

Perhaps the most obvious feature of the surface current distribution is the ring structure visible in the outer regions of the dish. This is due to diffraction from the subreflector rim and to the flange surrounding the subreflector, which is a special feature of the JPL 64 metre antennas and whose purpose is to reduce the antenna noise temperature by reducing the main reflector spillover.

Both results reveal good circular symmetry indicating the absence of any significant subreflector tilt. A particularly interesting localised minimum in the surface current is visible close to the lower right strut. This was not detected in earlier measurements[1] and is due to a depression in the surface resulting from accidental damage that occurred during the mechanical retrofit.

Adjacent to the right hand edge of the subreflector blockage can be seen a very small area of low illumination which is thought to be due to part of a structure, such as a winch or part of the subreflector positioner mechanism, which protrudes slightly beyond the subreflector. This minor feature was noted in the earlier measurements on DSS-63[1] and a similar feature can be seen also in the measurements made on the Canberra 64m antenna, DSS-43[2].

Line structures are visible in the areas surrounding each of the four strut shadows. These can be seen more clearly in the monochrome display of the result from the larger of the two S-band scans, scan 2, shown in plate 7. Similar patterning was found at S-band in DSS-43 and DSS-45 and arises due to scattering from the support struts. The ring formation caused by subreflector scattering is also shown clearly in the monochrome display.

Plate 5 shows the surface current distribution from scan 2, using a special colour table which provides a colour contouring effect. This shows, for example, that the vast majority of the surface lies within the range white to orange inclusive, and is thus within 12.5 dB of the maximum value.

3.2 K-band surface current distribution

Plate 3 K-band reflector surface current distribution from scan 3 shown in red/blue colour table

Plate 4 K-band reflector surface current distribution from scan 4 shown in red/blue colour table

Plate 6 K-band reflector surface current distribution from scan 4 shown in white/red/orange/blue colour table

Plate 8 K-band reflector surface current distribution from scan 4 shown in monochrome

Comparison of the two K-band scans indicates good repeatibility although it should be remembered that scan 4 yields a higher resolution than scan 3. The strut shadows in plates 3 and 4 are noticeably better defined than those in the S-band results in the previous section. This is to be expected at the shorter K-band wavelength since diffraction around the struts into the geometrical shadows is reduced. However it is observed that both maps show the shadows of the two upper struts to be more complete than the shadows of the lower struts. Since it is the upper struts which carry cables, ladders and hoists, whereas the lower ones do not, it seems likely that transmission through the struts is occurring in this band.

Diffraction from the subreflector rim appears here as a number of exceptionally well defined concentric rings close to the edge of the dish. The spacing of the rings is much less than in the S-band maps due to the difference in wavelength.

Many of the features seen at S-band, such as the patch of low illumination resulting from panel damage close to the lower right strut, are visible here. However, a number of additional localised features, which may also be the result of accidental damage, are revealed at K-band. The K-band data reveal another characteristic, not seen at S-band, in the form of radial

line stuctures emanating from the dish centre. These are perhaps more easily discerned in the monochrome display of the data from the larger of the two K-band scans, scan 4, shown in plate 8 and are thought to be associated with the sectored construction of the subreflector. As might be expected, in contrast to the S-band distribution, the monochrome display shows very little scattering from the struts.

Plate 6 shows the K-band surface current distribution using the colour contouring table. Comparison with the equivalent S-band display on the same page suggests the illumination taper to be slightly greater at K-band.

4. REFLECTOR SURFACE ERRORS

(See also explanatory notes section C)

Ring structures due to scattering from the subreflector rim have already been observed in the surface current distributions at S-band and K-band. This scattering perturbs not only the amplitude of the surface current but also the phase. Thus, in order to derive the surface errors of the dish from the phase component of the distribution, it is necessary to remove the variations due to subreflector scattering. The way in which this is done is described in section 4.2. First however it is useful to calculate surface error maps without removing the feed/subreflector phase function. Whilst these maps do not show the true mechanical surface errors they nevertheless show the equivalent errors which are effective in determining antenna performance.

4.1 Effective reflector surface errors

4.1.1 Effective reflector surface errors at S-band

Plate 9 Effective reflector surface errors at S-band from scan 1

Plate 10 Effective reflector surface errors at S-band from scan 2

At resolutions of 0.60m and 0.41m the r.m.s. deviations of the effective reflector surface errors from the two S-band scans, scans 1 and 2, are 3.05mm and 3.28mm respectively. Inspection of the two maps shows good repeatibility with ring structures due to scattering from the subreflector rim clearly visible on the outer three rings of panels.

Close to the lower right strut can be seen a single panel which appears depressed (blue). This is the panel which suffered accidental damage during the mechanical retrofit and which was seen to cause a localised minimum in both the S-band and the K-band surface current distributions.

4.1.2 Effective reflector surface errors at K-band

Plate 11 Effective reflector surface errors at K-band from scan 3

Plate 12 Effective reflector surface errors at K-band from scan 4

The r.m.s. deviation of the K-band effective reflector surface errors is found to be 1.48mm and 1.64mm at resolutions of 0.50m and 0.40m respectively. These values are only about half of those at S-band, illustrating the relative impact of subreflector edge diffraction in the two bands. Here, the ring structure is much finer and is discernible in the photographs only on the next-to-outermost panel ring.

The damaged panel close to the lower right strut is clearly visible as a blue patch in the higher resolution map shown in plate 12. It will be noted, however, that in the lower resolution map of plate 11 this panel does not appear uniformly blue. This is because, at K-band, the magnitude of the depression is comparable with the wavelength and causes the phase of the surface current distribution to change through an amount greater than π radians. Thus a 'phase flip' has occured on the damaged panel in plate 11. An algorithm is available to remove such features and hence to resolve the ambiguities caused by phase excursions which exceed $\pm \pi$ radians, but has not been applied to the effective surface error map from scan 3. (No phase flips occured in the in the map from scan 4.) Apart from the damaged panel and the difference in resolution, the two K-band scans produce extremely similar effective surface error maps.

4.2 Compensation for feed/subreflector phase pattern

Plate 13 Reflector surface errors from K-band test (scan 4) using JPL theoretical feed/subreflector phase function

Plate 14 Reflector surface errors from K-band test (scan 4) using derived feed/subreflector phase function

At the outset of the present programme of holographic testing of the DSN antennas, it was envisaged that compensation for the feed/subreflector phase function would be carried out by subtracting theoretical predictions of this function from the measured phase distribution of the antenna image. The theoretical predictions at S-band and K-band were supplied by JPL for this purpose. The procedure was first attempted on the S-band data obtained for DSS-43[2] but was not completely successful, as subtraction of the theoretical function did not satisfactorily eliminate the ring structure shown in the effective surface error maps. It was found that the ring structures in the measured results were not centred on the dish axis, presumably because of the asymmetric nature of the feed geometry which is not accounted for in the theoretical function. Thus the subtraction was tried again, this time with the JPL function offset from the antenna axis. Unfortunatley this action did not produce a significant improvement as the locations and widths of the rings appeared to differ slightly between the measured results and the theoretical function.

Following discussions with JPL it was concluded that the problem lies in the simplified symmetric model used to predict the phase functions and that development of the model to correctly account for the feed system asymmetry would involve considerable theoretical and computational effort.

In order to affect the required correction to the data the following alternative scheme was devised. The surface of the reflector is divided into a number of annuli, concentric with the ring structures observed in the surface current maps. The phase of the image is then averaged around each annulus to produce a phase distribution which is a function of radius from the ring structure centre. This function is then assumed to be the

phase pattern of the feed/subreflector and is used to correct the data. Since this new function is derived from the measured data it is referred to as a 'derived phase function'. Deriving the phase function from the data in this way introduces the risk that genuine circularly symmetric features of the dish shape may be lost but it is suggested that the accuracy provided is better than could be obtained using the theoretical function.

Here also, it has been necessary to adopt the derived phase function approach. For the S-band tests, the centre of the ring structures is found to lie about 0.5m to the right of tha antenna axis, viewed looking into the reflector bowl. The derived S-band phase function is shown in figure 4.1. Shown for comparison is the S-band phase function derived for the DSS-43, Canberra, 64m antenna, for which the centre of the ring structure also lies mostly to the right of the axis. Good agreemement is observed over most of the radius, with the greatest differences occuring in the poorly illuminated region close to the reflector edge.

An example of a K-band surface error map compensated using the JPL phase function is shown in plate 13. This particular result is obtained from scan 4, and ring features, which are undoubtedly due to subreflector diffraction and which should therefore have been removed by the compensation, are still apparent on the next-to-outermost ring of panels. The centre of the K-band ring structure is found to be offset from the antenna axis by a greater amount than at S-band and lies at X = 0.96m, Y = 0.96m. Simply offsetting the JPL theoretical function by this amount does not produce a significant improvement. Figure 4.2 shows the phase function derived from scan 4 using the method described above. Only the outer part of the radius is shown in order to permit a detailed comparison of this rapidly varying function with the JPL supplied data. Also, at this frequency, subreflector scattering does not cause significant phase perturbation of the illumination of the inner part of the reflector. Apart from the offset of the centre of the ring structure, over the range plotted, the two functions have similar form and peak-to-peak excursions but with slight misalignment of the phase peaks around 24m radius. The profile map from scan 4, obtained using the derived phase function, is shown in plate

14 and it will be observed that the ring features on the next-to-outermost panel ring are now greatly reduced.

4.3 Surface error maps

4.3.1 Surface error maps from K-band data

Plate 14 Reflector surface errors from K-band test (scan 4) shown in red/green/blue colour table

At the highest resolution of 0.40m obtained at K-band (scan 4) the r.m.s. deviation of the surface is found to be 1.53mm, measured normal to the surface of the best fit paraboloid. Inspection of the map shows little evidence of astigmatic distortion which would appear as a predominance of red at the top and bottom and blue at the sides, or vice versa. However, as found in the earlier tests[1] the reflector appears to possess a third order deformation about its axis, as indicated in the photograph by the tendency for blue to occur most predominantly at the top and at the lower left and right sides. That is, the reflector is asymmetric about the elevation axis. (This property of the reflector will be seen more clearly in section 4.5.)

4.3.2 Surface error maps from S-band data

Plate 16 Reflector surface errors from S-band test (scan 2) shown in red/green/blue colour table

At 0.41m resolution the r.m.s. deviation of the surface indicated by the S-band test is 2.73mm. Note that for this result it is necessary to use a ± 10mm display range in contrast to the K-band result in the previous section for which a display range of ± 5mm was sufficient.

Examination of this map suggests that the correction for subreflector edge diffraction using the derived phase function method may not be totally effective as residual ring structure is perhaps still visible on the left hand side of the dish.

4.4 Comparison of S-band and K-band surface error data

Plate 15 Reflector surface errors from K-band test (scan 4) shown in red/green/blue colour table

Plate 16 Reflector surface errors from S-band test (scan 2) shown in red/green/blue colour table

Plate 17 Reflector surface errors from S-band test (scan 2) shown in monochrome

Plate 18 Reflector surface errors from K-band test (scan 4) shown in monochrome

The r.m.s. deviations obtained from the highest resolution scans at S-band and K-band after phase function removal are as follows.

Scan	Band	Resolution	r.m.s. deviation
2	S	0.41m	2.73mm
4	K	0.40m	1.53mm

In order to investigate the reasons for the significant difference in r.m.s. values, the profile maps from the two scans are displayed using the same range in plates 15 and 16. Certain localised features, such as the damaged panel close to the lower right strut, appear essentially the same in both maps. The greatest differences are systematic rather than random and are seen to exist predominantly in the outer three panel rings, particularly the outermost ring, suggesting that they are associated with diffraction from the subreflector rim. Since subreflector diffraction is much less important at K-band, it follows that residual errors from the derived phase function method of compensation are also much less in this band.

Close to the reflector rim, discrepancies must also be anticipated due to the inferior profile mapping accuracy in this poorly illuminated region. In addition, differences in reflector shape may be present due to the

approximate 4.5° difference between the elevation angles of the S-band and K-band tests.

Another source of discrepancy between the tests carried out in the two bands is diffraction from the subreflector support struts. It will be recalled that line structures due to strut diffraction are visible around the bases of the struts in the S-band surface current distribution (plate 7), but not in the K-band distribution (plate 8). It seems likely that the red areas surrounding the shadows cast by the upper struts in the S-band result represent contamination due to strut diffraction.

To aid comparison of the small scale features revealed by the S-band and K-band tests the surface error maps from scans 2 and 4 are also shown in mononchrome in plates 17 and 18. Note that different display ranges are used here for the two maps. Particularly in this display format, many of the small scale features are seen to be associated with individual panels. For example, just below the right horizontal on panel ring 6 (ring 8 being the outermost) two adjacent raised (white) panels are readily identified in both results.

In summary, it is thought that differences between the S-band and K-band reflector surface error maps are largely associated with removal of the feed/subreflector phase function. The combination of an asymmetric feed system geometry and the subrelector flange, which serves to reduce main reflector spillover, is a particularly demanding application of phase function removal.

4.5 Comparison of reflector surface errors before and after structural bracing

Plate 19 Reflector surface errors from K-band test (Scan 4) at 3.14m resolution

The purpose of this section is to compare the reflector surface error data obtained here with data obtained from the holographic tests carried out in November 1984, before the mechanical retrofit[1]. During the previous tests considerable difficulty was encountered due to incorrect operation of the DATEX antenna position encoders which were fitted to the antenna at that time. These problems caused much of the raw data to be lost, both at S-band and K-band, and hence only low resolution reflector surface error data were obtained.

In order to facilitate a meaningful comparison with the results obtained before the mechanical retrofit, a low resolution surface error map has been generated from scan 4 (K-band) and is shown in Plate 19. This map has the same resolution of 3.14m and display range of ± 4.5mm as used in the K-band result shown in plate 5 of the earlier report[1]. Since both tests utilised the satellite ECS-1, the elevation angles of the measurements are identical also.

First inspection indicates remarkably good agreement between these two K-band results, obtained approximately six months apart. All the major features of the reflector shape shown in the results from the November 1984 tests are seen also in the present results, including the third order deformation around the reflector axis. However close inspection of the colour displays shows the new map to be less saturated. That is, whilst the form of the reflector shape seems to have remained largely unchanged, the addition of bracing to the reflector backing structure has reduced the peak to peak range of the surface errors at the test elevation angle of about 40°. This perhaps suggests that the new bracing has reduced the third order deformation component of the reflector.

At 3.14m resolution, the tests made before the mechanical retrofit revealed an r.m.s. value of 1.38mm. The additional bracing provides a worthwhile

reduction in the r.m.s. deviation of surface errors to 1.07mm, measured with the same resolution.

5. ASTIGMATISM ANALYSIS

(See also explanatory notes section D)

Analysis of the astigmatic component of reflector surface errors has been carried out on the data obtained from scan 2 (S-band) and scan 4 (K-band) and the focal differences found to be 1.8mm and 2.5mm respectively. Both of these focal differences are sufficiently small to have negligible impact on antenna gain.

6. REFLECTOR PANEL ADJUSTMENTS

(See also explanatory notes section E)

Plate 20 Predicted reflector surface errors after panel adjustments

Reflector panel adjustments are derived from the highest resolution K-band test, scan 4, and are given in the listing in appendix B. Adjustments are provided for rings 2 to 8 only, as ring 1 (innermost) is substantially blocked by the subreflector. Panels which are substantially blocked or shadowed by the struts are omitted from the listing also.

Plate 20 shows a prediction of the new reflector surface errors after panel adjustment. The recommended corrections adjust only the mean positions and tilting of panels and do not introduce panel re-shaping. Several panels are noticeably distorted, perhaps as the result of stressing due to their present multiple screw jack adjuster settings. It is possible that releasing certain of the adjusters on these panels will restore their correct shapes.

The r.m.s. deviation of the surface is predicted to reduce from 1.53mm (60 thou) to 0.86mm (34 thou) at a resolution of 0.4m and the resultant gain improvements at S-band and K-band are calculated as 0.09 dB and 0.94 dB respectively.

7. ACCURACY ANALYSIS FOR DETERMINATION OF REFLECTOR SURFACE ERRORS

The measurement inaccuracies due to receiver system noise are derived from the beam peak signal to noise ratios and are shown in figures 7.1 and 7.2.

At the S-band resolution of 0.406m provided by scan 2, figure 7.1 shows the standard deviation of errors due to noise to rise from about 0.4mm close to the reflector centre to about 2.4mm close to the dish edge. At K-band the standard deviation of errors due to noise is considerably less due to the higher signal to noise ratio and the shorter wavelength. Figure 7.2 shows the errors at K-band to possess a maximum standard deviation of only about 0.12mm close to the reflector edge, with a resolution of 0.400m. The K-band surface error measurements are thus around twenty times less noisy than the S-band results with similar resolutions.

The recommended panel corrections given in section 6 are derived from the K-band test (scan 4). The panel corrections are effectively derived by averaging the surface error data over each panel. Thus, since the surface area of the panels is considerably greater than that of the 0.400m resolution cell, the standard deviation of errors due to noise in determining the adjustments is reduced by a factor of about five and is shown as the lower curve in figure 7.2. The worst case error occurs at the rim of the dish but is less than 0.025mm (1 thou).

8. SUBREFLECTOR POSITION ADJUSTMENTS

(See explanatory notes section G)

8.1 Recommended adjustments for S-band

For the S-band tests, the automatic subreflector positioning mechanism was disabled with the subreflector fixed at the following position, as displayed on the operator's console.

x = 0.41 inches
y = 0.11 inches
z = 0.00 inches

IMPORTANT: ***This JPL co-ordinate system is not the same as the Eikontech co-ordinate system used below to define subreflector position corrections. The Eikontech co-ordinate system is decribed in section G of the explanatory notes provided at the back of this report. Before implementation, any corrections given here will need to be transferred to the JPL co-ordinate system.***

The recommended S-band subreflector adjustments derived from the two S-band scans are as follows.

	Scan 1	Scan 2
X	-9.38mm	-4.18mm
Y	-8.49mm	-0.95mm
Z	-4.45mm	-3.40mm

The first point to note about these recommended corrections is that the total subreflector position error is only a small fraction of the S-band test wavelength of about 130mm. Not surprisingly then the gain loss due to subreflector position error at S-band is negligible as will be shown in section 9.1.

The second point worthy of note is that, whilst the Z co-ordinate changes by only about 1mm between scans, the X and Y co-ordinates change by rather greater amounts of about 5mm and 7.5mm respectively. This may be due to the varying effects of wind loading, temperature, etc., or to non-repeatibility of the subreflector positioner mechanism. Interestingly the same order of fluctation in the X and Y subreflector position was detected in the K-band tests carried out on DSS-63 prior to the mechanical retrofit, and again the Z co-ordinate was found to be comparatively stable[1]. The tests carried out on the DSS-43 antenna at Canberra suggest that the Z co-ordinate of the subreflector on that antenna also is more stable than the transverse co-ordinates[2].

The present tests show the S-band subreflector position error to be greatly reduced from that found before the mechanical retrofit, where the transverse position error was almost half of a wavelength. It should be noted that the calibration of the subreflector position readout on the operators console was changed by an unknown amount during the mechanical work and thus, when expressed in the JPL readout co-ordinate system, the optimum subreflector positions will differ for the two sets of measurements.

8.2 Recommended adjustments for K-band

For the K-band tests, the automatic subreflector positioning mechanism was disabled with the subreflector fixed at the following position, as displayed on the operator's console.

x = 0.30 inches
y = 0.40 inches
z =-0.09 inches

IMPORTANT: ***This JPL co-ordinate system is not the same as the Eikontech co-ordinate system used below to define subreflector position corrections. The Eikontech co-ordinate system is decribed in section G of the explanatory notes provided at the back of this report. Before implementation, any corrections given here will need to be transferred to the JPL co-ordinate system.***

The recommended K-band subreflector adjustments derived from scans 3 and 4 are as follows.

	Scan 3	Scan 4
X	20.73mm	29.88mm
Y	16.37mm	15.31mm
Z	-8.11mm	-9.97mm

Clearly the overall adjustment required to optimise the K-band performance of the antenna is comparable with the wavelength of about 25mm. Again it is seen that the transverse subreflector co-ordinates are less stable than the Z co-ordinate. In this case greatest variation is observed in the X co-ordinate.

The gain loss due to subreflector position error for scans 3 and 4 is 0.26 dB and 0.41 dB respectively. The difference between these values is due to the differences of about 9mm and 2mm respectively between the X and Z co-ordinates of the subreflector for the two scans. This illustrates well

that seemingly small subreflector movements about a non-optimum position can cause noticeable variations in antenna gain.

8.3 Discussion of subreflector adjustments

Different subreflector positions were used for the S-band and K-band tests. The position for the S-band tests was set by driving the antenna to the satellite elevation and then disabling the automatic subreflector positioning mechanism which controls the Y and Z coordinates to compensate for gravitational deformation of the reflector. The same procedure was attempted for the K-band measurements. However, while experimenting with the subreflector position shortly before the first K-band test the subreflector adjuster mechanism developed a fault and ceased to operate. In order to avoid delays, the position at which the subreflector had stopped was accepted and was used for both K-band scans.

Referring all recommended subreflector position adjustments to the position used for the S-band tests gives the following results.

	S-band		K-band	
	Scan 1	Scan 2	Scan 3	Scan 4
X	-9.38mm	-4.18mm	23.53mm	32.68mm
Y	-8.49mm	-0.95mm	23.77mm	22.71mm
Z	-4.45mm	-3.40mm	-10.61mm	-12.47mm

Expressing the results in this way reveals the optimum subreflector positions for S-band and K-band to be significantly different, particularly in the transverse coordinates. The difference between the average adjustments for the two bands is approximately 21mm, 19mm, and 7mm in X, Y, and Z respectively.

It seems unlikely that gravitational deformation of the antenna structure is responsible for the observed difference, particularly since the S-band and K-band satellite sources differ in elevation by only about 4.5°. Furthermore gravitational deformation is not expected to influence the X-coordinate.

It is possible that the difference between the optimum subreflector positions for S-band and K-band arises due to incorrect location of one or

both of the feed horns. Note however that the corresponding feed position errors would be of the order of five times greater than the subreflector position errors, due to the magnification of the Cassegrain system, and it seems unlikely that such gross misalignments are present.

Another possible reason for the difference is subreflector tilt. It will be recalled that the subrelfector of the DSS-63 antenna can be rotated about the main reflector axis in order to position the secondary focus on the desired feed. It can easily be shown that if the subreflector is tilted by a small fraction of a degree, the circle described by the secondary focus as it rotates can fail to intersect the feed horns by amounts sufficient to cause the measured difference between optimum subreflector positions.

Before implementing the recomended subreflector adjustments the effect on antenna pointing must be considered. Based on the known positions of the S-band and K-band satellites, a brief investigation suggests that the subreflector adjustments produce the undesireable effect of causing the S-band and K-band beams to diverge. This confirms that the recommended subreflector position corrections represent an attempt to compensate for some other misalignment within the antenna. Thus it is suggested that the position of the feed horns should be checked, particularly the recently installed K-band horn. Should the horn positions be found to be satisfactory the best course of action is probably to relocate the relatively small K-band horn so that parallel beams and optimum gain are realised in both bands with a common subreflector position.

Considering now also X-band operation, it is understood that the reflex dichroic S/X band feed system possess different phase centres in its two bands. The relationship between the phase centres is well known to JPL and hence it should be possible to choose the subreflector position to be an acceptable compromise for dual S/X band operation.

9. GAIN LOSSES

(See also explanatory notes section I)

9.1 Gain losses at S-band

The gain loss factors derived from scan 2 are as follows.

Non-uniform illumination	-0.76 dB
Subreflector position error	0.00 dB
Measured loss due to reflector surface errors	-0.13 dB
Predicted loss due to surface errors after panel adjustment	-0.04 dB

At 0.76 dB the loss due to non-uniform illumination is slightly less than the theoretical value of 0.84 dB predicted by JPL. As anticipated in section 8.1, the loss due to the S-band subreflector position error of a small fraction of a wavelength is negligible at less than 0.01 dB. Apparently the gain loss due to surface errors can be reduced by almost one tenth of a decibel by readjustment of the reflector panels.

9.2 Gain losses at K-band

The gain loss factors derived from scan 4 are as follows.

Non-uniform illumination	-0.86 dB
Subreflector position error	-0.41 dB
Measured loss due to reflector surface errors	-1.35 dB
Predicted loss due to surface errors after panel adjustments	-0.41 dB

That the gain loss due to subreflector positioning error is as large as 0.41 dB is because no attempt was made, prior to the tests, to optimise the subreflector position for use with the specially installed K-band feed.

The loss of 1.35 dB due to reflector surface errors is obviously much greater than at the lower S-band test frequency. At K-band quite noticeable pattern degradation can be expected and minor changes in reflector shape, due to temperature variations, wind loading, etc., will produce significantly greater variation in antenna gain than at S-band. However it appears that the loss at 11.451 GHz can be reduced by almost one decibel by readjustment of the reflector surface.

10. ANALYSIS OF VARIATION WITH FREQUENCY OF GAIN LOSS DUE TO SURFACE ERRORS

(See also explanatory notes section J)

The purpose of this section is to illustrate how the reflector might be expected to perform at frequencies other than the test frequencies. The results given here are derived from scan 4, as the K-band tests are considered to provide superior accuracy compared to the S-band data. Also, of the two K-band scans, scan 4 provides the higher resolution.

The straight line in the graph of figure 10.1 shows how the antenna gain would increase with frequency in the absence of reflector surface errors, and assuming 100% aperture efficiency. Surface errors introduce a loss which increases with frequency and the net variation is also shown in the figure. Above about 23 GHz the surface error losses increase sufficiently rapidly that the antenna gain decreases with frequency. From this analysis, the gain loss due to reflector surface errors at X-band (8.4 GHz) is found to be 0.77 dB. (Note that this is the loss due to reflector surface errors only and that subreflector position will introduce an additional loss factor.)

The third curve in the figure shows the predicted behaviour following reflector panel readjustment. Maximum gain is now realised at around 48 GHz. The loss at X-band is reduced to 0.23 dB giving a 0.54 dB gain improvement in this band.

11. FAR FIELD RADIATION PATTERNS

(See also explanatory notes section H)

11.1 S-band radiation patterns

Plate 21 S-band far-field radiation pattern for optimised subreflector position

The measured far-field radiation patterns at the S-band test frequency of 2.2775 GHz are shown in figure 11.1. Shoulders are apparent on the side of the main beam in both the elevation and the azimuth cuts. In the elevation cut the highest shoulder is at about -22 dB whilst in the azimuth cut the highest shoulder is at about -20 dB. Interestingly the symmetry of the beam and the inner sidelobe structure in the elevation pattern is quite good, despite the top-to-bottom asymmetry of the reflector shape. This perhaps suggests that, at S-band, the feed/subreflector phase pattern is more significant in determining pattern shape than low order surface deformations.

Patterns showing the predicted effect of implementing the S-band subreflector position adjustment given in section 8.1 are presented in figure 11.2. It will be recalled that corrections of only a small fraction of a wavelength are required and hence the change in the patterns is barely detectable.

The pattern predicted for the optimum subreflector position is also shown as a false colour display in plate 21. Linear features associated with the subreflector support struts are clearly visible.

11.2 K-band radiation patterns

Plate 22 K-band far-field radiation pattern for optimum subreflector position

The measured K-band radiation patterns are shown in figure 11.3. As mentioned earlier the subreflector position was not optimised for use with the specially installed K-band feed. As a result a substantial subreflector position error, of the order of a wavelength, was present in the X co-ordinate. The pronounced asymmetry of the first sidelobes in the azimuth pattern is therefore not surprising.

Figure 11.4 shows the patterns predicted for the optimum K-band subreflector position. Asymmetry of the beam is apparent in both the azimuth and the elevation cuts, but more noticeably in the latter. This is almost certainly due to the asymmetry of the reflector about its horizontal diameter, which seems to be the dominant feature in determining beam shape and inner sidelobe structure at this frequency.

Plate 22 shows the K-band radiation pattern predicted for the optimum subreflector position, in the form of a false colour display. Interestingly, the cross formation seen in the S-band pattern in the previous section is hardly detectable here. This may be because the strut blockages are electrically narrower at the shorter wavelength. Alternatively, it is possible that the curved line features in the S-band pattern are primarily the result of scattering from the struts, an effect which is known to be more extensive at S-band.

12. SUMMARY OF TEST REPORT

High resolution holographic tests were carried out at S-band and K-band on DSS-63 during May 1985. The measurements were made shortly after the addition of structural bracing to the antenna backing structure.

At both S-band and K-band the antenna illumination is found to be reasonably circularly symmetric. Perturbation of the reflector surface current distribution, associated with minor panel damage that occurred during the mechanical work, is visible in both bands. However, diffraction from the subreflector support struts, which is prominent at S-band, is not detectable at the shorter K-band wavelength.

At a resolution of around 0.4m the r.m.s. deviation of the effective surface (that is the surface derived without correction for subreflector diffraction effects) is found to be 3.28mm and 1.64mm at S-band and K-band respectively. That the S-band effective surface errors are twice as large as the K-band errors illustrates the much greater impact of subreflector edge diffraction on the S-band performance of the antenna.

As in the high resolution measurements made on DSS-43 [2], straightforward subtraction of the theoretical feed/subreflector phase diffraction patterns supplied by JPL was found to be unsatisfactory. Thus it was once again necessary to correct the microwave image for subreflector diffraction effects using an approach which attempts to identify and remove features with circular symmetry. The reason for the inability to make the correction with the theoretical data is thought to be because the latter does not taken account of the asymmetry of the feed systems used on the 64m antennas. Whilst the approach used introduces the risk that genuine circularly symmetric properties of the dish shape may be lost, it is nevetheless considered to provide superior results. Compensation for subreflector diffraction is particularly important at S-band and if further high resolution measurements are to be carried out in this band, other than for the purpose of monitoring any changes with time in the antenna shape, it is suggested that effort be devoted to improving the accuracy of the theoretical feed/subreflector phase pattern predictions.

After removal of subreflector diffraction effects using the derived phase function technique, the r.m.s. deviation of the surface, measured normal to the best-fit paraboloid, is found to be 2.73mm and 1.53mm at S-band and K-band respectively, again with a resolution of about 0.4m. By far the major cause of the discrepancy between these values is thought to be due to residual contamination from subreflector diffraction in the S-band result. Correction for subreflector diffraction is relatively unimportant at K-band and it follows that any residual errors in this band can be expected to be insignificant. It is also known that the S-band profile map suffers contamination by diffraction from the subreflector support struts whereas the K-band map does not.

Inspection of the S-band and K-band surface error maps shows negligible astigmatic distortion. As found in tests carried out shortly before the installation of the structural bracing [1], the antenna possess a third order deformation about its axis. Interestingly, however, this deformation component appears to have reduced as a result of the added bracing. It is also interesting that the K-band test is sufficiently sensitive to show radial line features believed to be associated with the sectored construction of the subreflector.

A list of corrections to be applied to the reflector panel adjusters is derived from the K-band surface error map. At 0.4m resolution the r.m.s. deviation of the surface is predicted to reduce from 1.53mm to 0.86mm. The associated gain improvements at S, X, and K-band are predicted to be 0.09 dB, 0.54 dB, 0.94 dB respectively.

At S-band the subreflector position error is found to be only a small fraction of a wavelength and is responsible for negligible gain loss. At K-band a position error comparable with the wavelength was detected. It is worth noting that in these and the earlier tests the axial position of the subreflector is found to be quite stable whereas the transverse position appears to vary by several millimetres. Interestingly the optimum subreflector positions for K-band and S-band differ by a few tens of millimetres, particularly in the transverse coordinates, and cause the K-band and S-band beams to diverge. This indicates some other misalignment

in the antenna, such as feed horn position error or subreflector tilt. Whilst this does not seem to adversely affect the S-band operation of the antenna, it is suggested that the locations of the feed horns should at least be checked, particularly the recently installed K-band horn.

The results given here demonstrate well the superiority of K-band holographic tests over S-band tests. Firstly, K-band testing is not heavily dependent upon the computational correction of data for the effects of subreflector diffraction, which has proved to be a formidable problem at S-band. Secondly, unlike the S-band results, the K-band surface error map is not noticeably contaminated by diffraction from the subreflector support struts. Thirdly, measurement errors due to receiver system noise are greatly reduced at K-band. Here, errors due to noise at K-band are about twenty times less than at S-band.

The accuracy of S-band surface error mapping could almost certainly be improved by devoting further effort to the prediction of feed/subreflector phase scatter patterns. It has also been suggested that algorithms might be developed for the removal of subreflector support scattering by spatial filtering. However, despite the shortcomings of the use of S-band for accurate surface mapping, use of this frequency band for future measurements should perehaps not be dismissed entirely as it offers the potential for long term monitoring of changes of reflector shape without the need to use feeds other than those normally employed in the DSN antennas.

13. REFERENCES

1. 'Final report on holographic tests at S-band and K-band on the DSS-63 64 metre antena', Test dates: 19 to 27 November 1984, Eikontech Limited report prepared for JPL under contract No. 956984, January 1986.

2. 'Final report on S-band holographic tests on the DSS-43 64 metre antenna', Test dates: 19 to 23 January 1985, Eikontech Limited report prepared for JPL under contract No. 956984, September 1985.

3. 'Final report on S-band holographic tests on the DSS-45 34 metre antenna', Test dates: 28 to 30 Jan 1985, Eikontech Limited report prepared for JPL under contract No. 956984, October 1985.

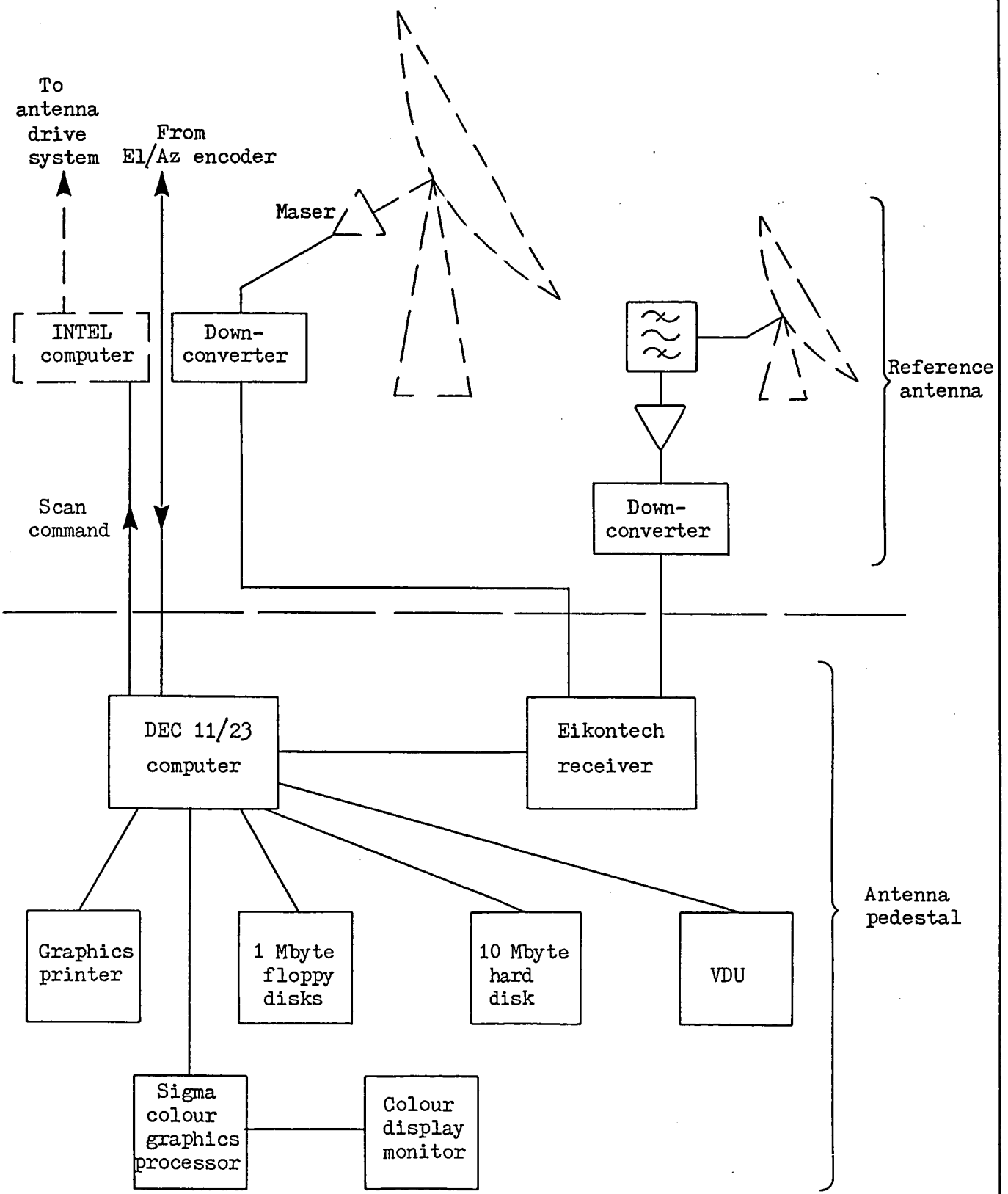

Holographic test system

Figure No 2.1

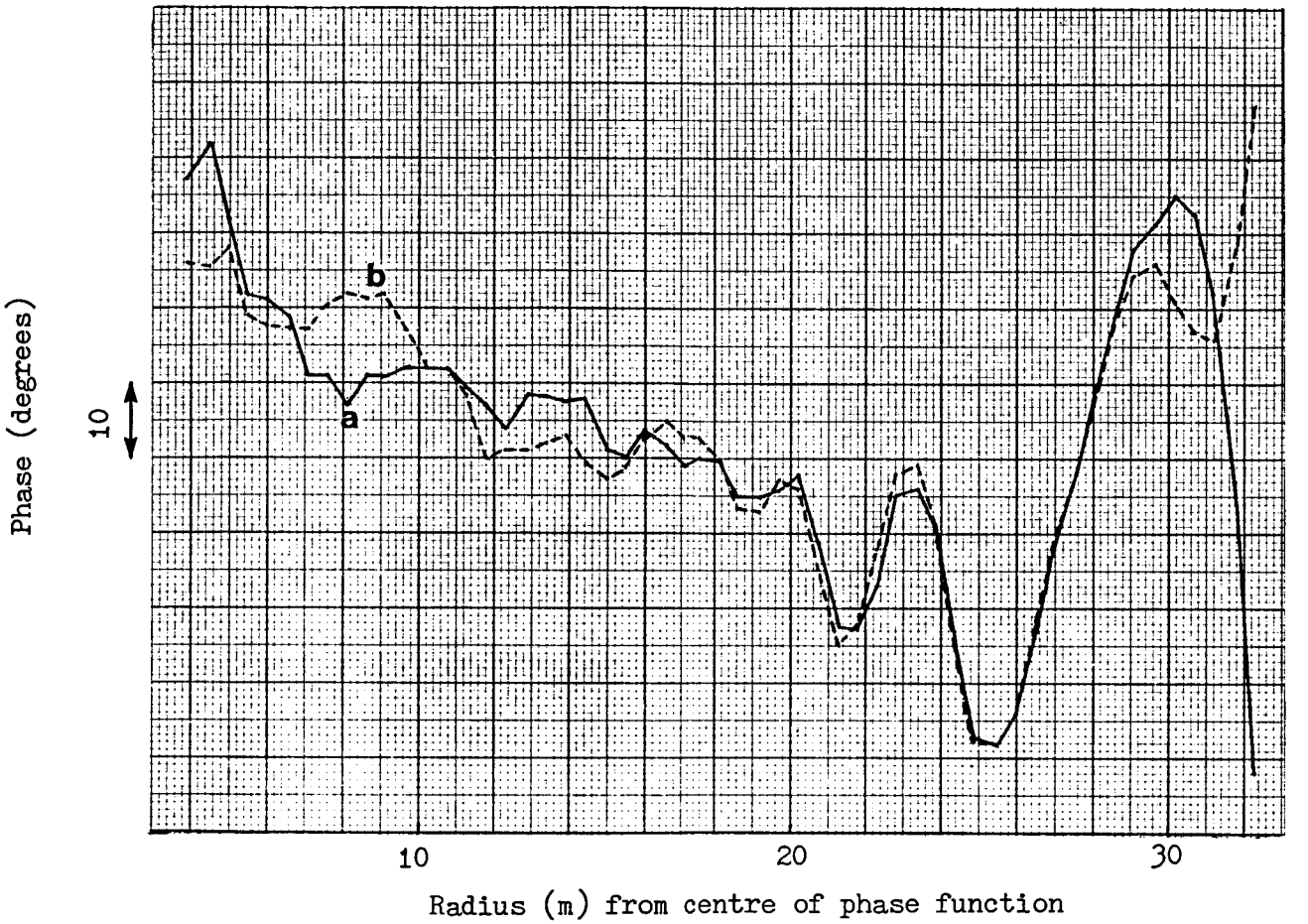

Comparison of phase functions at 2.2725 GHz.
a. Derived from results for DSS-43 (see reference 2).
b. Derived from scan 2.

Figure No 4.1

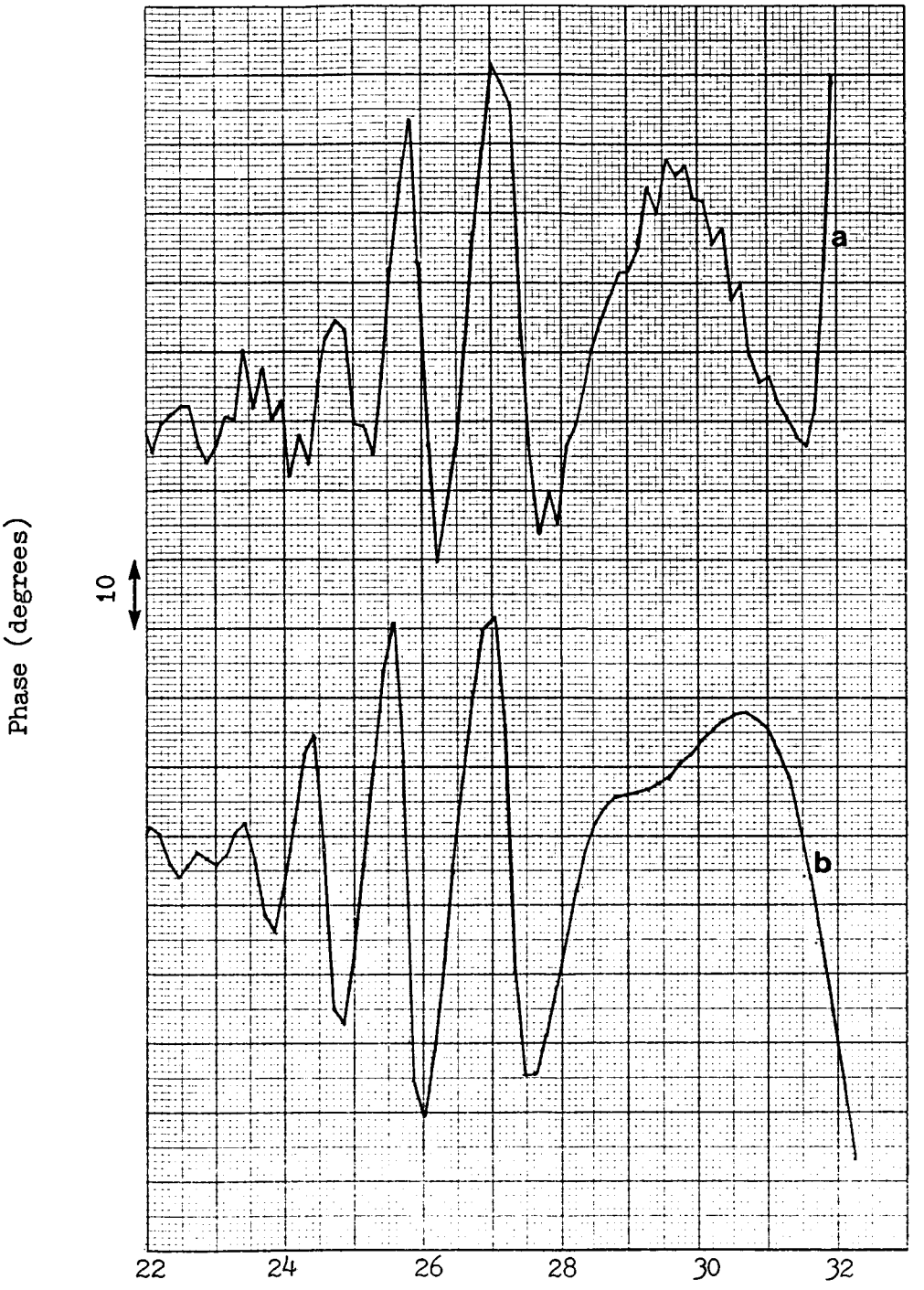

Phase distribution due to feed/subreflector scatter at 11.451 GHz
a. Derived from scan 4
b. Predicted by JPL

Figure No 4.2

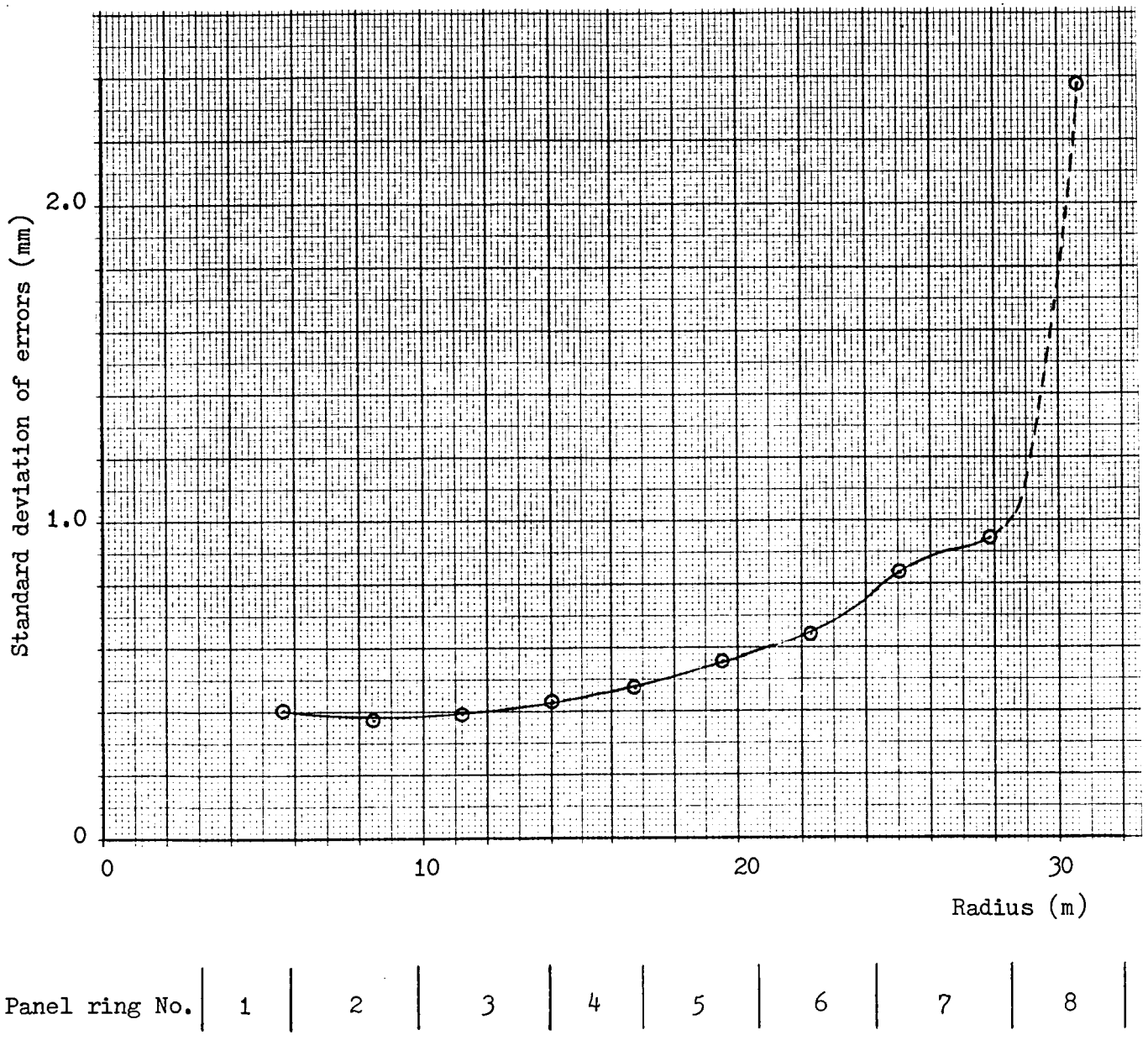

S-band profile mapping accuracy (from Scan 2)

Figure No 7.1

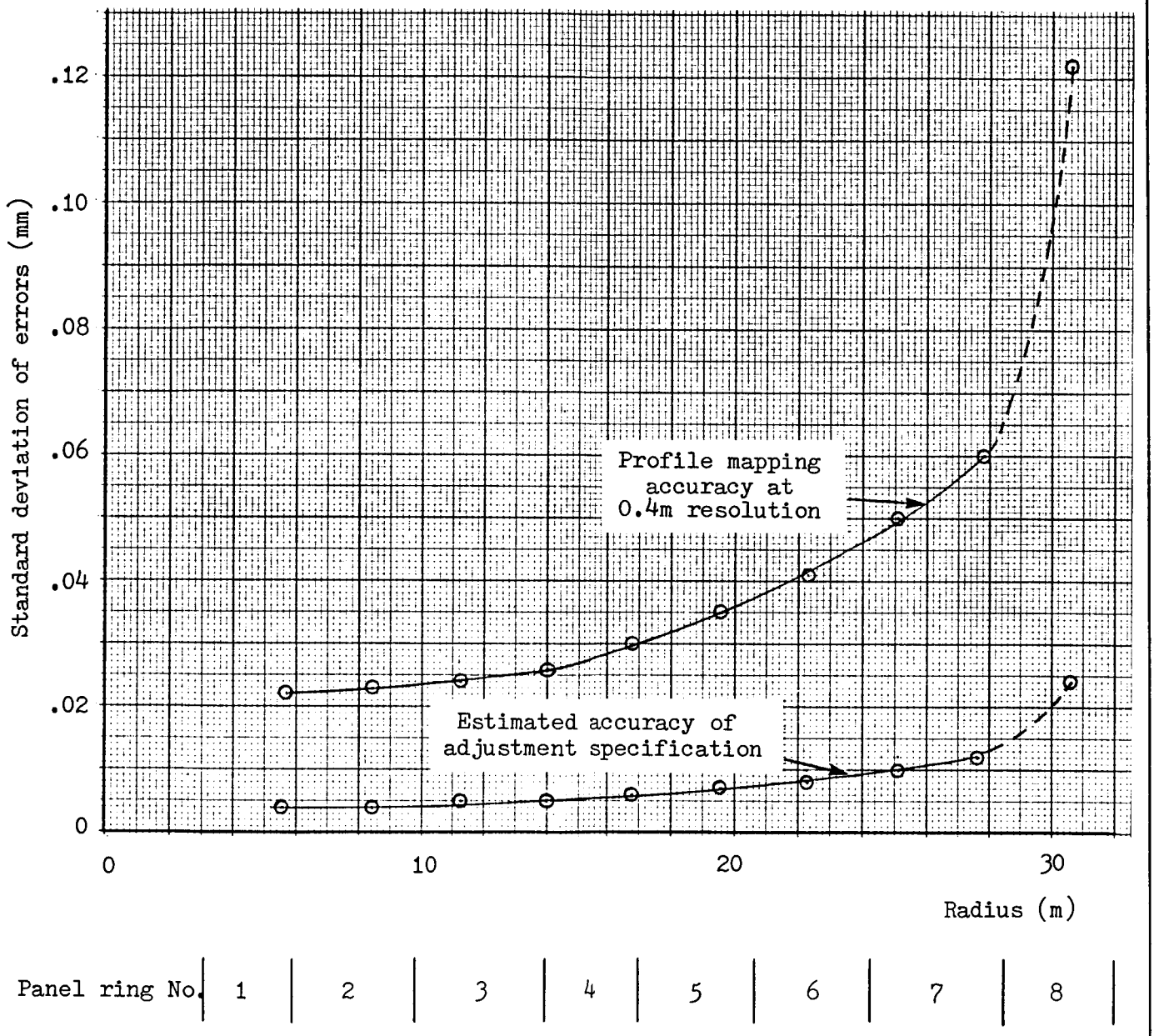

K-band profile mapping accuracy and estimated accuracy of specified panel adjustments (from Scan 4)

Figure No 7.2

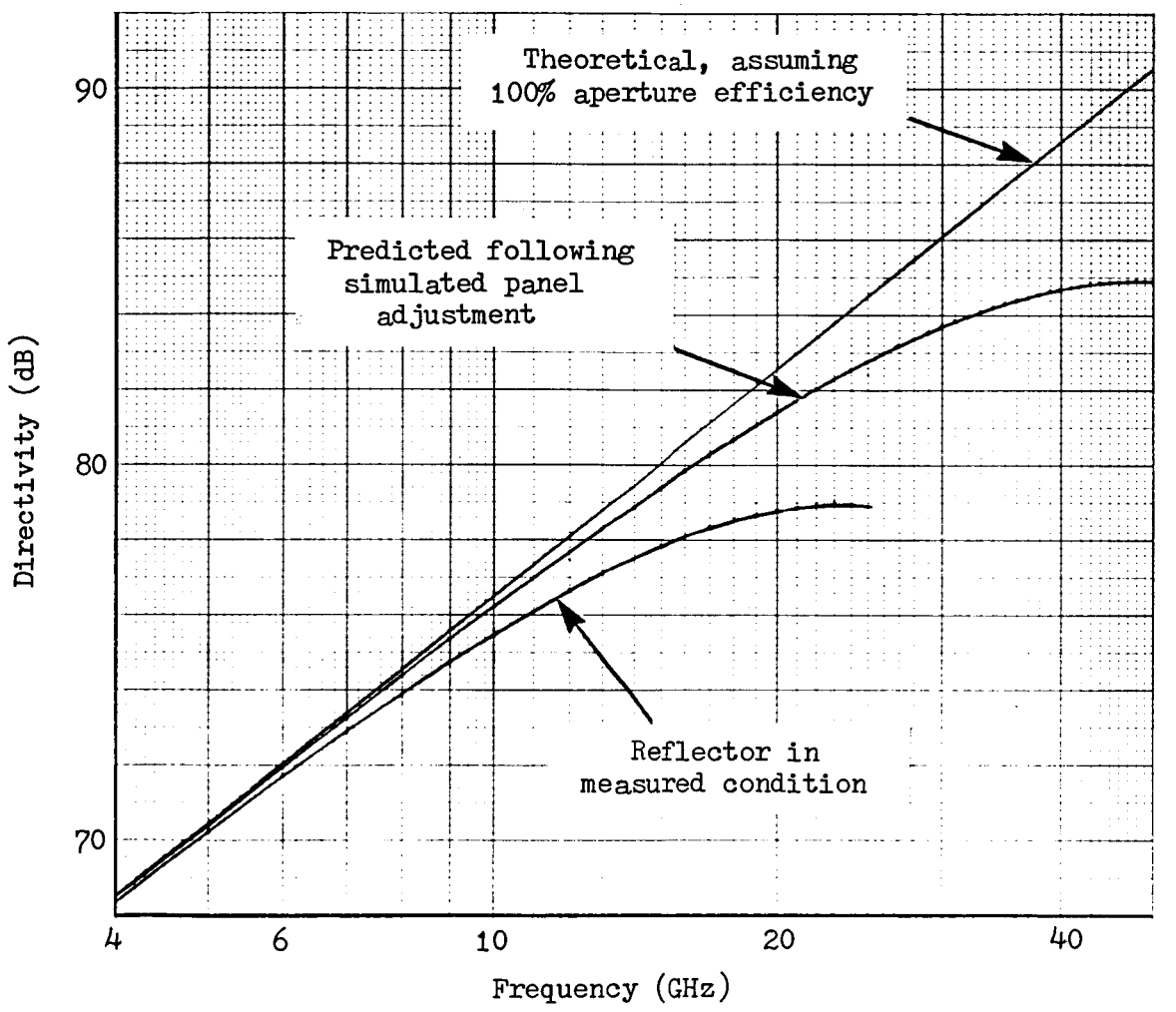

Variation of directivity with frequency

Figure No 10.1

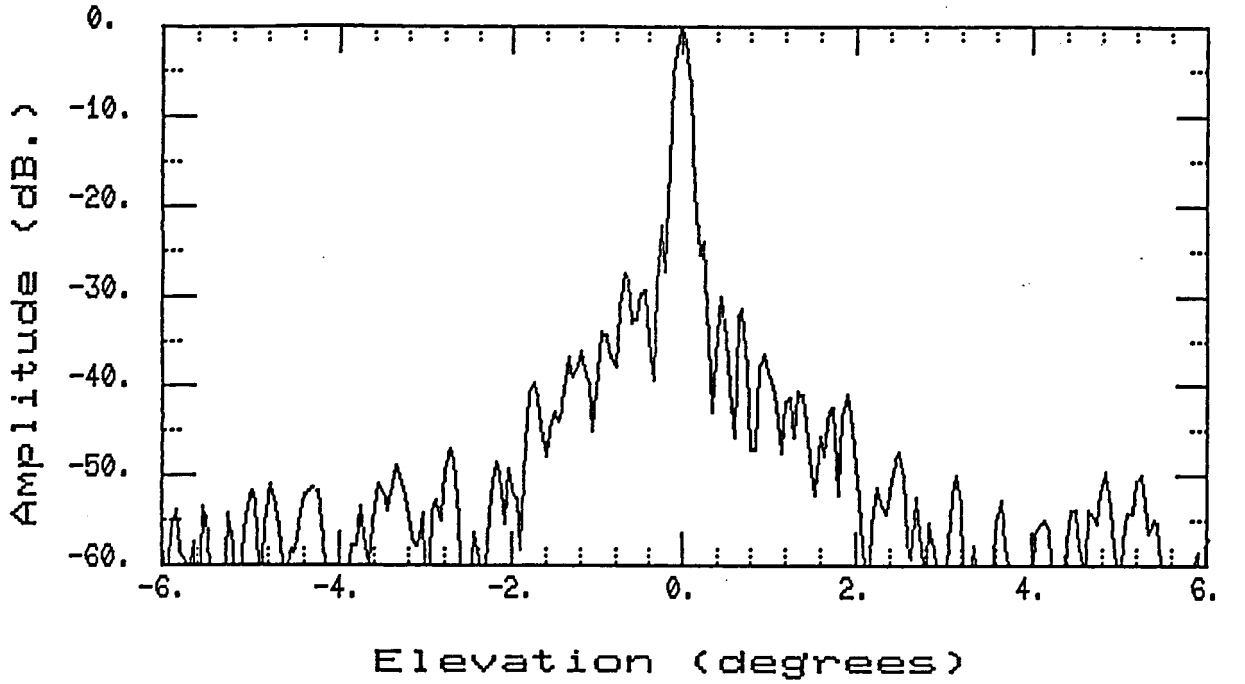

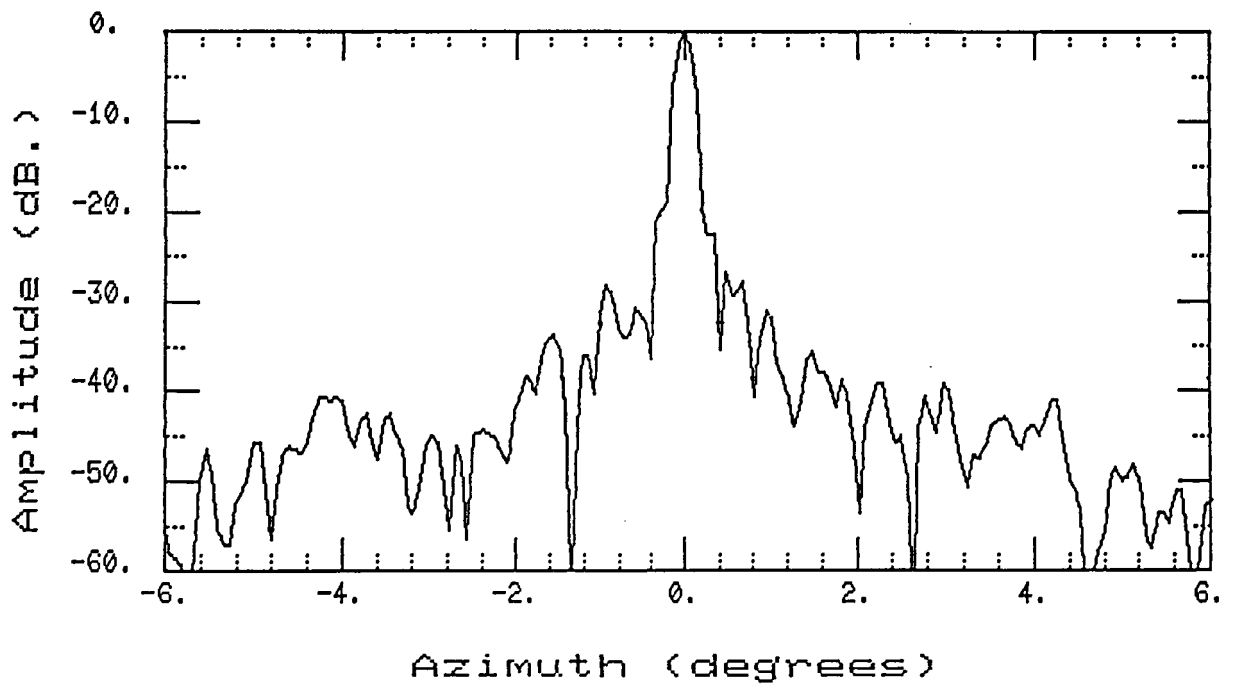

Measured radiation patterns at 2.2775 GHz

Figure No 11.1

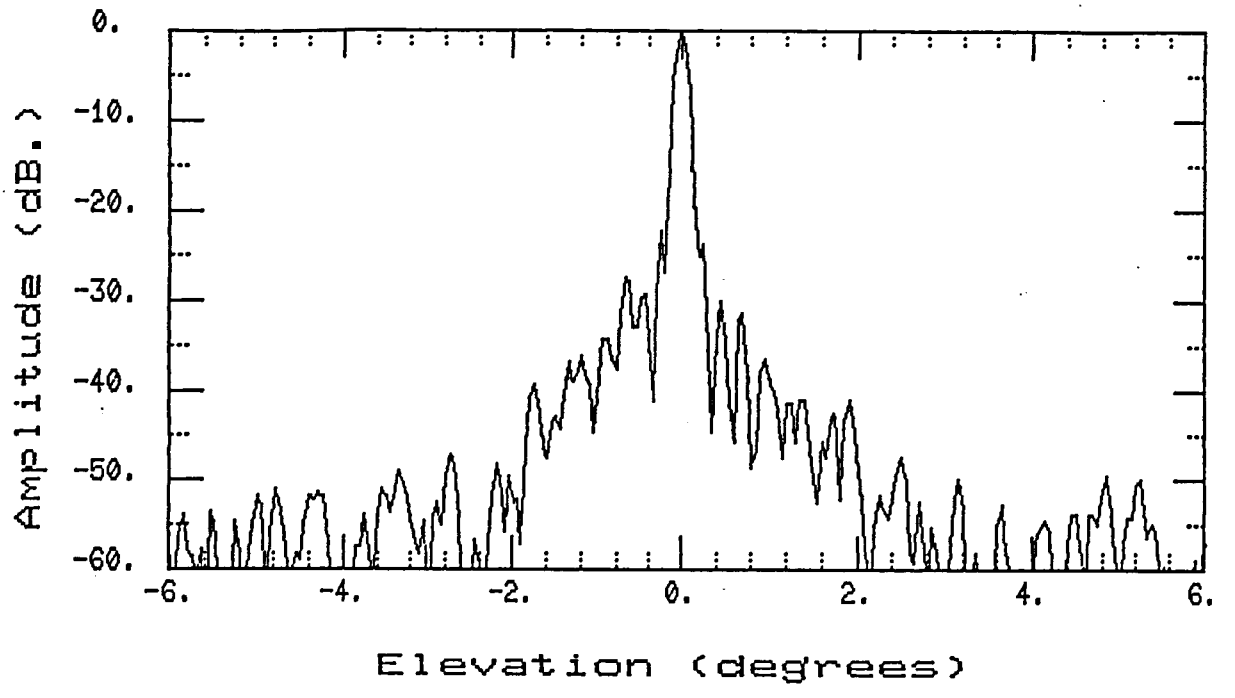

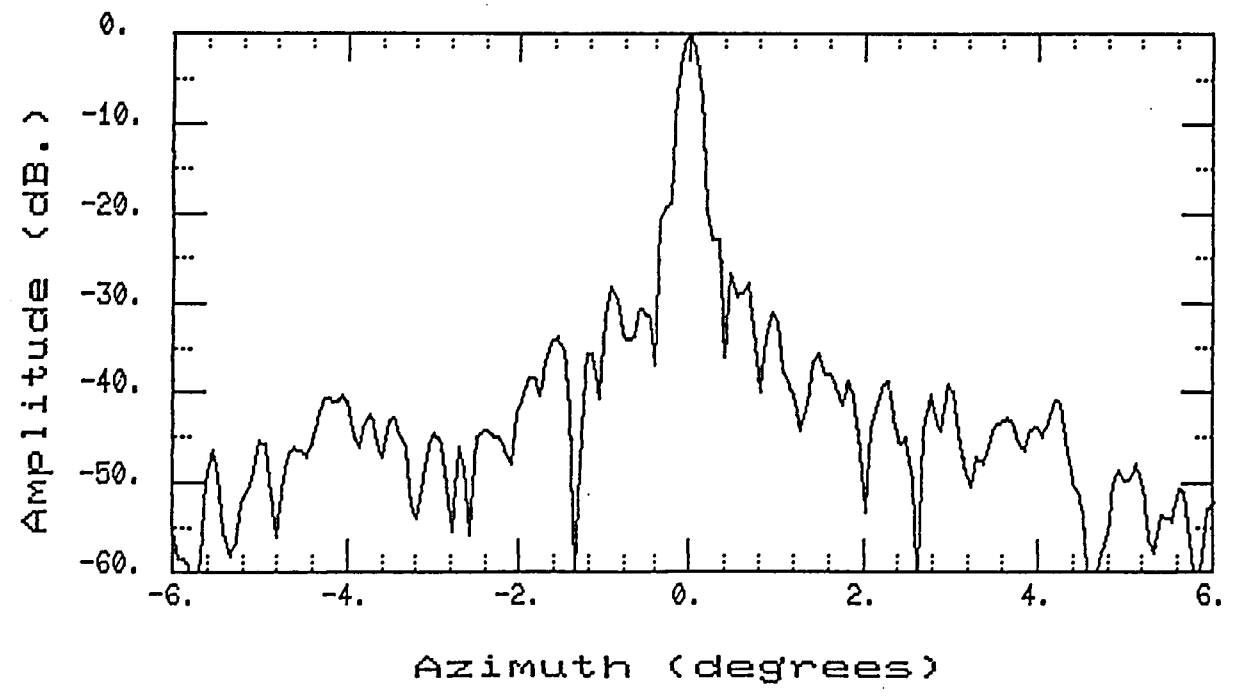

Predicted radiation patterns after simulated subreflector adjustment to optimise performance at 2.2775 GHz

Figure No 11.2

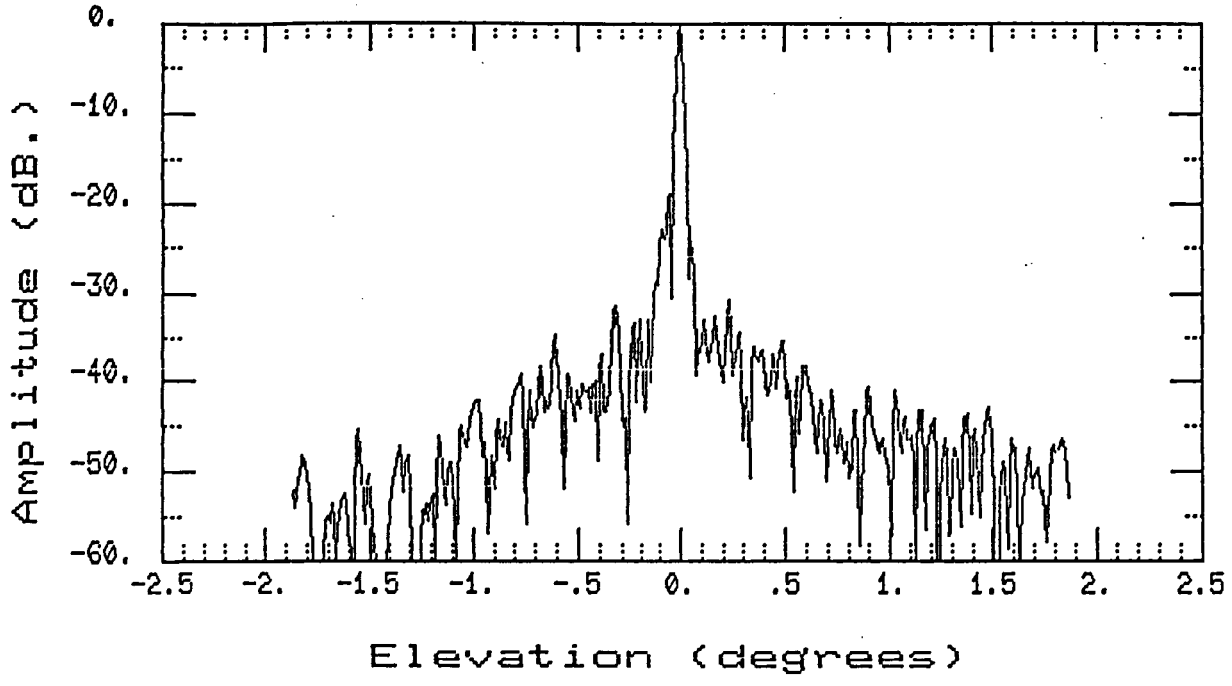

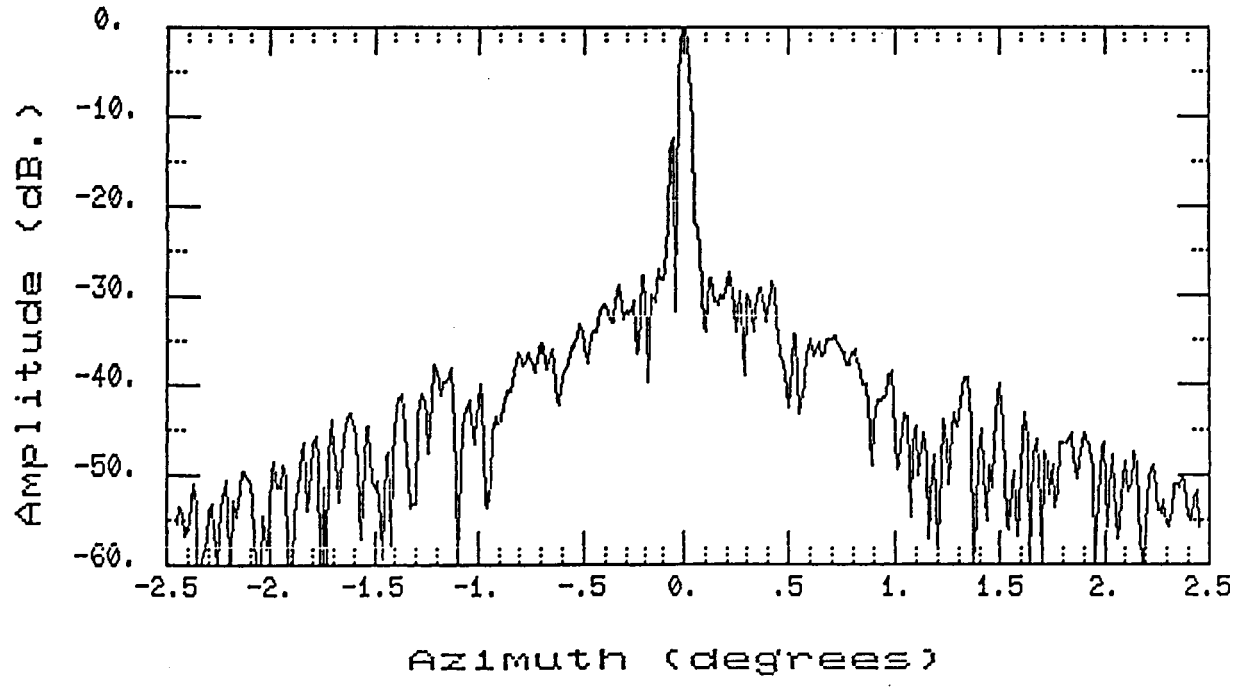

Measured radiation patterns at 11.451 GHz.

Figure No 11.3

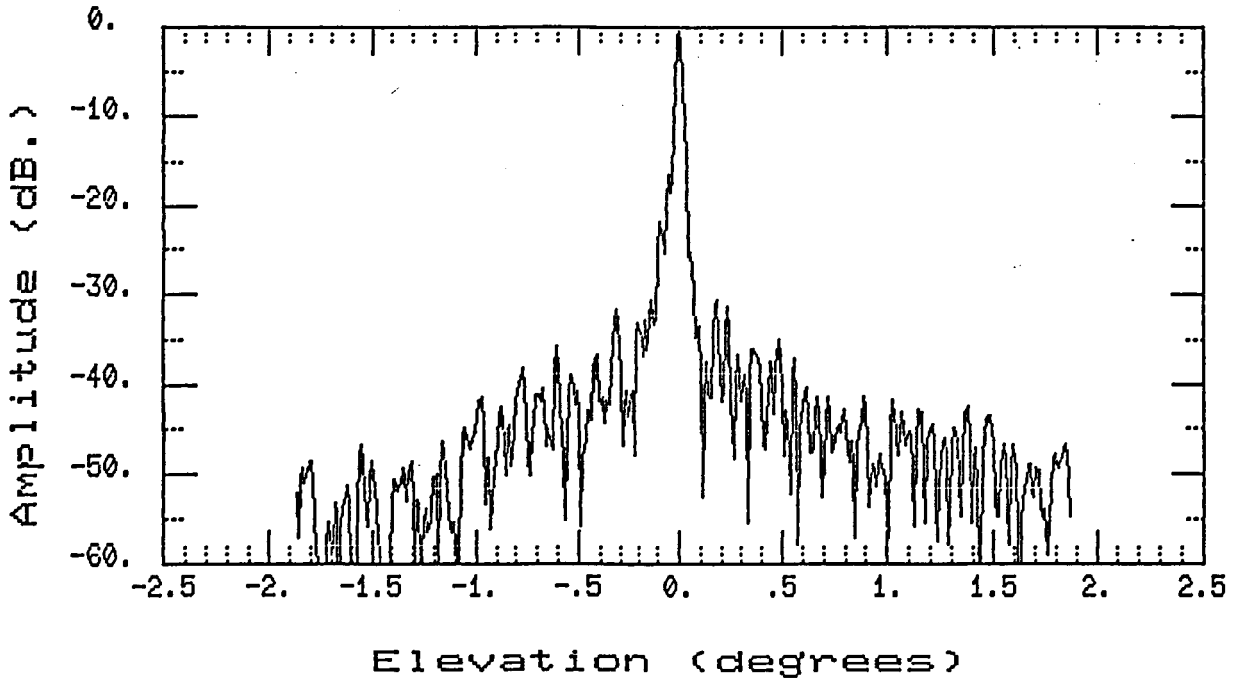

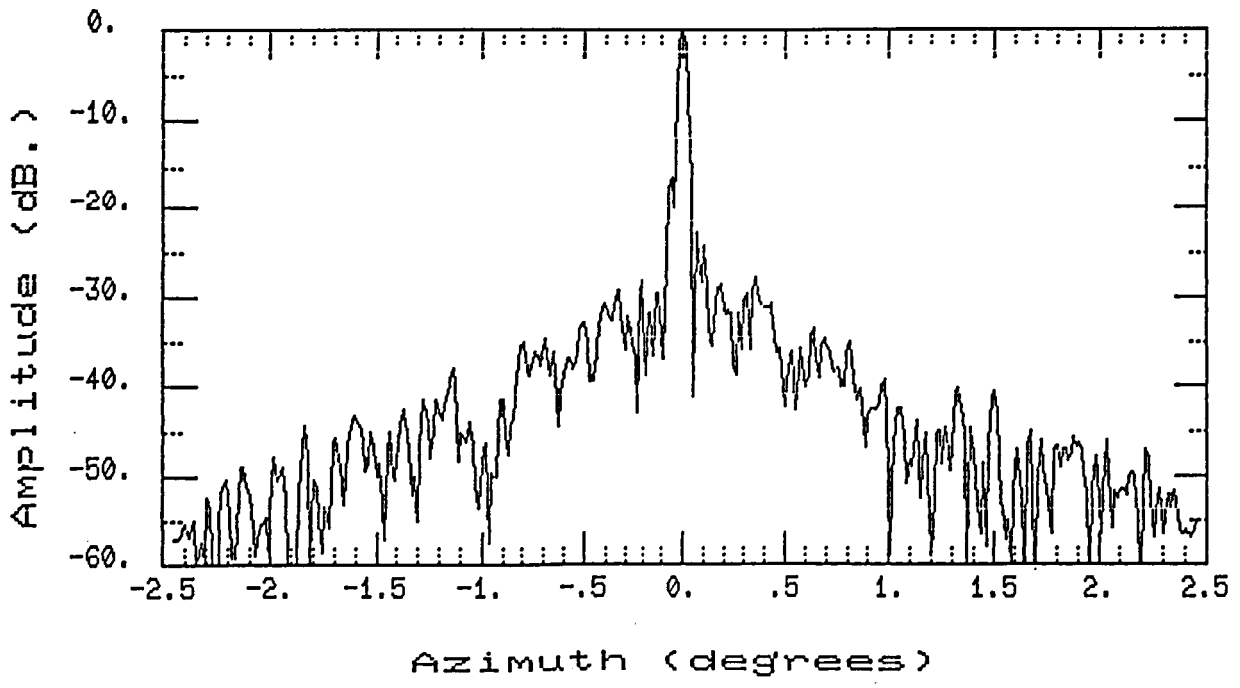

Predicted radiation patterns after simulated subreflector adjustment to optimise performance at 11.451 GHz.

Figure No 11.4

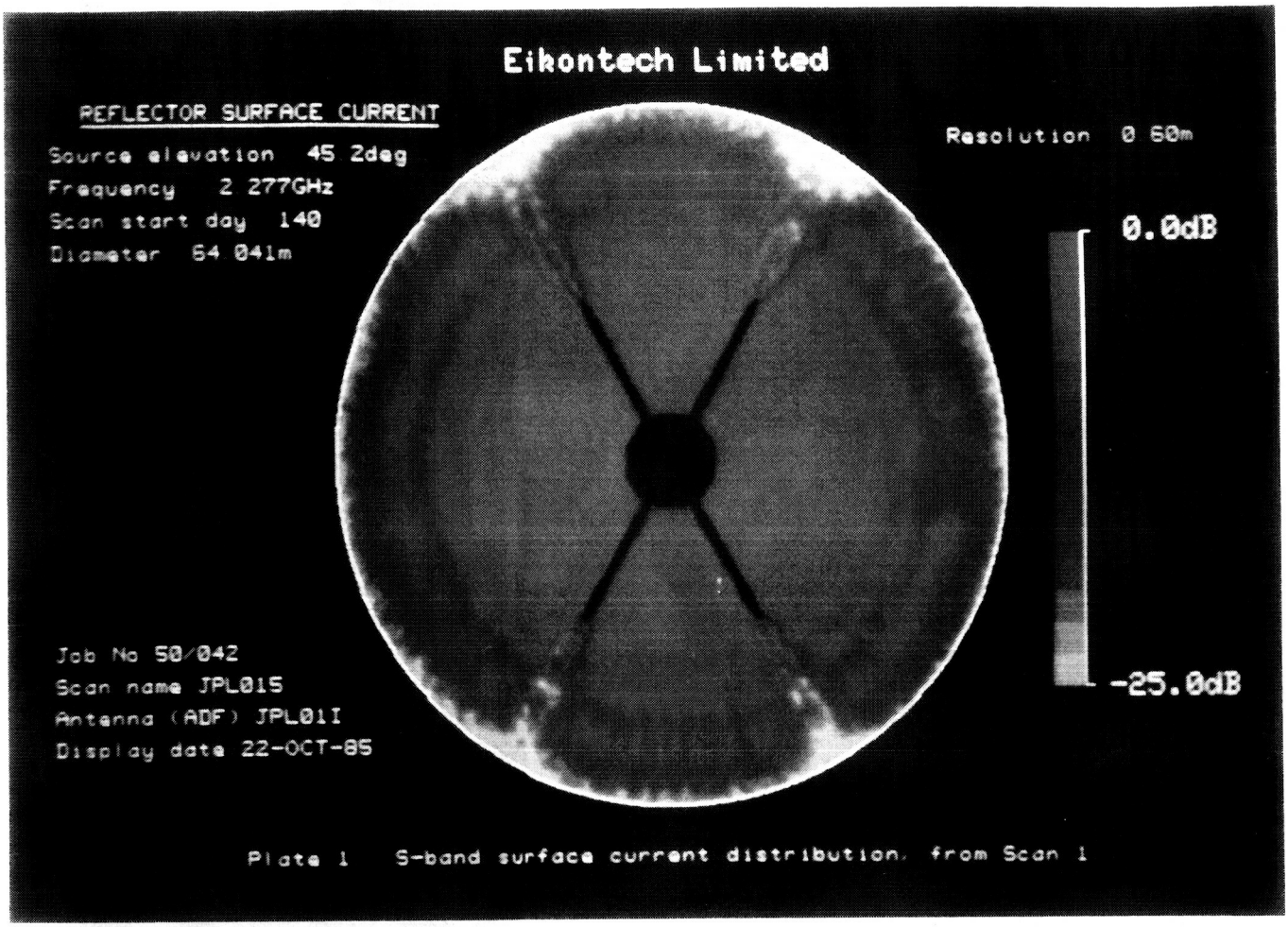

Plate 1 S-band surface current distribution, from Scan 1

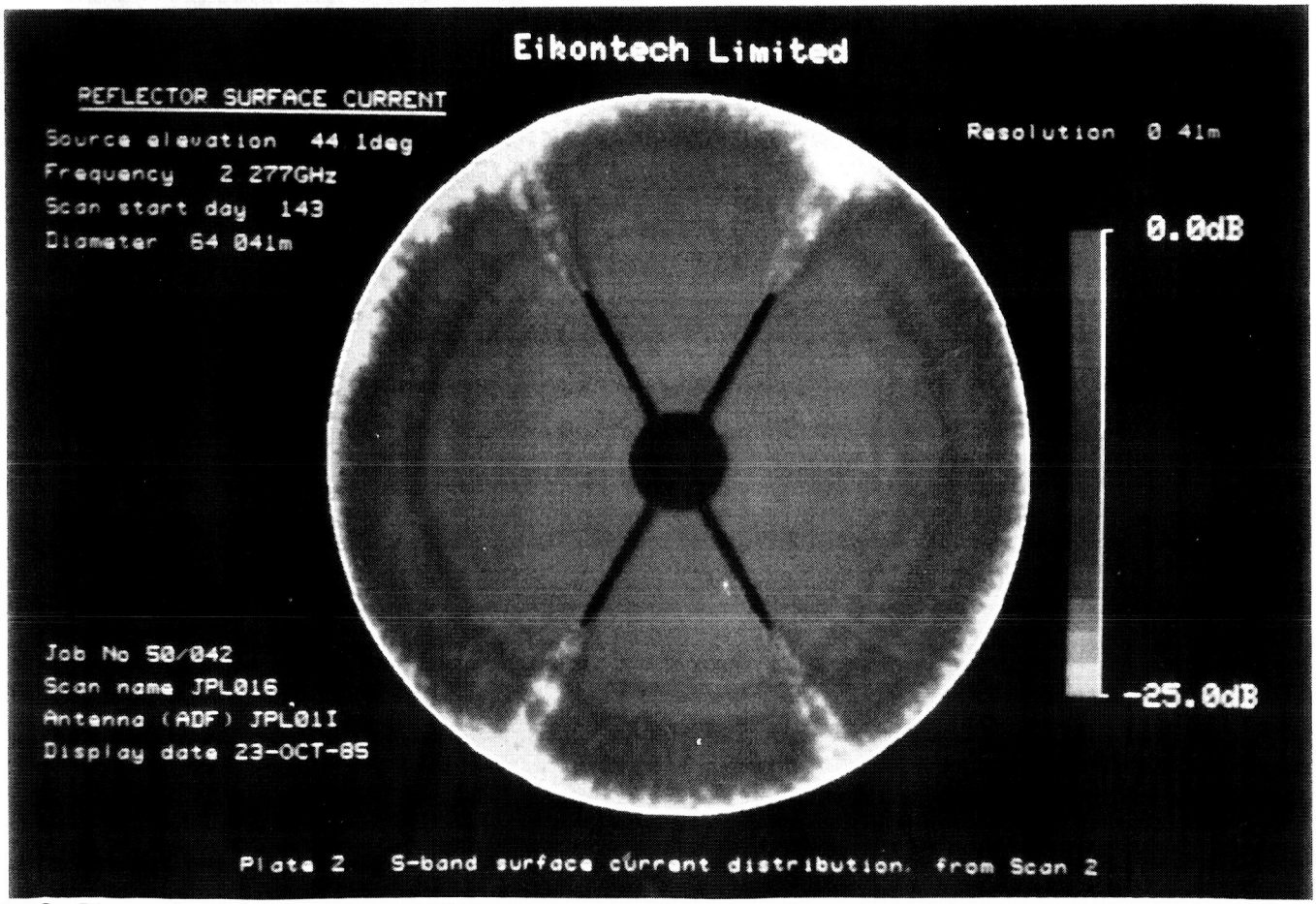

Plate 2 S-band surface current distribution, from Scan 2

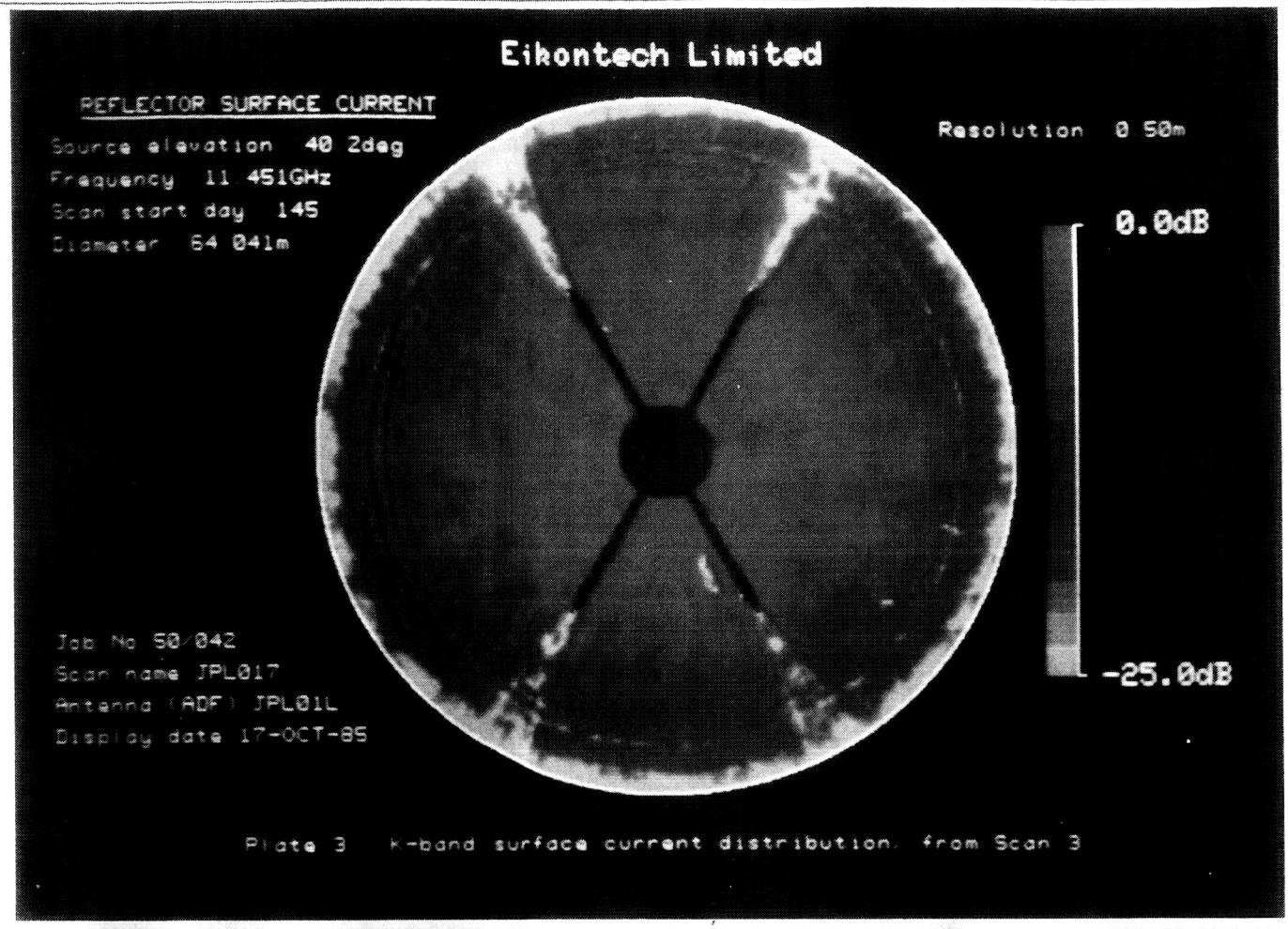

Plate 3 K-band surface current distribution from Scan 3

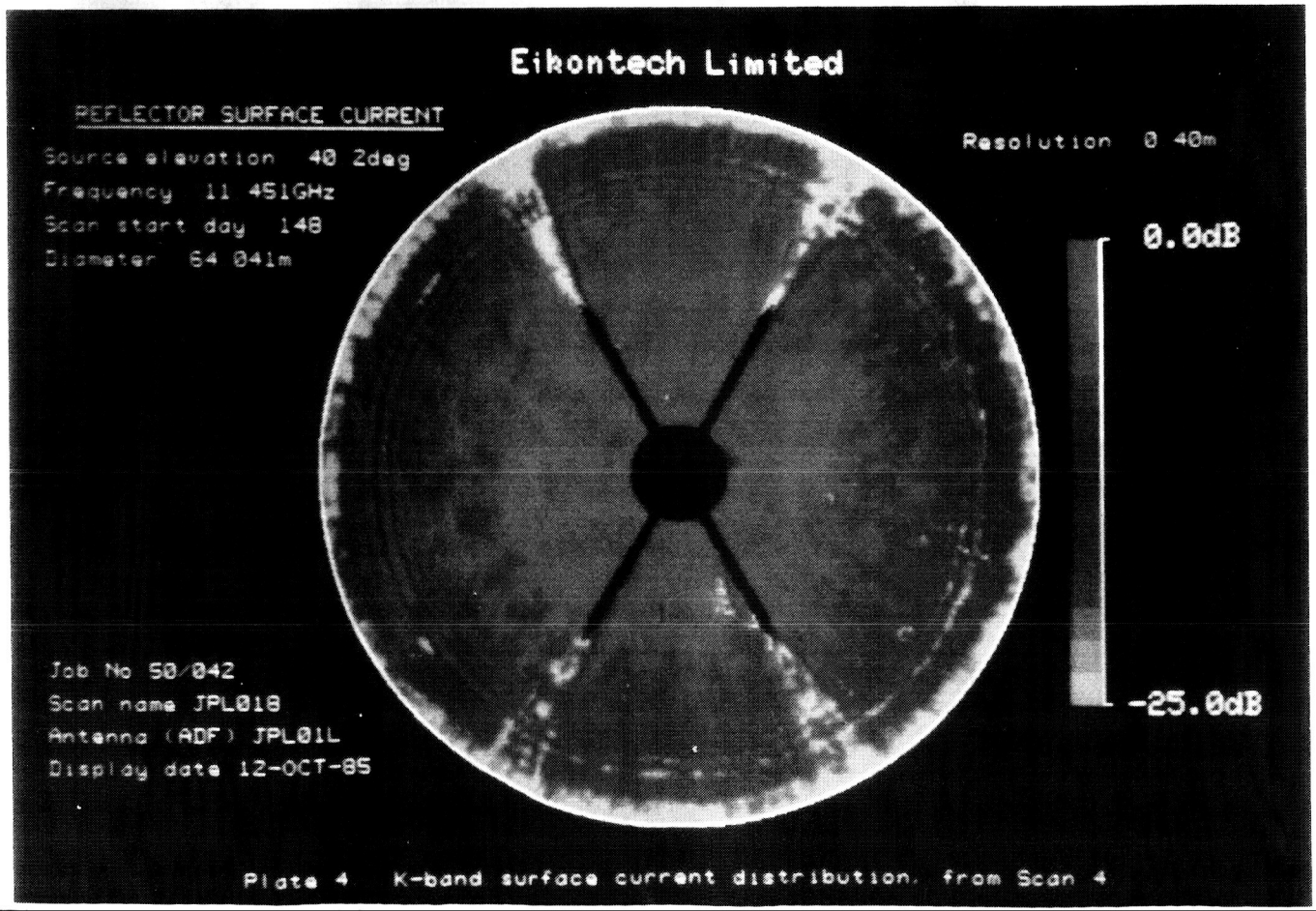

Plate 4 K-band surface current distribution from Scan 4

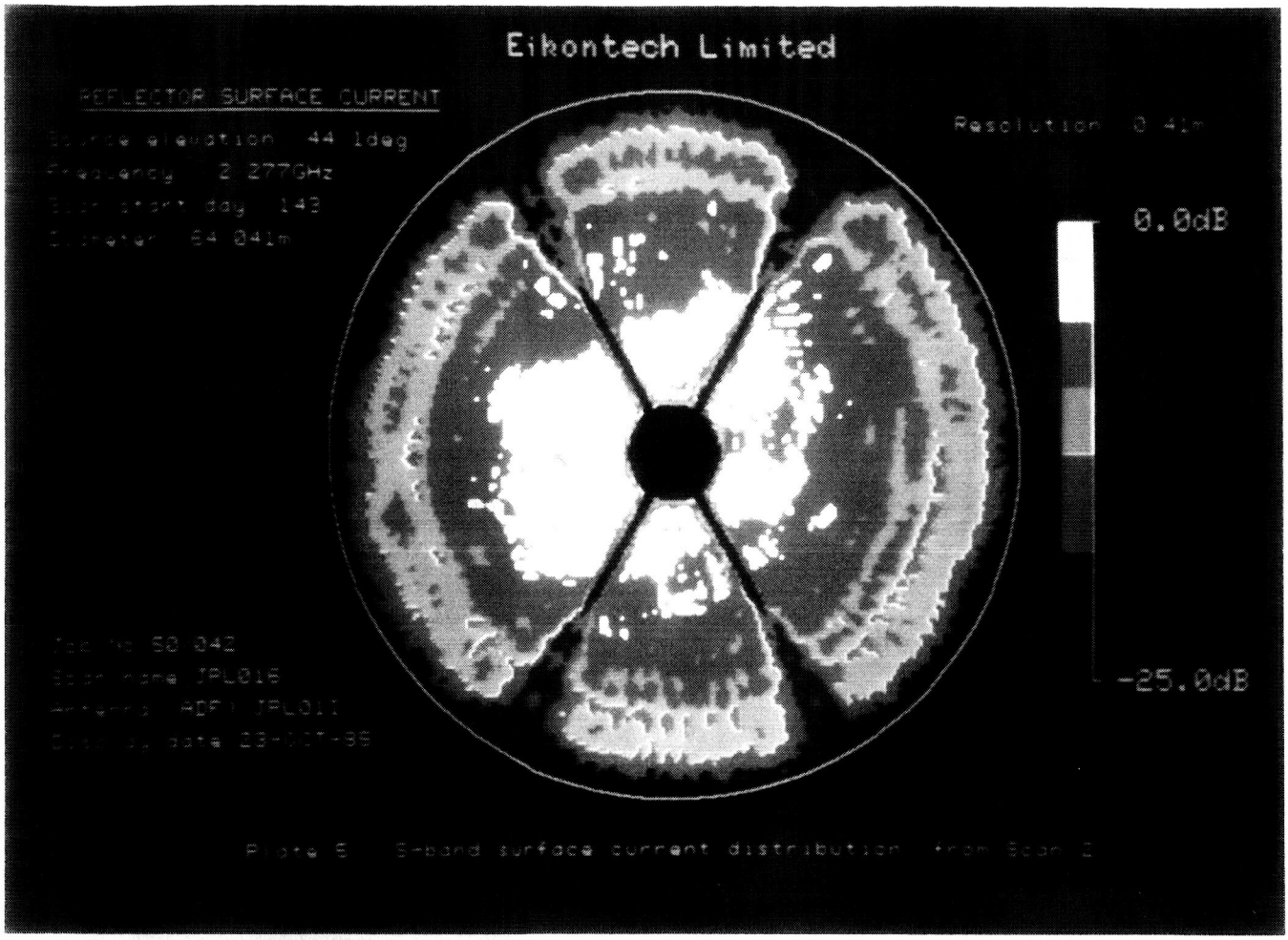

Plate 5 S-band surface current distribution from Scan 3

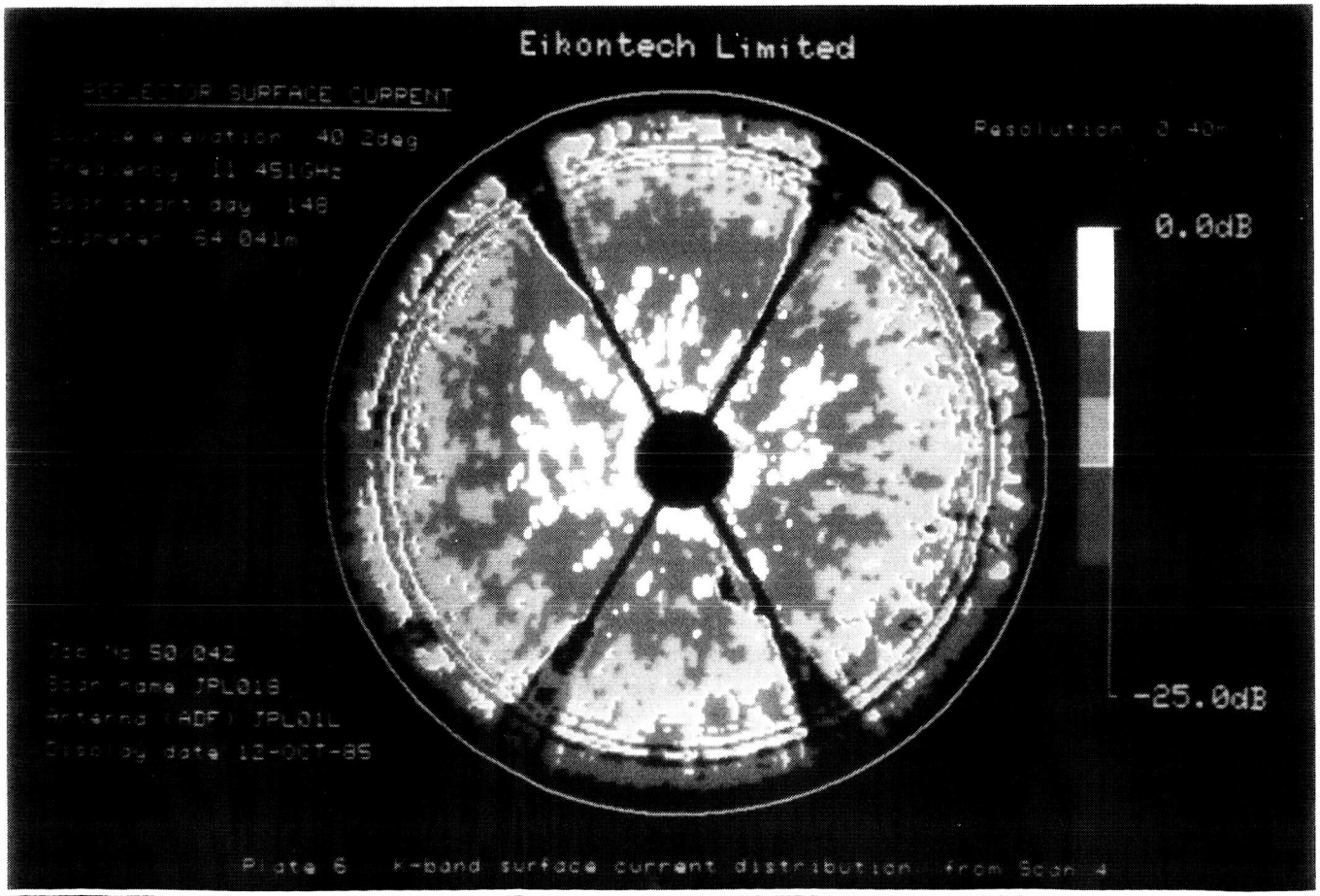

Plate 6 X-band surface current distribution from Scan 4

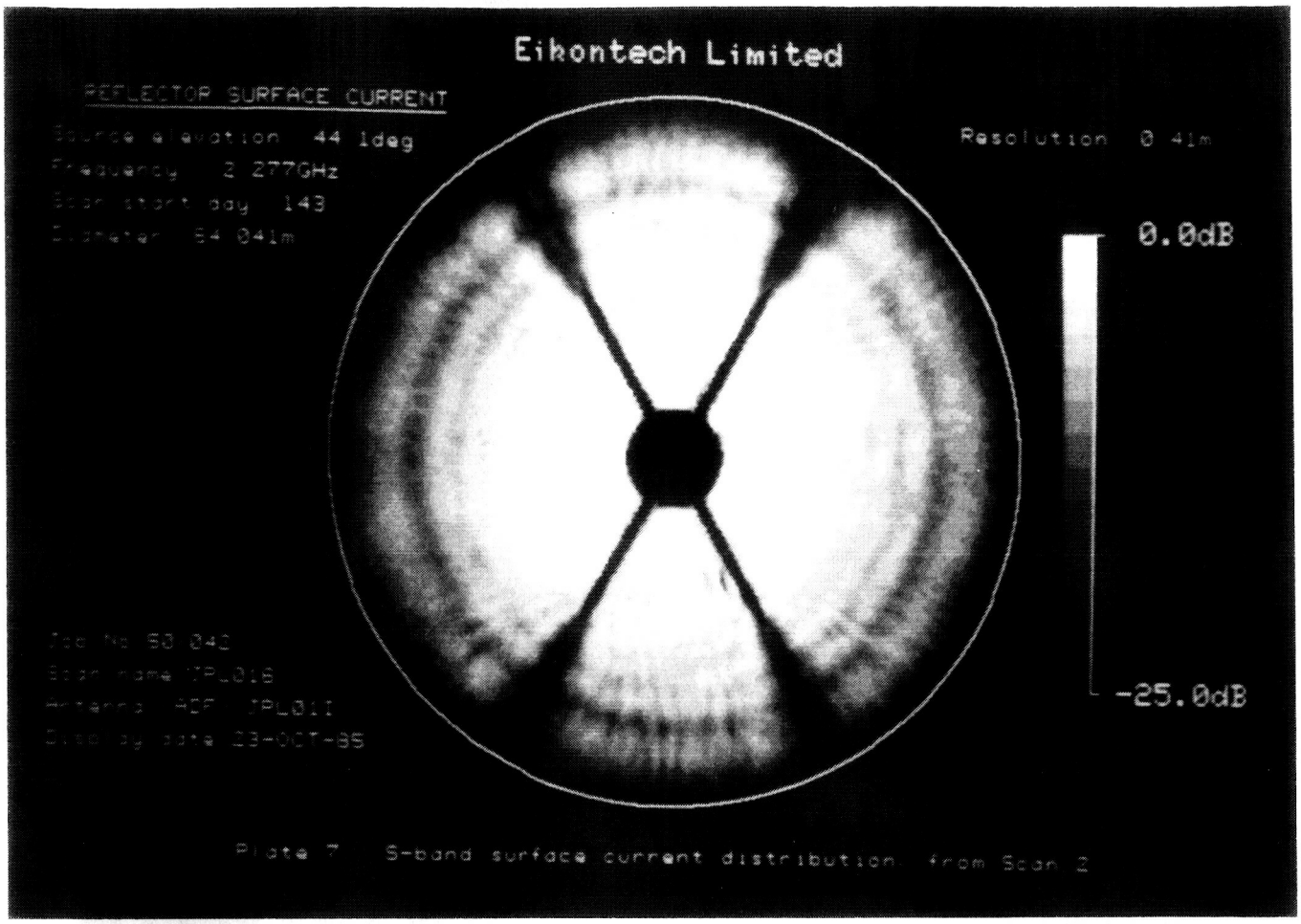

Plate 7 S-band surface current distribution from Scan 2

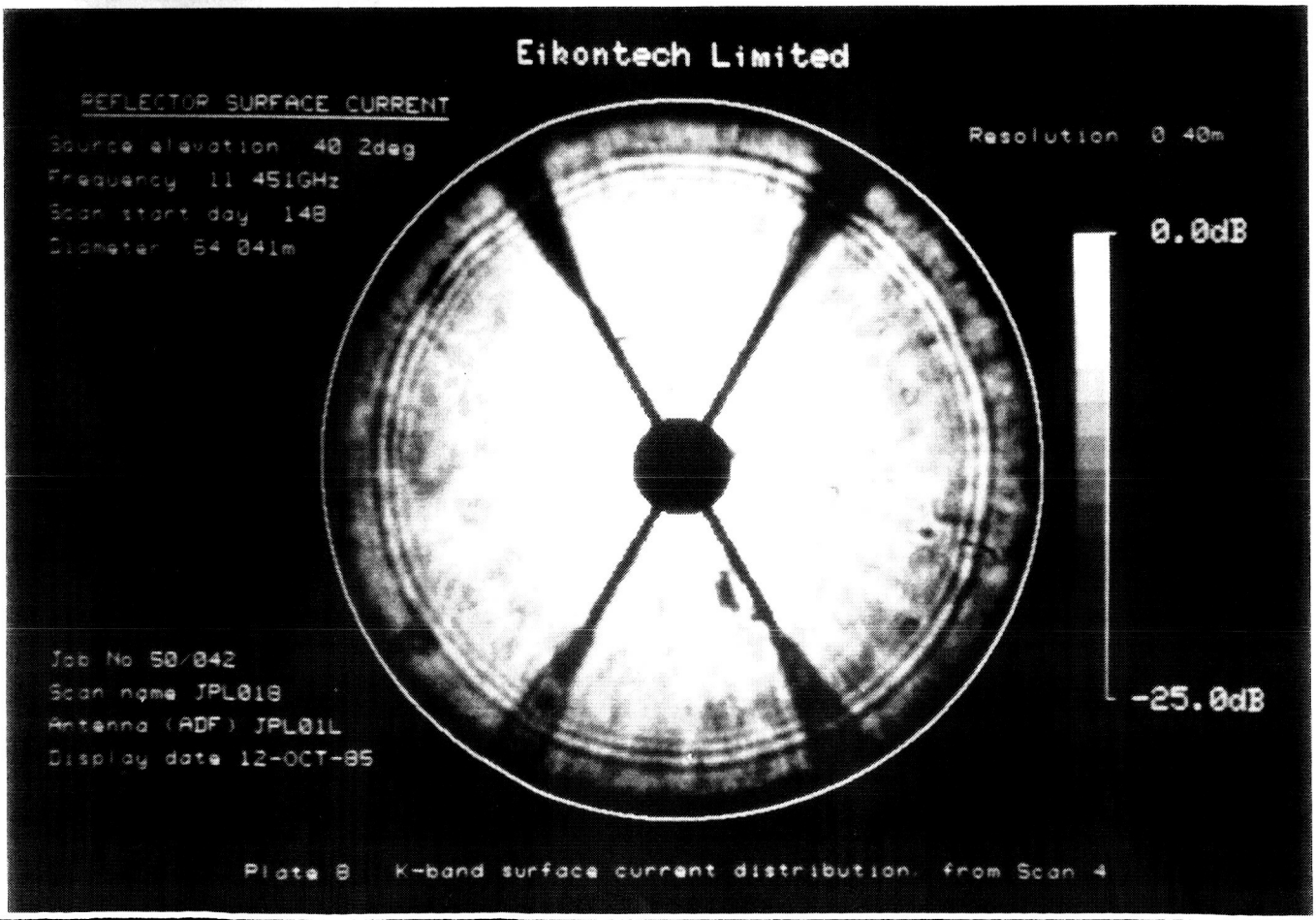

Plate 8 K-band surface current distribution from Scan 4

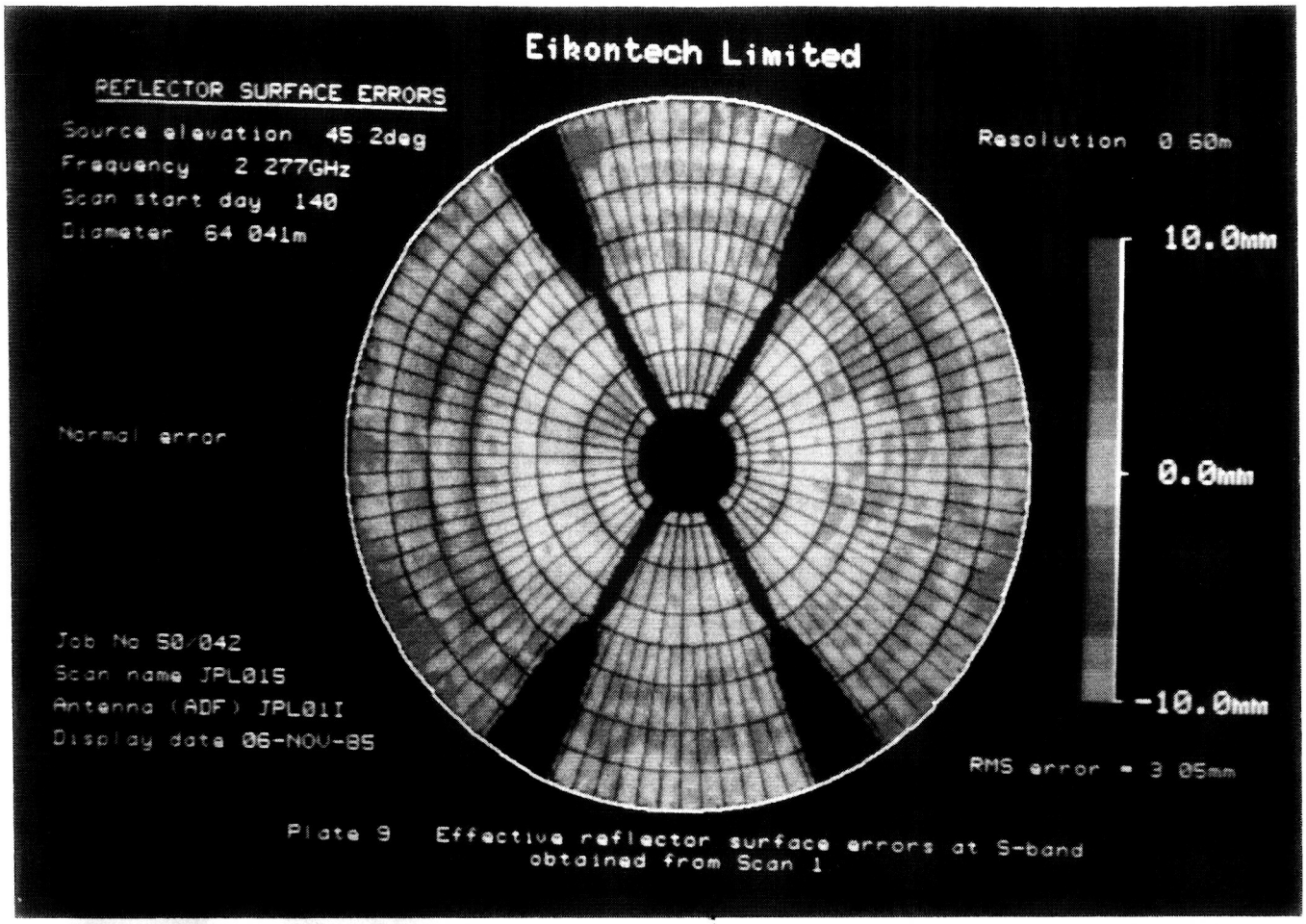

Plate 9 Effective reflector surface errors at S-band obtained from Scan 1

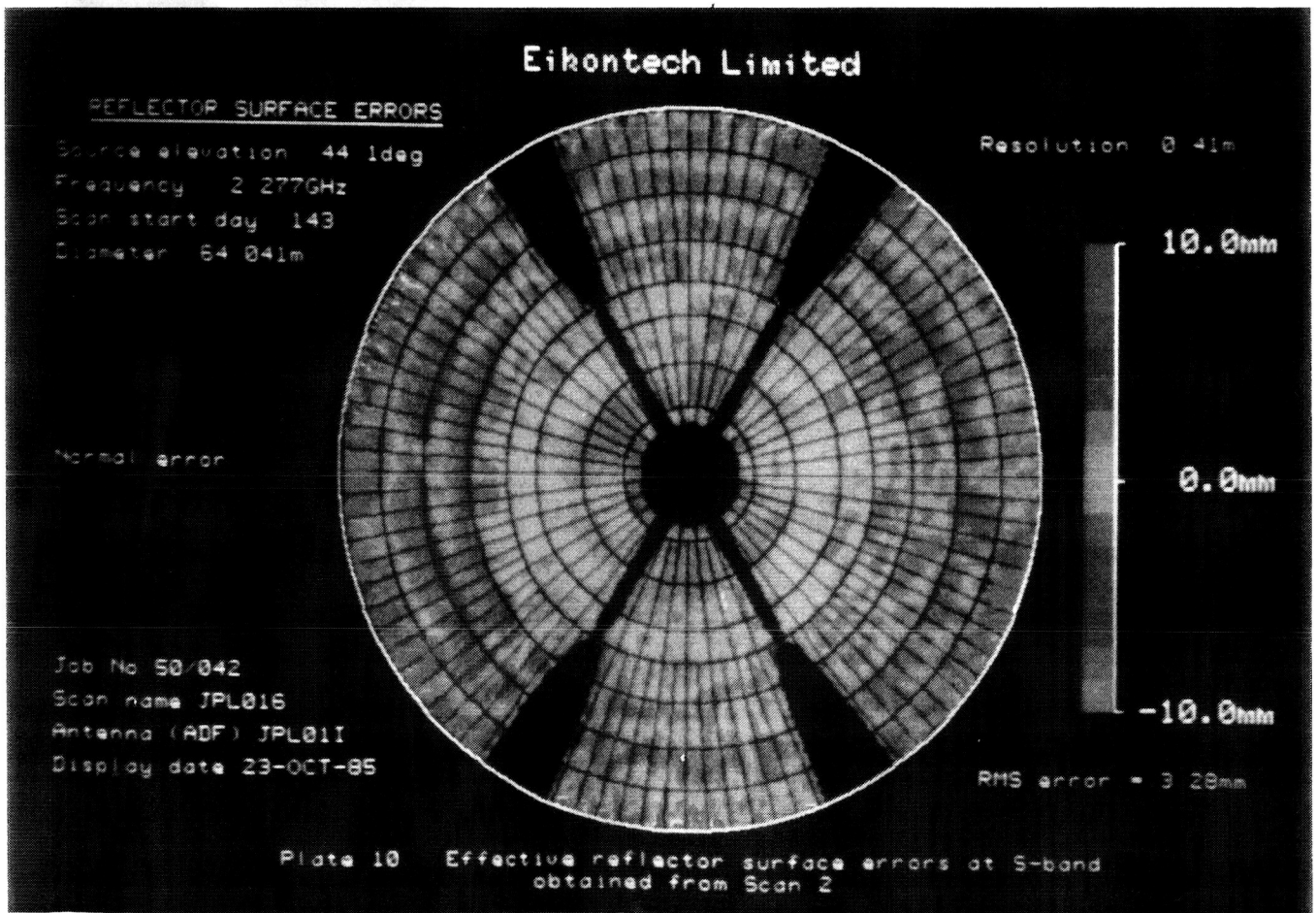

Plate 10 Effective reflector surface errors at S-band obtained from Scan 2

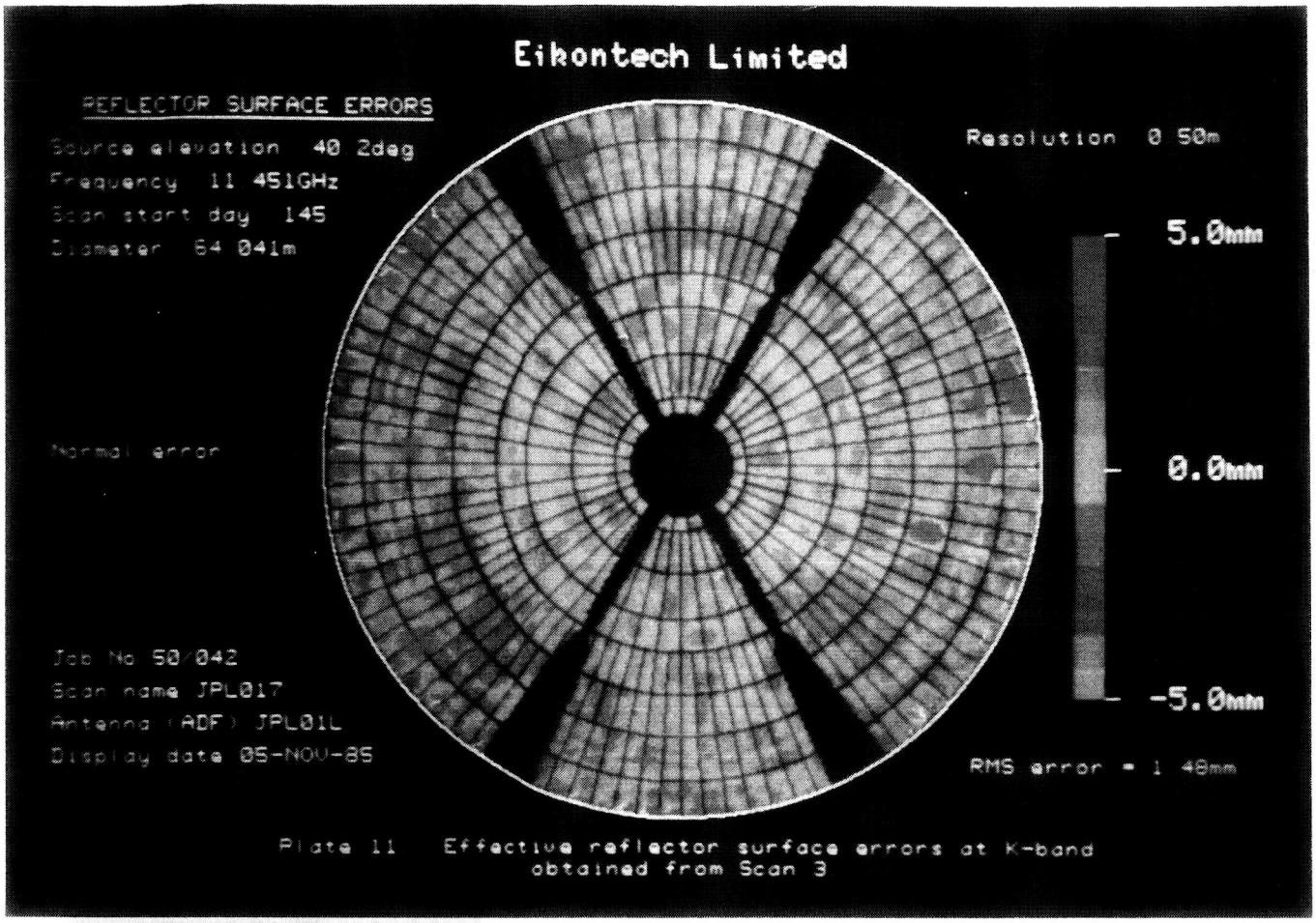

Plate 11 Effective reflector surface errors at K-band obtained from Scan 3

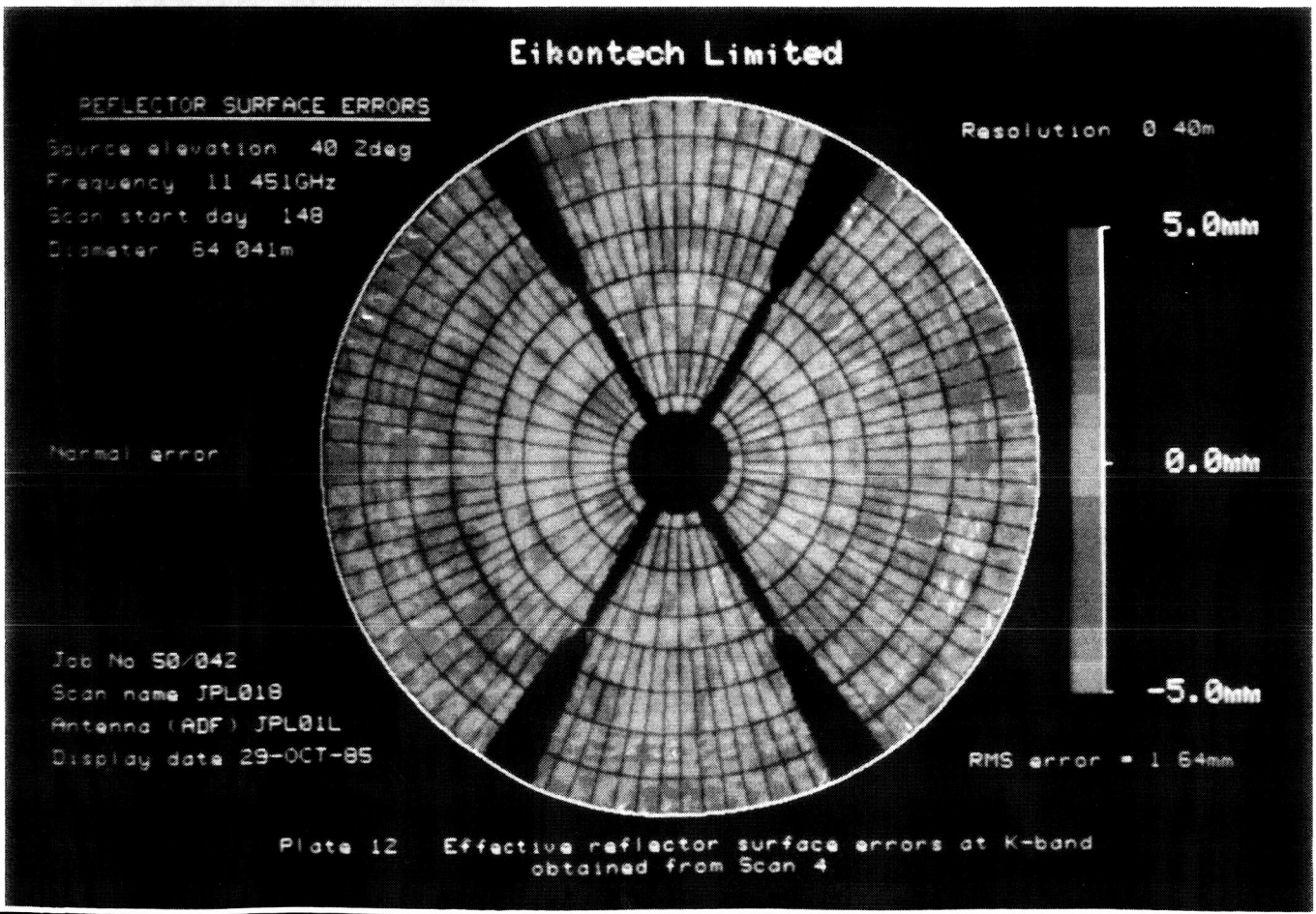

Plate 12 Effective reflector surface errors at K-band obtained from Scan 4

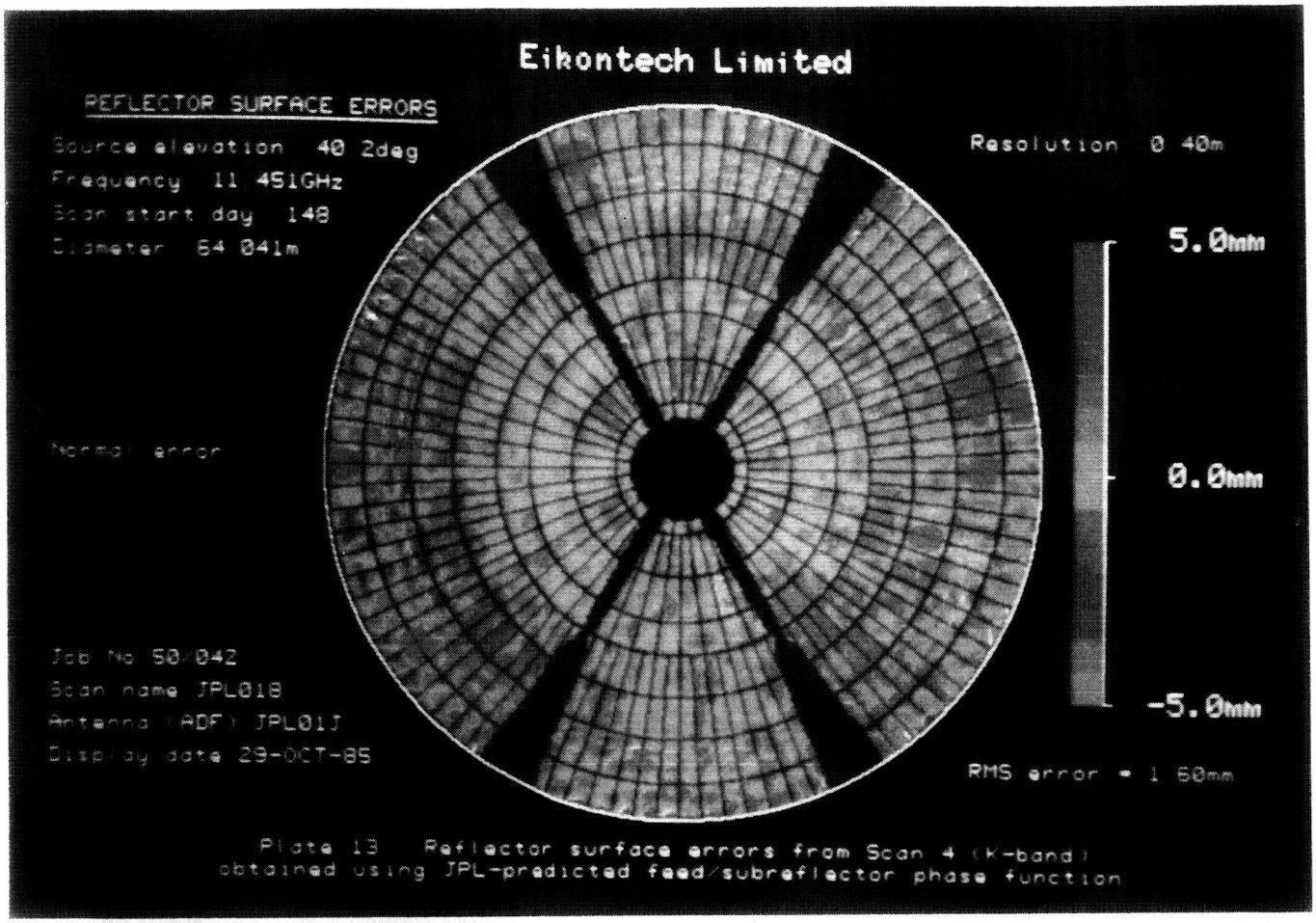

Plate 13 Reflector surface errors from Scan 4 (K-band) obtained using JPL-predicted feed/subreflector phase function

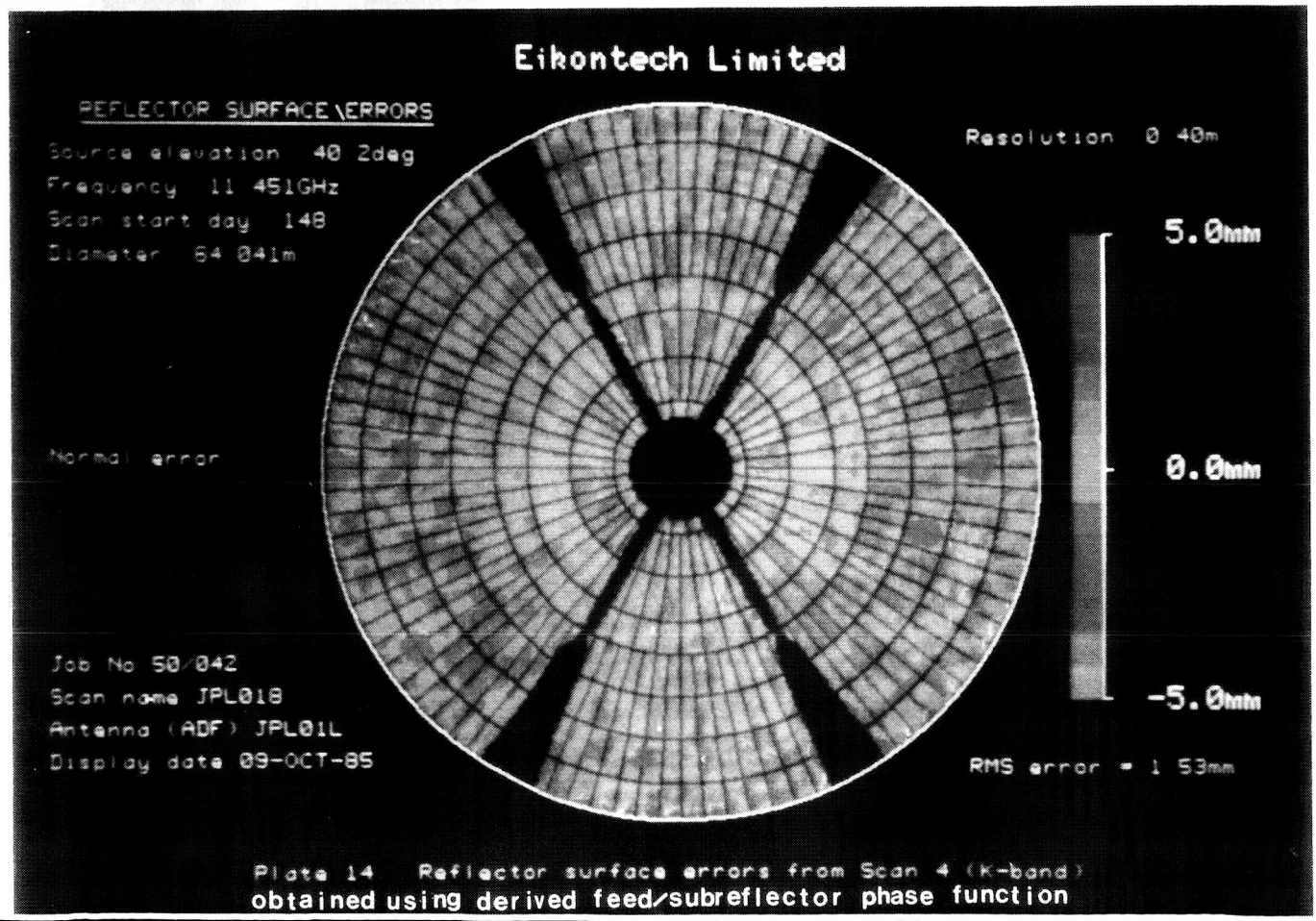

Plate 14 Reflector surface errors from Scan 4 (K-band) obtained using derived feed/subreflector phase function

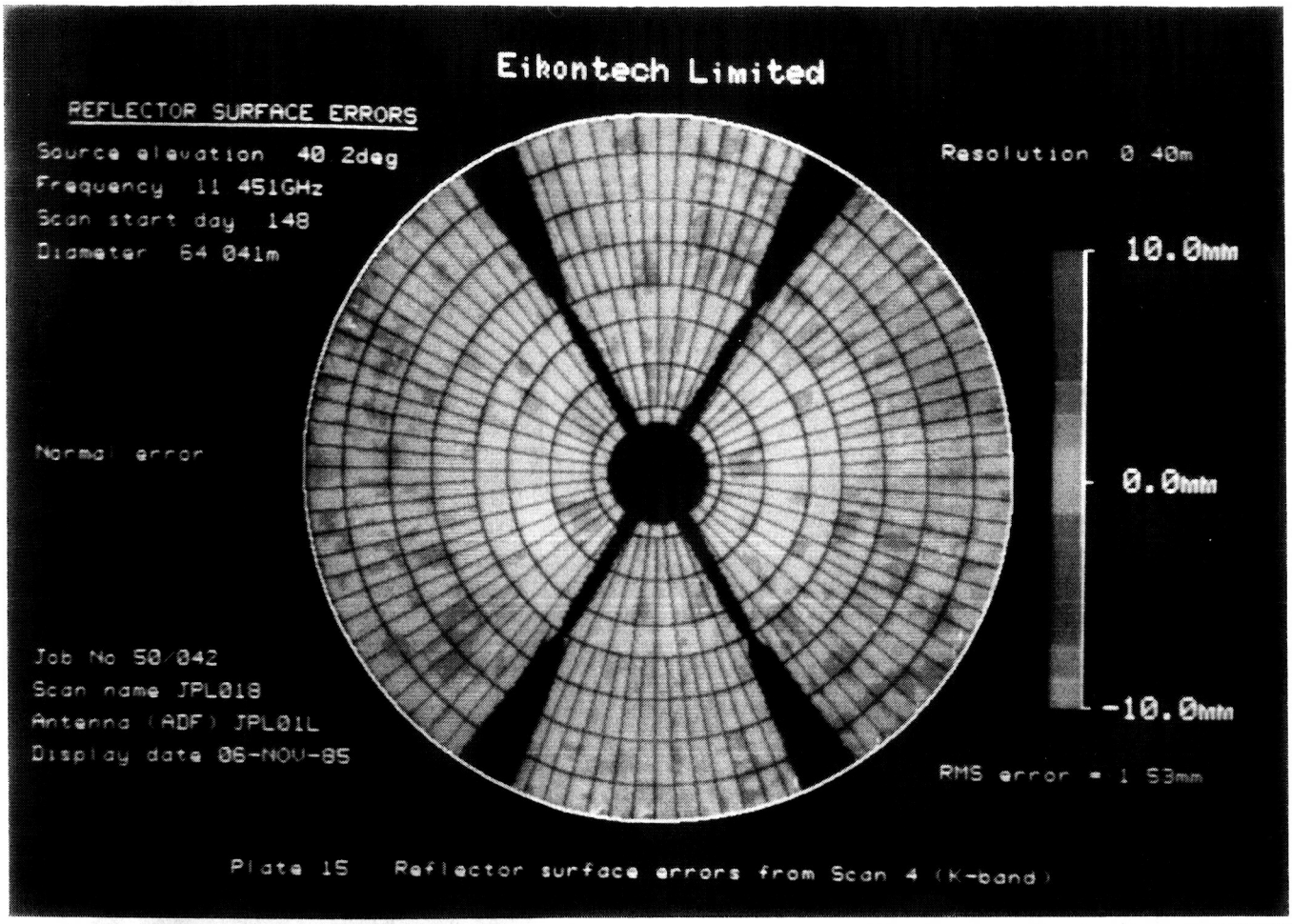

Plate 15 Reflector surface errors from Scan 4 (K-band)

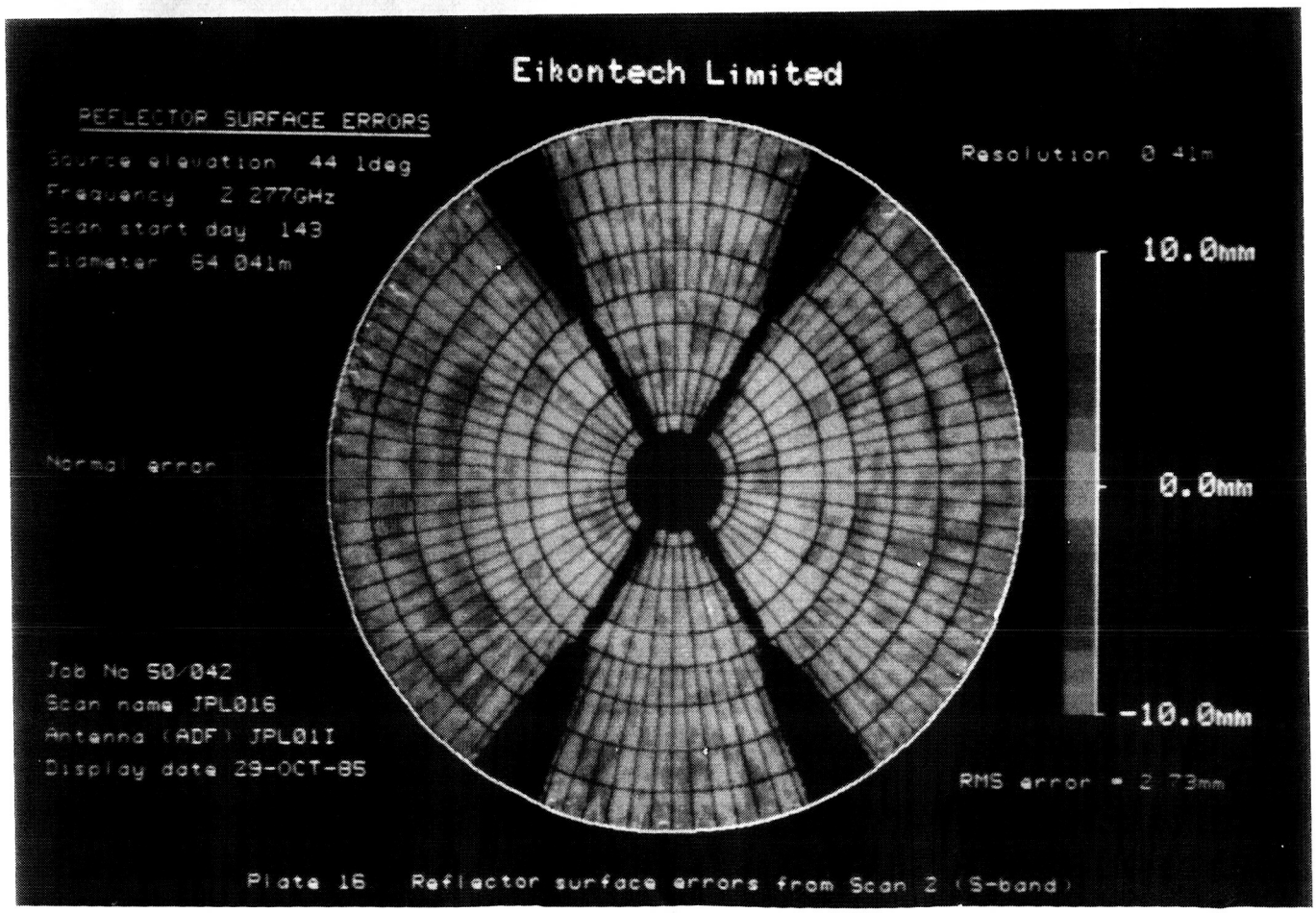

Plate 16 Reflector surface errors from Scan 2 (S-band)

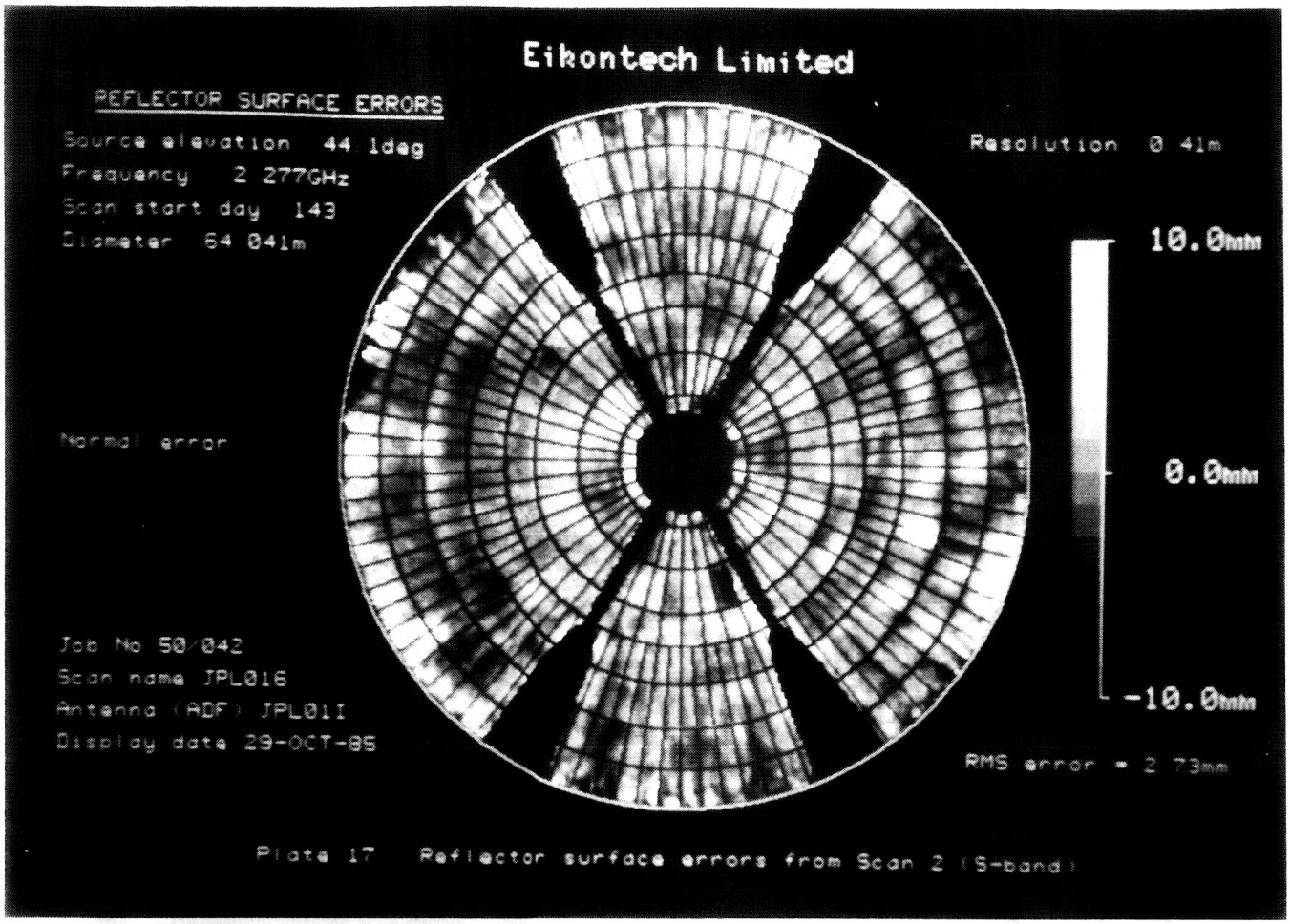

Plate 17 Reflector surface errors from Scan 2 (S-band)

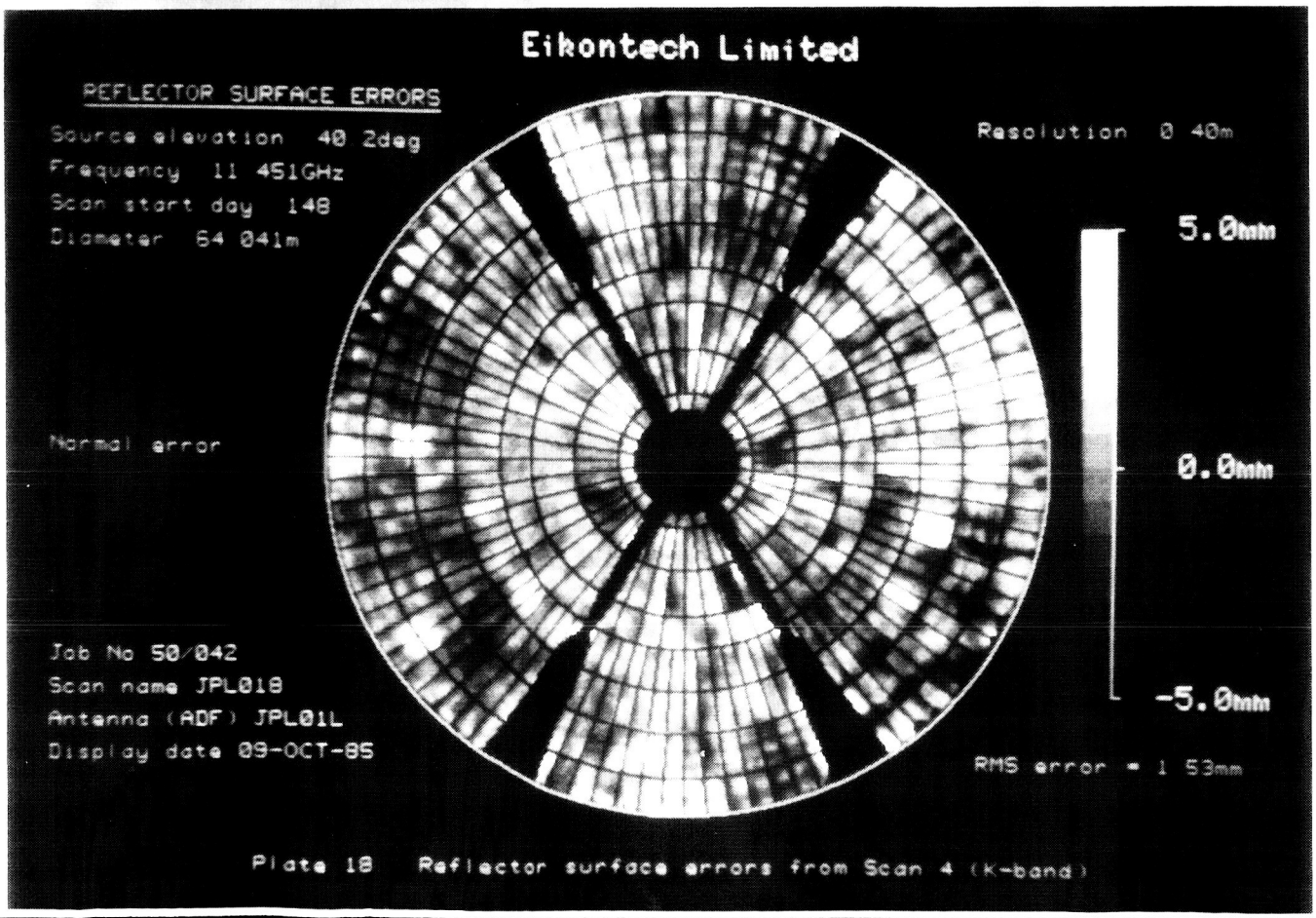

Plate 18 Reflector surface errors from Scan 4 (K-band)

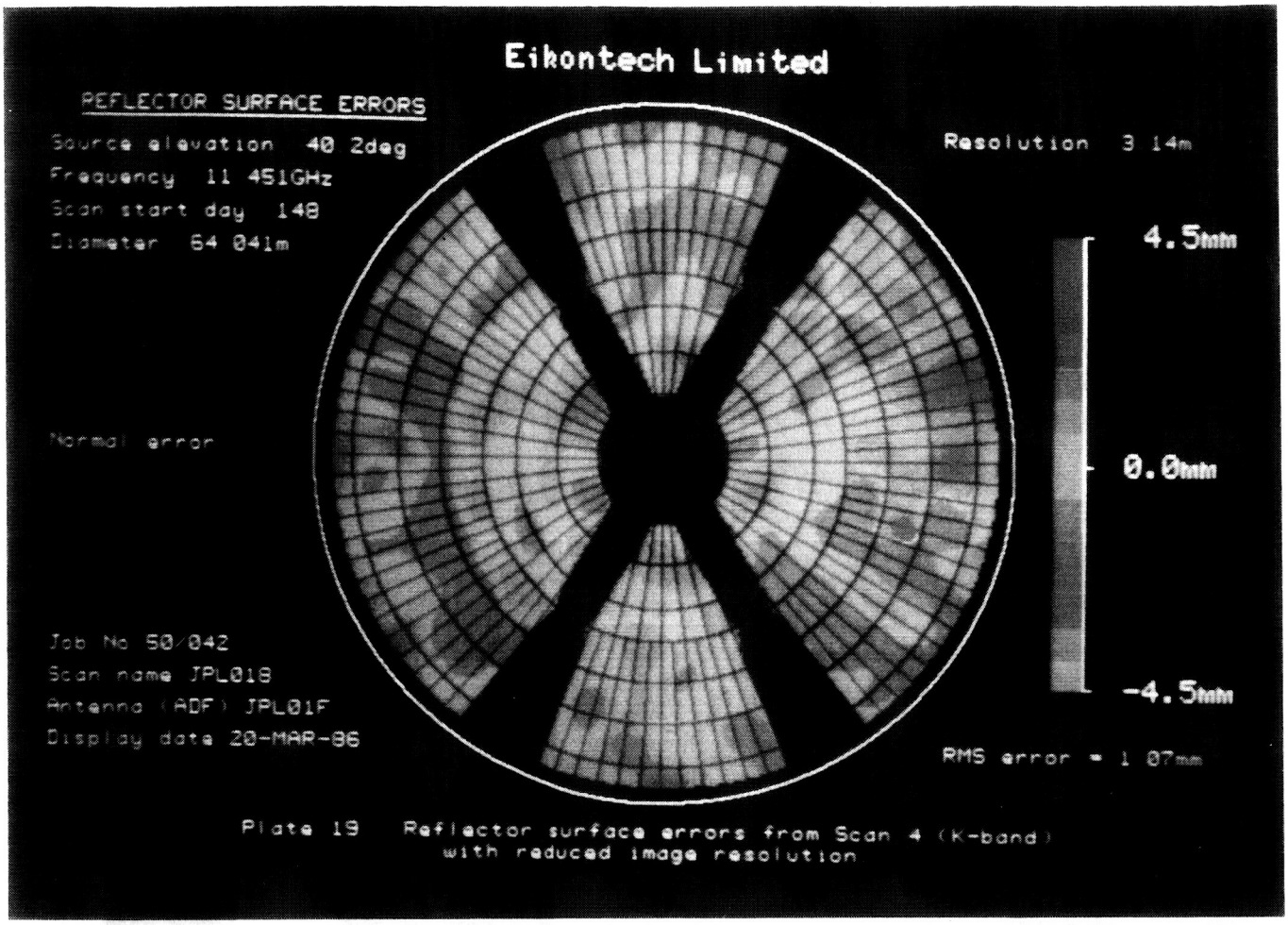

Plate 19 Reflector surface errors from Scan 4 (K-band) with reduced image resolution

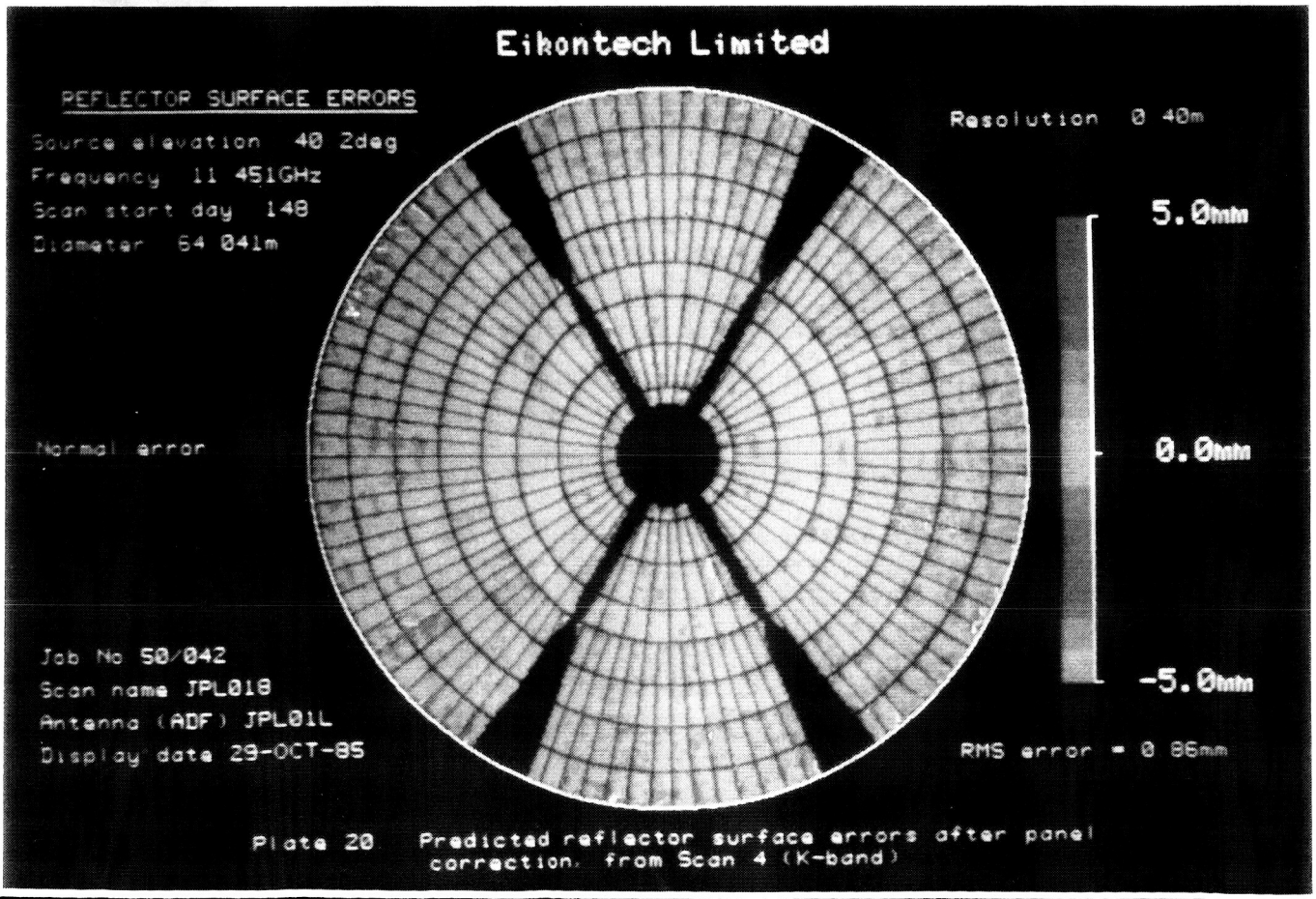

Plate 20 Predicted reflector surface errors after panel correction, from Scan 4 (K-band)

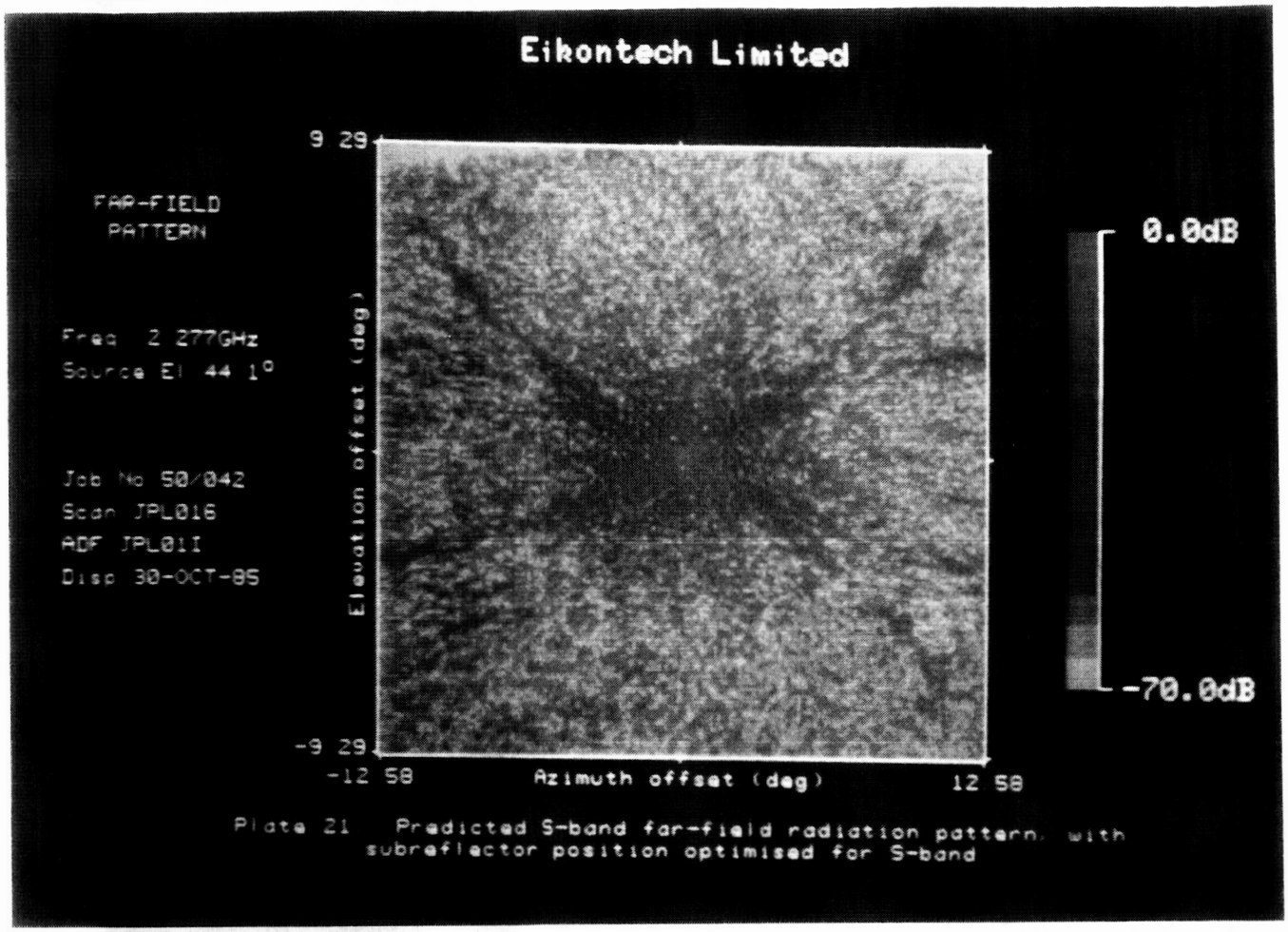

Plate 21 Predicted S-band far-field radiation pattern, with subreflector position optimised for S-band

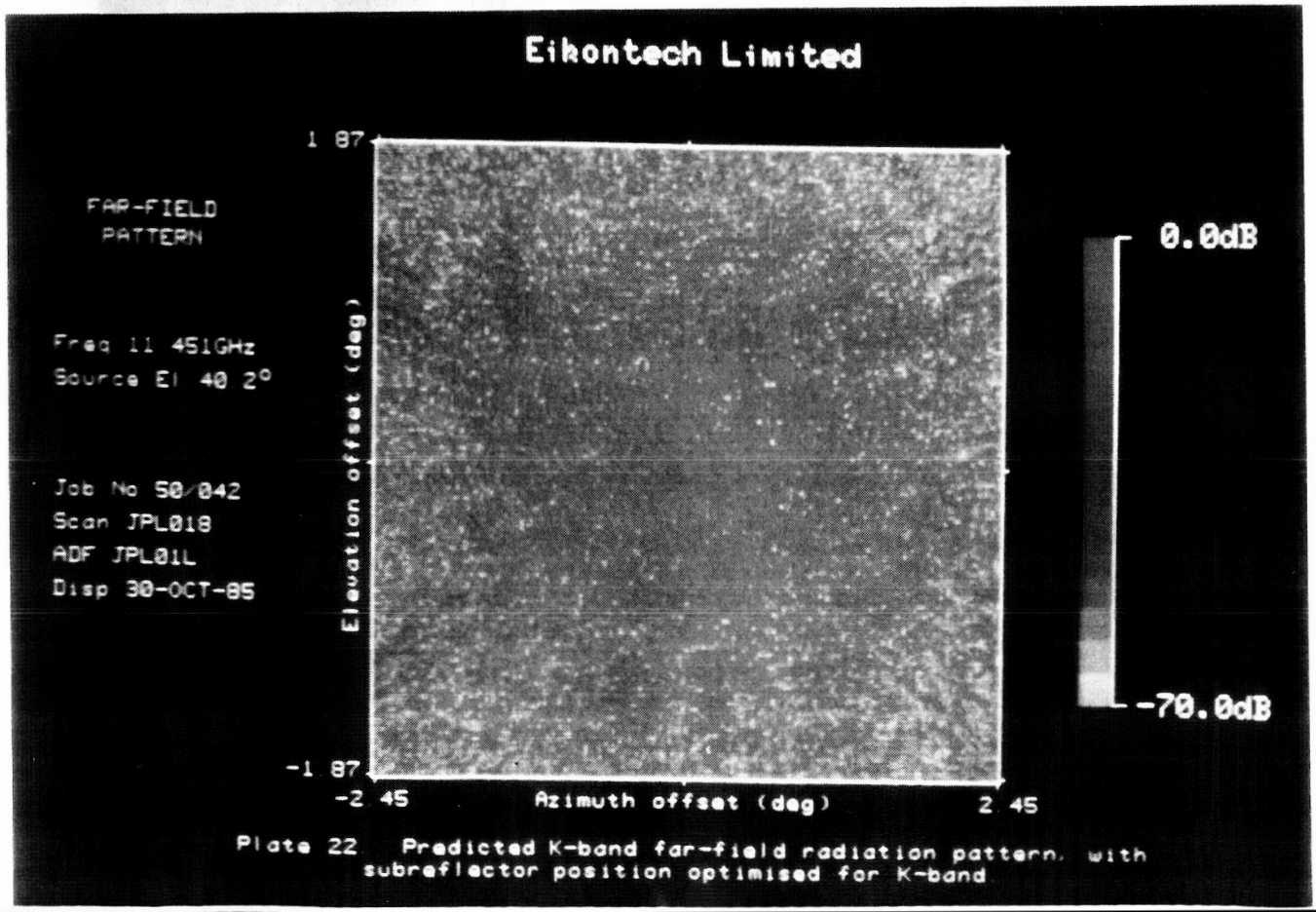

Plate 22 Predicted K-band far-field radiation pattern, with subreflector position optimised for K-band

Appendix A - Processing details (for Eikontech use)

Scan names: JPL015,JPL016,JPL017,JPL018

ADF names: JPL01F/I/J/L

Processing software:

STAGE1(256)	VIH0701
STAGE2(256)	VIH1603-IH1604
STAGE3(256)	VIH0301
STAGE4(256)	VIH0105-IH0106
PLTCUT	VIH0301
PHFUNC(256)	VIH0101
XST256	VIH0201
XTALK	VIH0201
SDFDSP	VIH0201
STAGE1(128)	VIH0801
STAGE2(128)	VIH1501
ENLARG	VIH0201

Data files:

JPL015. PP1,PP2,TP1,TP2,MK1,MK2,PA1,PA2,PB2,PB3,PB4,PB5.PC1,PR1,PR2,
PR3,PR4,PR5,PR6,PR7,SC1,SC2,SC9,FP1,FF1,AM1

JPL016. PP1,PP2,TP1,TP2,MK1,MK2,PA2,PB2,PB3,PB4,PB5,PC1,PR1,PR2,PR3,
PR4,PR5,SC1,SC2,SC3,SC4,FP1,FF1,AM1,AM2,AM3

JPL017. PP1,PP2,TP1,TP2,PA2,PB1,PB2,PB3,PB4,PB5,PC1,PC2,PR1,PR2,PR3,
PR4,PR5,PR6,PR7,PR8,SC1,SC2,MK1,MK2,FF1,FP1,AM1,AM2

JPL018. PP1,PP2,TP1,TP2,TP3,PA2,PB0,PB2,PB3,PB4,PB5,PB9,PC1,PRA,PR0,
PR1,PR2,PR3,PR4,PR5,PR6,PR7,PR8,PR9,SC1,SC2,SC3,SC4,MK1,MK2,
MK3,FF1,FP1,AM1,AM2,AM3,AM4,ST3

Appendix B - Reflector panel adjustments

(See also explanatory notes section E)

The numbering scheme used to define the reflector panels in the attached listing is as follows.

Ring No.	Panels	Inner radius	Outer radius	Start angle
1	24	3.109m	5.913m	352.5°
2	48	5.913m	9.813m	0.0°
3	48	9.813m	13.947m	0.0°
4	48	13.947m	16.987m	0.0°
5	96	16.987m	20.632m	0.0°
6	96	20.632m	24.274m	0.0°
7	96	24.274m	28.528m	0.0°
8	96	28.528m	32.032m	0.0°

The nomenclature used for the panel adjusters is defined in figure B.1.

Note that, at the request of JPL, *the adjustments in the following listing are in inches.*

Rings 2, 3, 5, 6, 7 and 8

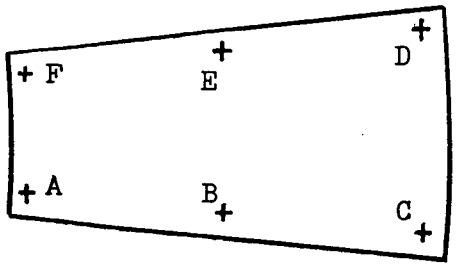

Ring 4 (all panels except 9, 16, 33 and 40)

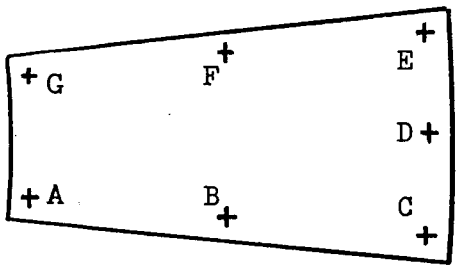

Ring 4, panels 9 and 33

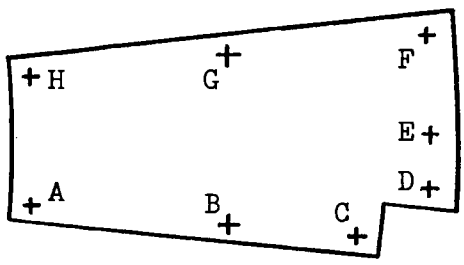

Ring 4, panels 16 and 40

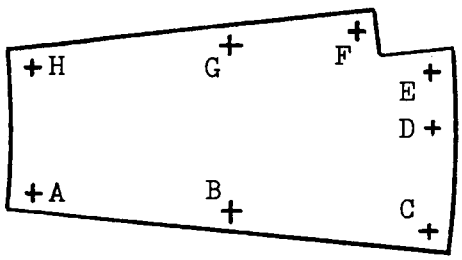

In all cases, the observer is assumed to be looking into the reflector (i.e. from the subreflector).

Nomenclature used to define panel adjusters

Figure No B.1

Reflector panel adjustments for ring 2 - inches

Panel	A	B	C	D	E	F
1	0.095	0.090	0.085	0.072	0.080	0.088
2	0.107	0.053	-0.001	0.096	0.129	0.162
3	0.045	0.115	0.185	-0.022	-0.046	-0.071
4	-0.046	-0.038	-0.030	0.050	0.025	-0.001
5	0.009	0.023	0.037	-0.091	-0.077	-0.063
6	-0.115	-0.105	-0.096	0.088	0.039	-0.011
7	0.030	0.040	0.051	-0.036	-0.028	-0.019
10	-0.027	-0.019	-0.011	-0.072	-0.067	-0.061
11	-0.063	-0.023	0.017	-0.032	-0.061	-0.091
12	-0.023	-0.055	-0.087	-0.087	-0.055	-0.023
13	0.019	0.002	-0.015	0.130	0.116	0.101
14	-0.031	-0.003	0.025	0.037	0.006	-0.025
15	0.036	0.019	0.003	-0.037	-0.012	0.013
18	-0.033	-0.024	-0.015	-0.050	-0.051	-0.053
19	-0.046	-0.075	-0.104	-0.084	-0.059	-0.034
20	-0.116	-0.085	-0.054	-0.068	-0.096	-0.124
21	-0.105	-0.081	-0.057	0.029	-0.014	-0.057
22	-0.042	-0.043	-0.044	-0.003	-0.011	-0.019
23	-0.019	-0.023	-0.027	0.009	0.005	0.001
24	-0.005	0.004	0.013	0.047	0.031	0.014
25	0.015	0.010	0.006	0.046	0.042	0.037
26	0.034	0.044	0.053	0.025	0.022	0.018
27	-0.038	-0.006	0.026	0.217	0.143	0.070
28	0.111	0.104	0.097	0.021	0.044	0.068
29	0.052	0.047	0.041	0.080	0.077	0.074
30	0.064	0.054	0.045	0.048	0.057	0.066
31	0.016	0.036	0.057	-0.051	-0.048	-0.045
34	-0.035	0.010	0.056	-0.009	-0.040	-0.072
35	-0.106	-0.070	-0.035	-0.011	-0.052	-0.093
36	-0.040	-0.040	-0.040	0.005	-0.005	-0.015
37	0.024	0.005	-0.014	-0.052	-0.025	0.002
38	-0.001	-0.023	-0.046	0.033	0.038	0.044
39	0.018	-0.000	-0.019	-0.014	0.003	0.021
42	-0.001	0.007	0.014	0.037	0.025	0.012
43	-0.029	-0.003	0.023	0.021	-0.004	-0.030
44	0.028	-0.002	-0.032	-0.066	-0.029	0.008
45	0.125	0.001	-0.123	-0.185	-0.048	0.090
46	-0.055	-0.028	-0.003	-0.029	-0.050	-0.070
47	-0.073	-0.073	-0.073	-0.015	-0.028	-0.041
48	0.035	0.019	0.003	0.033	0.042	0.052

Reflector panel adjustments for ring 3 - inches

Panel	A	B	C	D	E	F
1	-0.004	-0.012	-0.020	-0.019	-0.011	-0.003
2	0.008	0.025	0.042	-0.020	-0.028	-0.035
3	-0.000	0.007	0.014	0.060	0.046	0.031
4	0.006	0.002	-0.002	-0.005	-0.001	0.004
5	-0.021	-0.008	0.006	-0.025	-0.034	-0.042
6	-0.032	-0.031	-0.031	-0.017	-0.020	-0.022
7	0.016	-0.001	-0.017	0.004	0.018	0.031
10	-0.025	-0.022	-0.019	0.000	-0.006	-0.011
11	-0.032	-0.006	0.020	0.106	0.066	0.026
12	-0.064	-0.046	-0.028	-0.080	-0.090	-0.099
13	0.033	0.001	-0.031	0.048	0.067	0.087
14	-0.012	-0.024	-0.035	0.028	0.029	0.031
15	0.032	0.042	0.051	0.051	0.042	0.032
18	-0.009	0.004	0.017	-0.008	-0.017	-0.026
19	-0.039	-0.037	-0.034	-0.033	-0.036	-0.039
20	0.059	0.016	-0.027	-0.072	-0.022	0.028
21	-0.025	-0.054	-0.083	-0.060	-0.035	-0.009
22	-0.015	-0.023	-0.030	-0.021	-0.015	-0.009
23	0.006	-0.018	-0.042	-0.019	0.001	0.021
24	0.030	0.012	-0.006	-0.040	-0.017	0.007
25	-0.039	-0.030	-0.021	0.021	0.006	-0.010
26	-0.003	0.003	0.010	-0.019	-0.021	-0.023
27	-0.030	-0.010	0.010	0.019	-0.002	-0.023
28	-0.039	-0.018	0.002	0.018	-0.005	-0.028
29	-0.030	0.014	0.059	0.031	-0.009	-0.049
30	-0.021	-0.028	-0.035	-0.015	-0.011	-0.008
31	0.029	0.025	0.021	-0.054	-0.039	-0.023
34	0.004	-0.022	-0.049	-0.010	0.010	0.031
35	0.018	-0.016	-0.049	-0.115	-0.072	-0.028
36	0.050	0.086	0.122	-0.002	-0.019	-0.035
37	-0.043	-0.034	-0.024	-0.025	-0.035	-0.044
38	-0.019	-0.050	-0.082	-0.062	-0.034	-0.005
39	0.184	0.109	0.035	0.219	0.264	0.310
42	-0.025	0.009	0.042	0.051	0.016	-0.019
43	0.072	0.077	0.082	0.020	0.025	0.030
44	0.031	0.009	-0.013	-0.008	0.014	0.035
45	0.033	0.029	0.026	-0.013	-0.003	0.006
46	-0.014	-0.012	-0.010	-0.040	-0.038	-0.036
47	-0.076	-0.026	0.023	0.144	0.076	0.007
48	-0.034	-0.049	-0.064	0.022	0.024	0.025

Reflector panel adjustments for ring 4 - inches

Panel	A	B	C	D	E	F	G	H
1	-0.008	-0.013	-0.017	-0.000	0.015	0.017	0.018	
2	-0.001	-0.013	-0.025	-0.036	-0.045	-0.031	-0.018	
3	0.020	0.014	0.009	0.008	0.007	0.013	0.019	
4	0.076	0.032	-0.012	-0.003	0.008	0.050	0.093	
5	-0.008	-0.007	-0.005	-0.014	-0.023	-0.023	-0.023	
6	-0.059	-0.053	-0.047	-0.050	-0.053	-0.058	-0.064	
7	-0.013	-0.051	-0.089	-0.070	-0.051	-0.017	0.018	
8	0.063	0.047	0.030	0.093	0.149	0.155	0.160	
9	0.068	0.062	0.056	0.038	0.019	-0.013	-0.000	0.013
10	-0.024	0.004	0.032	0.040	0.046	0.017	-0.012	
11	0.007	0.052	0.096	0.055	0.015	-0.021	-0.059	
12	0.004	-0.002	-0.008	-0.008	-0.008	-0.002	0.004	
13	-0.006	0.034	0.074	0.059	0.043	0.006	-0.031	
14	0.066	0.061	0.056	0.025	-0.002	0.008	0.019	
15	0.030	-0.017	-0.064	-0.060	-0.053	-0.007	0.039	
16	-0.052	-0.047	-0.042	-0.021	-0.012	-0.005	-0.011	-0.020
17	0.048	0.087	0.126	0.055	-0.012	-0.037	-0.064	
18	-0.013	-0.000	0.012	-0.008	-0.026	-0.035	-0.044	
19	-0.038	-0.043	-0.047	-0.003	0.037	0.035	0.032	
20	0.080	0.098	0.116	0.036	-0.038	-0.042	-0.046	
21	-0.057	-0.051	-0.045	-0.025	-0.007	-0.016	-0.026	
22	0.029	0.008	-0.012	-0.068	-0.116	-0.086	-0.055	
23	0.015	0.002	-0.010	-0.026	-0.040	-0.025	-0.010	
24	0.020	0.004	-0.012	-0.021	-0.029	-0.011	0.006	
25	0.022	0.025	0.028	0.006	-0.014	-0.013	-0.012	
26	-0.016	-0.031	-0.044	-0.020	0.002	0.012	0.022	
27	0.049	-0.004	-0.056	-0.046	-0.035	0.015	0.066	
28	0.043	0.007	-0.029	-0.037	-0.042	-0.005	0.033	
29	0.075	0.070	0.065	0.023	-0.015	-0.002	0.010	
30	-0.014	-0.043	-0.073	-0.052	-0.032	-0.006	0.020	
31	-0.032	-0.012	0.007	0.008	0.007	-0.012	-0.032	
32	-0.064	-0.041	-0.019	0.024	0.061	0.031	0.000	
33	-0.070	-0.067	-0.065	-0.042	-0.018	0.025	0.014	0.003
34	-0.032	-0.035	-0.038	0.006	0.046	0.041	0.036	
35	0.001	-0.013	-0.027	-0.038	-0.047	-0.031	-0.016	
36	-0.019	-0.038	-0.058	-0.060	-0.060	-0.041	-0.021	
37	-0.012	-0.029	-0.045	-0.005	0.033	0.042	0.051	
38	0.045	0.051	0.057	-0.009	-0.069	-0.063	-0.057	
39	-0.000	-0.024	-0.048	-0.083	-0.113	-0.083	-0.053	
40	-0.124	-0.076	-0.030	-0.059	-0.072	-0.099	-0.129	-0.171
41	0.057	0.061	0.065	0.056	0.048	0.045	0.043	
42	0.028	0.066	0.103	0.093	0.082	0.046	0.011	
43	0.034	0.052	0.069	0.058	0.047	0.031	0.015	
44	0.011	0.020	0.029	-0.006	-0.039	-0.042	-0.045	
45	0.119	0.031	-0.055	-0.044	-0.028	0.056	0.141	
46	0.007	0.025	0.043	0.029	0.016	0.000	-0.015	
47	0.024	0.051	0.078	0.019	-0.036	-0.052	-0.068	
48	-0.050	-0.038	-0.027	0.009	0.041	0.023	0.005	

Reflector panel adjustments for ring 5 - inches

Panel	A	B	C	D	E	F
1	-0.025	-0.035	-0.046	-0.077	-0.064	-0.050
2	0.018	-0.044	-0.104	-0.064	-0.007	0.050
3	0.020	0.022	0.024	-0.037	-0.033	-0.029
4	-0.059	-0.069	-0.079	-0.018	-0.014	-0.010
5	0.040	0.028	0.017	-0.000	0.013	0.026
6	0.005	0.008	0.012	-0.010	-0.011	-0.013
7	0.016	0.011	0.007	0.002	0.007	0.012
8	0.000	-0.007	-0.014	0.010	0.014	0.019
9	0.026	0.005	-0.015	0.013	0.031	0.049
10	0.108	0.085	0.063	-0.016	0.014	0.044
11	0.002	0.030	0.058	-0.126	-0.136	-0.147
12	-0.049	-0.031	-0.014	0.142	0.109	0.077
13	-0.026	0.006	0.038	0.044	0.012	-0.021
14	-0.080	-0.013	0.053	0.115	0.042	-0.031
15	0.011	0.074	0.137	0.026	-0.026	-0.079
18	0.015	-0.013	-0.040	0.007	0.030	0.053
19	0.028	0.050	0.072	0.116	0.090	0.064
20	0.025	0.036	0.045	0.063	0.051	0.039
21	0.080	0.074	0.067	0.072	0.078	0.084
22	0.021	0.050	0.079	0.054	0.028	0.001
23	-0.037	0.005	0.046	0.060	0.017	-0.026
24	-0.035	-0.007	0.022	0.057	0.025	-0.007
25	0.098	0.045	-0.007	0.058	0.104	0.151
26	0.084	0.062	0.040	0.027	0.050	0.074
27	0.011	0.014	0.017	-0.002	-0.003	-0.005
28	0.032	-0.009	-0.048	-0.064	-0.023	0.019
29	0.034	0.037	0.041	-0.050	-0.044	-0.039
30	-0.055	-0.055	-0.056	0.010	0.004	-0.001
31	-0.006	-0.003	-0.000	0.040	0.033	0.026
34	0.015	-0.030	-0.074	-0.017	0.022	0.062
35	0.092	0.064	0.036	-0.054	-0.018	0.019
36	-0.027	-0.012	0.002	0.005	-0.009	-0.024
37	-0.032	-0.003	0.026	0.022	-0.007	-0.036
38	-0.001	0.020	0.041	0.001	-0.016	-0.034
39	-0.059	-0.053	-0.048	0.044	0.029	0.015
40	0.053	0.007	-0.038	-0.092	-0.041	0.010
41	0.016	-0.020	-0.057	-0.100	-0.060	-0.019
42	-0.031	-0.010	0.011	-0.000	-0.020	-0.040
43	-0.016	0.005	0.025	0.004	-0.015	-0.033
44	-0.033	-0.043	-0.052	-0.028	-0.021	-0.014
45	-0.050	-0.033	-0.015	-0.005	-0.024	-0.042
46	-0.021	0.001	0.022	0.001	-0.018	-0.038
47	-0.102	-0.045	0.010	0.072	0.010	-0.052
48	-0.035	-0.022	-0.008	0.036	0.018	0.000
49	-0.036	-0.033	-0.030	0.009	0.003	-0.004
50	-0.042	-0.015	0.011	0.044	0.015	-0.014

Reflector panel adjustments for ring 5 (continued)

Panel	A	B	C	D	E	F
51	-0.027	-0.000	0.026	0.005	-0.019	-0.043
52	-0.031	-0.046	-0.061	-0.074	-0.058	-0.042
53	-0.025	-0.010	0.006	0.033	0.015	-0.003
54	-0.020	0.007	0.033	0.033	0.007	-0.020
55	-0.009	0.027	0.064	-0.022	-0.050	-0.078
56	-0.013	-0.017	-0.020	-0.027	-0.023	-0.019
57	0.019	0.009	-0.002	0.015	0.023	0.032
58	-0.064	-0.004	0.055	0.012	-0.043	-0.099
59	-0.053	-0.050	-0.047	-0.055	-0.057	-0.059
60	-0.084	-0.078	-0.073	-0.031	-0.041	-0.050
61	0.017	-0.001	-0.018	0.020	0.034	0.048
62	-0.035	-0.020	-0.005	-0.014	-0.028	-0.042
63	-0.051	-0.030	-0.008	-0.080	-0.095	-0.110
64	-0.051	-0.038	-0.025	0.033	0.015	-0.004
67	0.009	-0.015	-0.039	-0.037	-0.013	0.011
68	-0.047	-0.025	-0.003	0.010	-0.014	-0.037
69	-0.045	-0.023	-0.001	-0.059	-0.075	-0.092
70	0.000	-0.020	-0.040	-0.023	-0.004	0.014
71	0.002	-0.013	-0.028	-0.067	-0.048	-0.030
72	-0.039	-0.016	0.008	-0.059	-0.076	-0.093
73	-0.057	-0.057	-0.056	-0.016	-0.020	-0.025
74	0.024	0.023	0.023	0.041	0.041	0.040
75	0.049	0.047	0.045	-0.013	-0.005	0.002
76	0.045	0.010	-0.025	-0.044	-0.007	0.030
77	-0.022	-0.035	-0.046	-0.046	-0.035	-0.022
78	-0.026	-0.017	-0.008	0.009	-0.001	-0.012
79	0.007	0.041	0.076	0.058	0.025	-0.008
82	0.022	0.023	0.025	0.061	0.056	0.051
83	0.080	0.063	0.045	0.035	0.054	0.072
84	0.116	0.089	0.061	0.033	0.063	0.094
85	0.027	0.009	-0.010	0.023	0.038	0.054
86	0.042	0.028	0.013	0.016	0.030	0.044
87	0.068	0.047	0.026	0.010	0.032	0.055
88	0.076	0.045	0.015	-0.046	-0.009	0.027
89	0.002	-0.023	-0.047	0.007	0.025	0.045
90	0.051	0.019	-0.011	-0.018	0.013	0.045
91	0.085	0.041	-0.003	-0.012	0.033	0.078
92	0.082	0.023	-0.035	0.005	0.059	0.114
93	0.154	0.052	-0.048	-0.076	0.027	0.131
94	0.037	0.016	-0.005	0.037	0.054	0.071
95	0.094	0.034	-0.026	-0.025	0.035	0.095
96	-0.029	-0.044	-0.060	-0.091	-0.073	-0.054

Reflector panel adjustments for ring 6 - inches

Panel	A	B	C	D	E	F
1	-0.058	-0.056	-0.055	-0.056	-0.057	-0.058
2	-0.050	-0.023	0.004	0.023	-0.006	-0.034
3	-0.029	-0.044	-0.058	-0.059	-0.044	-0.030
4	-0.088	-0.061	-0.034	-0.048	-0.074	-0.100
5	-0.004	-0.082	-0.160	-0.131	-0.056	0.020
6	-0.122	-0.091	-0.060	-0.024	-0.057	-0.092
7	-0.070	-0.062	-0.055	0.080	0.062	0.043
8	0.065	0.084	0.103	0.016	0.004	-0.008
9	-0.015	0.009	0.032	0.017	-0.005	-0.027
10	0.155	0.103	0.052	-0.099	-0.035	0.029
11	-0.049	-0.044	-0.038	-0.050	-0.054	-0.059
12	0.027	-0.013	-0.053	-0.098	-0.054	-0.010
13	-0.046	-0.061	-0.077	-0.029	-0.018	-0.007
14	0.068	0.040	0.013	-0.016	0.014	0.044
15	0.102	0.061	0.020	-0.098	-0.048	0.003
18	0.060	0.020	-0.020	0.019	0.056	0.093
19	0.046	0.043	0.040	0.060	0.062	0.064
20	0.172	0.144	0.116	-0.056	-0.014	0.027
21	0.035	-0.010	-0.055	0.053	0.089	0.126
22	0.171	0.146	0.121	0.032	0.064	0.097
23	0.030	0.021	0.012	-0.028	-0.015	-0.003
24	0.043	0.038	0.034	0.020	0.026	0.031
25	0.054	0.050	0.047	-0.019	-0.011	-0.002
26	0.032	0.018	0.004	-0.013	0.002	0.017
27	0.028	0.051	0.074	-0.022	-0.037	-0.052
28	-0.095	-0.041	0.014	0.005	-0.049	-0.103
29	-0.028	-0.021	-0.015	-0.091	-0.091	-0.092
30	-0.004	-0.084	-0.164	-0.096	-0.022	0.053
31	0.114	0.018	-0.078	-0.115	-0.017	0.083
34	-0.007	-0.020	-0.033	0.054	0.060	0.066
35	0.029	0.018	0.007	-0.022	-0.009	0.005
36	0.052	0.010	-0.032	-0.009	0.031	0.071
37	0.073	0.043	0.013	-0.058	-0.022	0.013
38	-0.071	-0.048	-0.026	0.040	0.013	-0.015
39	0.071	0.030	-0.011	-0.059	-0.014	0.032
40	-0.006	0.000	0.007	-0.027	-0.030	-0.034
41	-0.016	-0.015	-0.014	0.022	0.018	0.014
42	0.035	0.013	-0.009	0.003	0.024	0.045
43	0.047	0.044	0.041	0.018	0.022	0.027
44	0.083	0.059	0.035	0.004	0.031	0.057
45	-0.002	0.001	0.003	0.036	0.031	0.026
46	0.006	0.021	0.036	0.049	0.033	0.017
47	0.087	-0.017	-0.121	-0.139	-0.034	0.071
48	0.079	-0.034	-0.147	-0.114	-0.004	0.107
49	-0.015	-0.005	0.005	-0.041	-0.047	-0.054
50	-0.001	-0.060	-0.119	0.005	0.054	0.103

Reflector panel adjustments for ring 6 (continued)

Panel	A	B	C	D	E	F
51	0.065	0.025	-0.014	-0.015	0.024	0.064
52	0.009	0.012	0.014	0.069	0.062	0.055
53	0.004	0.022	0.040	0.070	0.050	0.029
54	0.103	0.085	0.067	0.037	0.057	0.078
55	0.087	0.045	0.004	-0.015	0.027	0.070
56	0.018	0.007	-0.004	0.039	0.047	0.055
57	0.063	0.026	-0.011	-0.023	0.015	0.053
58	0.084	0.091	0.098	0.078	0.073	0.068
59	0.028	0.038	0.048	0.097	0.083	0.069
60	0.042	0.086	0.130	0.059	0.021	-0.017
61	-0.042	-0.008	0.027	0.066	0.029	-0.009
62	0.031	0.046	0.062	0.064	0.048	0.032
63	0.094	0.056	0.018	-0.052	-0.009	0.035
66	-0.010	0.009	0.027	0.025	0.007	-0.011
67	-0.005	-0.009	-0.013	0.054	0.052	0.051
68	0.020	0.041	0.062	0.018	0.001	-0.017
69	-0.029	-0.044	-0.059	-0.019	-0.008	0.004
70	-0.038	-0.005	0.027	-0.004	-0.034	-0.064
71	-0.067	-0.057	-0.047	-0.019	-0.031	-0.043
72	-0.067	-0.049	-0.031	0.003	-0.017	-0.038
73	-0.077	-0.040	-0.003	0.062	0.020	-0.022
74	0.077	0.067	0.058	-0.060	-0.041	-0.022
75	-0.064	-0.063	-0.061	-0.006	-0.012	-0.018
76	-0.069	-0.033	0.003	-0.003	-0.038	-0.074
77	-0.073	-0.037	-0.002	-0.022	-0.056	-0.090
78	0.005	-0.011	-0.027	-0.012	0.003	0.018
79	0.110	0.037	-0.035	-0.149	-0.068	0.014
82	-0.069	-0.066	-0.064	0.090	0.076	0.061
83	-0.034	-0.016	0.001	0.006	-0.012	-0.030
84	-0.019	0.042	0.102	0.122	0.060	-0.003
85	-0.003	0.050	0.103	0.133	0.078	0.023
86	-0.014	-0.010	-0.006	0.012	0.006	0.001
87	-0.015	-0.013	-0.010	0.021	0.016	0.011
88	-0.123	-0.086	-0.050	-0.055	-0.091	-0.127
89	-0.070	-0.058	-0.047	0.114	0.090	0.065
90	-0.002	0.048	0.098	0.103	0.053	0.002
91	-0.018	0.071	0.160	0.121	0.035	-0.051
92	-0.080	-0.029	0.021	-0.338	-0.359	-0.382
93	-0.326	-0.313	-0.302	-0.027	-0.061	-0.095
94	-0.072	-0.037	-0.002	0.027	-0.010	-0.047
95	-0.052	-0.012	0.027	-0.052	-0.085	-0.118
96	-0.108	-0.095	-0.083	-0.035	-0.051	-0.067

Reflector panel adjustments for ring 7 - inches

Panel	A	B	C	D	E	F
1	-0.179	-0.183	-0.186	-0.031	-0.039	-0.048
2	-0.040	-0.057	-0.071	-0.066	-0.052	-0.035
3	-0.013	-0.003	0.005	-0.114	-0.113	-0.113
4	-0.140	-0.144	-0.146	-0.107	-0.108	-0.108
5	-0.128	-0.117	-0.108	-0.106	-0.115	-0.126
6	-0.092	-0.102	-0.111	-0.092	-0.085	-0.076
7	-0.061	-0.053	-0.046	-0.049	-0.055	-0.063
8	-0.065	-0.054	-0.044	-0.062	-0.070	-0.080
9	-0.073	-0.096	-0.117	-0.064	-0.047	-0.028
10	-0.109	-0.026	0.044	0.029	-0.040	-0.122
11	-0.032	0.001	0.030	-0.003	-0.029	-0.060
12	-0.004	-0.001	0.002	-0.074	-0.071	-0.068
13	-0.016	-0.040	-0.061	-0.071	-0.050	-0.025
14	0.016	-0.005	-0.023	-0.101	-0.077	-0.049
15	-0.035	0.049	0.119	0.067	-0.000	-0.079
18	0.125	0.159	0.188	0.069	0.049	0.025
19	0.040	0.062	0.081	0.063	0.046	0.025
20	0.089	0.151	0.204	0.001	-0.037	-0.082
21	-0.017	-0.004	0.007	0.056	0.042	0.024
22	0.051	0.063	0.074	0.041	0.033	0.023
23	0.037	0.030	0.024	-0.022	-0.013	-0.002
24	0.026	0.028	0.029	-0.003	-0.002	-0.000
25	-0.067	-0.035	-0.007	0.053	0.021	-0.017
26	0.065	0.020	-0.019	-0.031	0.008	0.054
27	-0.054	-0.007	0.032	0.016	-0.023	-0.068
28	-0.032	-0.027	-0.022	-0.013	-0.019	-0.025
29	-0.023	-0.013	-0.005	-0.134	-0.133	-0.132
30	-0.085	-0.141	-0.189	-0.122	-0.079	-0.028
31	-0.036	-0.065	-0.091	-0.144	-0.114	-0.080
34	-0.047	-0.116	-0.175	-0.098	-0.045	0.017
35	0.053	0.041	0.030	-0.033	-0.018	-0.000
36	-0.011	-0.003	0.005	-0.022	-0.028	-0.034
37	-0.041	-0.031	-0.022	0.068	0.053	0.036
38	0.090	0.079	0.069	-0.060	-0.041	-0.019
39	0.011	-0.030	-0.065	0.010	0.040	0.075
40	-0.074	-0.041	-0.012	0.020	-0.011	-0.048
41	0.064	0.075	0.085	0.025	0.020	0.013
42	0.088	0.095	0.101	0.048	0.046	0.044
43	0.070	0.054	0.041	0.044	0.056	0.072
44	0.052	0.058	0.064	0.024	0.021	0.018
45	0.034	0.030	0.026	0.061	0.062	0.064
46	0.125	0.079	0.039	-0.048	-0.002	0.052
47	-0.075	-0.034	0.000	-0.023	-0.056	-0.095
48	-0.081	-0.013	0.045	0.021	-0.035	-0.101
49	0.062	0.004	-0.045	0.016	0.061	0.113
50	0.032	0.028	0.024	0.021	0.025	0.029

Reflector panel adjustments for ring 7 (continued)

Panel	A	B	C	D	E	F
51	-0.005	-0.006	-0.008	0.028	0.026	0.025
52	0.027	0.008	-0.008	0.003	0.018	0.036
53	0.077	0.031	-0.008	-0.012	0.027	0.073
54	0.067	0.066	0.066	0.015	0.019	0.025
55	-0.008	0.005	0.016	-0.002	-0.012	-0.023
56	0.038	-0.009	-0.050	-0.008	0.029	0.073
57	0.163	-0.016	-0.168	-0.314	-0.151	0.040
58	0.048	-0.163	-0.343	-0.181	-0.013	0.185
59	0.079	0.054	0.032	0.018	0.041	0.067
60	0.118	0.055	0.002	0.009	0.062	0.124
61	0.073	0.054	0.038	0.015	0.033	0.054
62	0.040	0.034	0.029	-0.008	0.000	0.009
63	0.036	-0.008	-0.045	-0.099	-0.058	-0.010
66	-0.015	-0.056	-0.092	-0.077	-0.042	-0.002
67	0.056	0.022	-0.006	-0.081	-0.048	-0.008
68	0.046	0.025	0.007	0.028	0.044	0.063
69	0.094	0.027	-0.029	-0.150	-0.085	-0.008
70	-0.043	-0.041	-0.039	-0.129	-0.124	-0.119
71	-0.151	-0.118	-0.091	-0.025	-0.057	-0.095
72	-0.045	-0.047	-0.049	-0.072	-0.069	-0.065
73	0.026	-0.014	-0.048	-0.043	-0.010	0.030
74	0.101	0.084	0.069	-0.065	-0.041	-0.012
75	-0.068	-0.051	-0.036	-0.005	-0.021	-0.041
76	0.020	0.009	-0.000	0.038	0.044	0.052
77	0.054	0.038	0.025	0.065	0.075	0.087
78	0.013	0.058	0.096	0.051	0.016	-0.025
79	0.077	0.005	-0.056	-0.226	-0.152	-0.065
82	-0.177	-0.087	-0.010	0.138	0.050	-0.052
83	0.014	0.054	0.088	0.007	-0.021	-0.054
84	-0.010	0.015	0.035	0.135	0.107	0.074
85	0.016	0.070	0.116	0.096	0.052	-0.001
86	0.037	0.059	0.078	0.027	0.012	-0.006
87	0.051	-0.020	-0.080	-0.064	-0.005	0.065
88	-0.002	-0.007	-0.010	0.015	0.016	0.018
89	-0.036	0.057	0.135	0.222	0.137	0.037
90	0.048	0.171	0.275	0.119	0.026	-0.084
91	0.050	0.039	0.029	-0.033	-0.019	-0.003
92	-0.097	-0.028	0.030	0.427	0.339	0.237
93	-0.022	0.001	0.020	0.125	0.098	0.066
94	0.083	0.104	0.123	-0.025	-0.033	-0.042
95	-0.091	-0.072	-0.055	-0.011	-0.030	-0.054
96	-0.081	-0.018	0.036	-0.128	-0.170	-0.220

Reflector panel adjustments for ring 8 - inches

Panel	A	B	C	D	E	F
1	0.049	0.065	0.081	-0.029	-0.038	-0.048
2	-0.024	-0.064	-0.100	-0.056	-0.022	0.015
3	-0.018	-0.070	-0.117	-0.199	-0.147	-0.090
4	-0.134	-0.162	-0.187	-0.120	-0.099	-0.075
5	-0.108	-0.097	-0.087	-0.056	-0.068	-0.081
6	0.006	0.006	0.006	-0.100	-0.094	-0.087
7	-0.105	-0.092	-0.081	0.022	0.005	-0.014
8	-0.013	0.055	0.116	0.046	-0.012	-0.075
9	-0.038	0.050	0.129	0.117	0.039	-0.049
10	0.088	0.091	0.093	0.009	0.011	0.014
11	0.115	0.130	0.144	0.017	0.010	0.003
12	0.026	0.043	0.058	-0.001	-0.013	-0.025
13	0.044	-0.002	-0.043	-0.062	-0.020	0.027
14	-0.034	0.017	0.064	-0.113	-0.150	-0.191
15	-0.213	-0.145	-0.084	0.009	-0.057	-0.130
18	0.023	-0.048	-0.112	-0.025	0.034	0.099
19	0.019	0.052	0.083	0.052	0.023	-0.009
20	0.057	0.081	0.102	0.010	-0.006	-0.024
21	0.082	0.079	0.076	0.066	0.070	0.074
22	0.154	0.090	0.032	-0.063	0.000	0.070
23	0.099	0.057	0.019	-0.079	-0.036	0.012
24	0.047	0.050	0.053	-0.012	-0.012	-0.011
25	0.026	0.022	0.018	0.040	0.042	0.045
26	0.192	0.168	0.146	-0.025	0.006	0.041
27	0.031	-0.043	-0.109	-0.075	-0.010	0.062
28	0.005	0.016	0.027	0.020	0.010	-0.001
29	-0.061	0.041	0.133	-0.019	-0.102	-0.195
30	-0.126	-0.066	-0.011	-0.079	-0.130	-0.186
31	-0.006	-0.035	-0.060	-0.168	-0.137	-0.102
34	-0.100	-0.092	-0.085	0.059	0.044	0.027
35	0.069	0.024	-0.017	-0.125	-0.078	-0.026
36	-0.036	-0.051	-0.065	-0.003	0.008	0.019
37	-0.065	-0.046	-0.028	0.012	-0.008	-0.030
38	-0.099	-0.033	0.027	0.035	-0.025	-0.092
39	-0.079	-0.033	0.009	-0.003	-0.044	-0.090
40	-0.107	-0.018	0.062	0.100	0.018	-0.073
41	0.001	0.056	0.105	0.113	0.063	0.008
42	0.074	0.077	0.080	0.056	0.054	0.052
43	0.082	0.117	0.148	0.052	0.026	-0.002
44	-0.001	0.008	0.017	0.033	0.024	0.013
45	0.033	0.077	0.117	0.061	0.024	-0.016
46	0.016	0.015	0.015	-0.001	0.000	0.002
47	0.003	-0.038	-0.075	-0.093	-0.055	-0.014
48	-0.053	-0.061	-0.069	-0.158	-0.146	-0.132
49	-0.103	-0.139	-0.171	-0.045	-0.020	0.007
50	0.017	-0.026	-0.066	-0.025	0.013	0.054

Reflector panel adjustments for ring 8 (contimued)

Panel	A	B	C	D	E	F
51	0.045	0.044	0.044	0.058	0.058	0.057
52	0.131	0.054	-0.015	-0.050	0.021	0.100
53	0.041	-0.010	-0.056	-0.021	0.023	0.072
54	0.068	0.044	0.022	-0.031	-0.007	0.021
55	-0.021	-0.006	0.007	0.002	-0.011	-0.026
56	0.010	-0.002	-0.013	-0.020	-0.009	0.004
57	-0.134	0.008	0.136	-0.012	-0.132	-0.265
58	-0.216	-0.092	0.019	0.118	0.001	-0.128
59	0.034	0.044	0.053	-0.043	-0.047	-0.051
60	0.022	0.009	-0.003	-0.050	-0.035	-0.019
61	0.052	-0.004	-0.055	-0.043	0.007	0.063
62	0.040	0.023	0.007	-0.028	-0.010	0.009
63	-0.012	-0.035	-0.055	-0.076	-0.055	-0.031
66	-0.215	-0.158	-0.108	0.047	-0.012	-0.078
67	0.025	0.056	0.083	0.046	0.020	-0.008
68	-0.020	-0.066	-0.108	-0.109	-0.067	-0.021
69	0.013	-0.045	-0.097	-0.037	0.012	0.066
70	0.094	0.008	-0.070	-0.222	-0.136	-0.040
71	0.008	-0.031	-0.065	-0.205	-0.163	-0.116
72	0.007	-0.065	-0.130	-0.203	-0.134	-0.058
73	-0.059	-0.072	-0.084	-0.088	-0.076	-0.062
74	-0.073	-0.134	-0.189	-0.069	-0.020	0.033
75	0.001	0.050	0.095	-0.018	-0.057	-0.100
76	0.060	0.056	0.052	-0.012	-0.005	0.003
77	0.092	0.104	0.115	0.035	0.028	0.021
78	0.028	0.030	0.031	0.046	0.043	0.041
79	-0.169	0.005	0.162	0.201	0.042	-0.134
82	-0.006	-0.177	-0.331	-0.200	-0.053	0.110
83	-0.041	-0.055	-0.068	-0.004	0.006	0.016
84	-0.044	-0.000	0.040	0.105	0.062	0.013
85	0.011	-0.015	-0.039	-0.042	-0.018	0.009
86	0.010	0.054	0.094	0.238	0.190	0.137
87	0.071	0.222	0.359	0.216	0.087	-0.055
88	-0.025	0.062	0.141	0.119	0.042	-0.044
89	-0.085	0.010	0.097	0.278	0.182	0.075
90	0.112	0.105	0.098	-0.017	-0.003	0.011
91	0.060	0.021	-0.014	-0.096	-0.056	-0.012
92	0.011	-0.066	-0.135	-0.021	0.041	0.111
93	0.043	0.088	0.129	-0.034	-0.065	-0.101
94	0.021	-0.001	-0.020	0.006	0.024	0.044
95	-0.006	-0.030	-0.051	-0.032	-0.012	0.011
96	-0.012	0.041	0.089	0.026	-0.018	-0.067

EXPLANATORY NOTES

A	Notes on scan parameters
B	Reflector surface current
C	Reflector surface errors
D	Astigmatism
E	Panel corrections
G	Subreflector position adjustments
H	Far-field radiation patterns
I	Gain losses
J	Analysis of gain versus frequency

A. NOTES ON SCAN PARAMETERS

Type of source:

If a terrestrial source is used, the co-ordinates of the source relative to the test antenna will be fixed. In this case, the data will usually be acquired in the "Fresnel" zone (or radiating near-field) of the antenna.

In the case of a satellite source, the measurement will effectively be in the true far-field of the antenna. Satellite motion corrections are required both in the scan software (for the changing pointing) and in the processing (for the resultant drift in the relative phase of signals received by the reference and test antennas).

Subscan co-ordinate:

A grid of samples of the antenna radiation pattern (in amplitude and phase) is acquired, with the main beam located at the centre of the grid. The grid is formed by taking a number of separate pattern cuts (termed "subscans") either in elevation or in azimuth, with the other co-ordinate being incremented between subscans.

Type of scan:

The scan may be performed with the antenna moving in the same direction for each subscan (raster scan) or with reversal of motion for alternate subscans (zig-zag scan).

Data array size:

This parameter defines the number of data points acquired in the sample grid.

Resolution of measurement:

In the holographic technique, a microwave image of the reflector surface current (in amplitude and phase) is formed by convolution of the true distribution with a narrow convolving function. Thus, in the maps of reflector surface current and surface profile errors, the value at any point is essentially a weighted average of the true distribution, the weighting taking place over a small surrounding area. The resolution parameter indicates the 3dB width of the

Continued ...

convolving function and hence the diameter of the weighting area. It is thus a measure of the definition available in the image.

Calibration scan:

Over a period of hours, small changes can occur in the r.f. equipment, cables etc., which may cause a slow drift in the measured amplitude and phase. In addition, any minor discrepancy between the predicted satellite motion and that actually achieved may result in an uncompensated drift in the relative phase between the signals received by the test and reference antennas. A calibration scan consists of a small number of subscans acquired perpendicular to the subscans in the 'main' scan. Assuming that the drift over the relatively short period of a single subscan is negligible, it is possible to generate a correction function by comparing the corresponding samples of the main and calibration scans.

Beam-peak monitoring:

This is an alternative method of drift correction. The amplitude and phase of the signal, at a suitable reference pointing angle (usually the beam peak), are logged at the scan start and periodically throughout the scan. Any drift is thus quantified and can be removed from the data.

B. REFLECTOR SURFACE CURRENT MAP

A map of the amplitude of the reflector surface current is normally presented in the form of a 14-level false colour display with high amplitudes shown as peak red and low amplitudes as peak blue. The map may also be presented in other special colour schemes or as a monochrome display if important features are revealed better in this format.

This map is particularly useful in verifying correct operation of the feed system. For most antennas, the illumination may be expected to be circularly symmetric so that an offset illumination may indicate feed tilt. Other feed system malfunctions, such as overmoding, are commonly revealed in the surface current map. The map also enables the edge illumination taper to be checked and the shadowing effect of the feed struts etc. to be examined.

C. REFLECTOR SURFACE ERROR MAP

A map of the reflector surface profile errors is most commonly presented in the form of a 14-level false colour display using a blue-green-red colour table such that depressions of the reflecting surface (away from the primary focus) are shown as negative (blue) while protruberances (towards the primary focus) appear as red. Areas close to the ideal (best-fit) surface appear as green. This form of display is particularly useful for showing large-scale features of the reflector. Finer detail is, however, sometimes more clearly visible in a monochrome display which is therefore used where appropriate.

The errors are referred to the best-fit paraboloid which is defined as that paraboloid which, when used as the reference surface, yields the minimum r.m.s. error. The errors are usually measured normal to the reflector surface but can also be measured parallel to the reflector axis. The convention used in any particular case is indicated on the map.

Information in those portions of the map corresponding to blocked and shadowed areas is meaningless and is therefore suppressed. The r.m.s. error is calculated only over the remaining unobstructed areas of the map.

In the calculation of reflector surface error maps and r.m.s. surface deviation, illumination-weighting is optional. That is, the best-fit paraboloid may be determined such that,

i. the r.m.s. surface deviation is minimised, or

ii. the r.m.s. of the illumination-weighted surface errors is minimised. In this case, the r.m.s. quoted would normally be that of the illumination-weighted errors.

Unless otherwise specified, procedure i is adopted.

Continued ...

Dual-reflector antennas only:

It is important to note that no attempt is normally made, in the processing, to distinguish between surface errors on the main reflector and those on the subreflector. That is, the effects of subreflector imperfections are automatically interpreted as errors on the surface of the main reflector. This means that any corrections recommended will automatically tend to compensate for distortions of the subreflector at the test frequency.

D. ASTIGMATISM

Astigmatism is a symmetric distortion of the reflector about two perpendicular planes such that the reflector curvature is greater in one plane than in the other. A best-fit focal length can be determined for each of the planes and the astigmatism may then be quantified in terms of the difference between the two focal lengths and the orientation of the planes. Astigmatism often arises through the action of gravitational forces upon the reflector structure.

The orientation of the plane of shorter focal length is specified as an angle measured from the vertical. The angle is measured counter-clockwise viewed looking into the dish.

E. PANEL CORRECTIONS

In all cases, the observer is considered to be looking into the dish from the direction of main beam. A panel is identified by means of its ring number (ring 1 being the innermost) and a panel number on that ring. The panels on each ring are numbered by counting counter-clockwise around the ring. Panel 1 of a ring is defined as that panel whose clockwise-most edge is at an angular position described as the "start angle". The start angle for each ring is measured counter-clockwise, in degrees, from the right-horizontal. This is illustrated in Figure E.1.

Panel correction information may be supplied in three forms:

i. Corner corrections. This is perhaps the most convenient form for practical implementation where panel adjusters are located very near the corners of the panel. Four parameters are supplied, these describing the required adjustments, usually perpendicular to the reflector surface, at each of the corners of the panel. A positive correction requires movement of the panel towards the observer (i.e. towards the primary focus). The correction points are labelled inner and outer A and B. Those points labelled A lie on the more clockwise edge of the panel while those points labelled B lie on the more counter-clockwise edge, as shown in Figure E.2.

ii. Resolved corrections. These enable the required adjustment to be evaluated for any point on the panel, by use of the geometry shown in Figure E.3. In this form of presentation, three parameters are provided; an adjustment, s, at a reference point (with sign convention as for corner corrections) and two "tilts", α about the radial axis and β about the circumferential axis (both in degrees). It should be noted that α and β are not the physical tilts to be applied to the panel but are merely parameters used for calculating the adjustment at any point. The reference point is taken to be the centre of the inner edge of the panel and the two tilt axes pass through this point. Referring to Figure E.3, the correction at any point Q may be calculated as,

Continued ...

$$\text{correction} = s + d \tan(\alpha) + e \tan(\beta)$$

where d and e are distances from the tilt axes, measured as projections onto a plane normal to the reflector axis. The sign convention for the resulting adjustment is as for corner corrections.

iii. Corrections at adjusters. Where details of the positions of panel adjusters are provided, the appropriate values may be substituted into the above expression to yield direct figures for adjuster movements. The sign convention will be as for corner corrections.

The recommended adjustments are calculated on the basis of a stiff panel assumption. That is, the recommended adjustments change the mean position and tilt of the panel without introducing any significant bending. Adjustments are most often specified in mm. although they may be provided in inches, if requested.

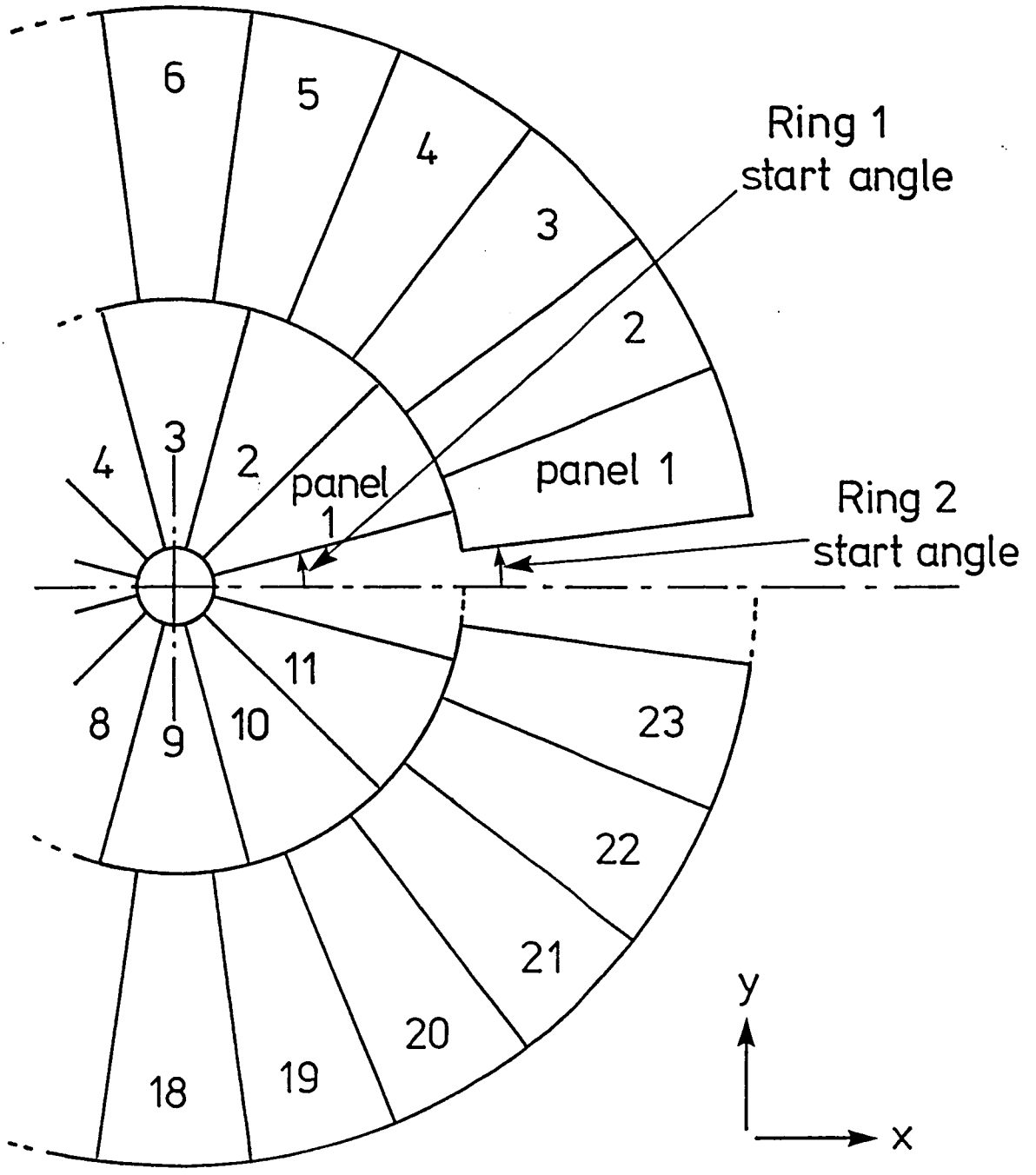

Figure E.1 Typical antenna panel layout illustrating panel numbering scheme and definition of panel start angle

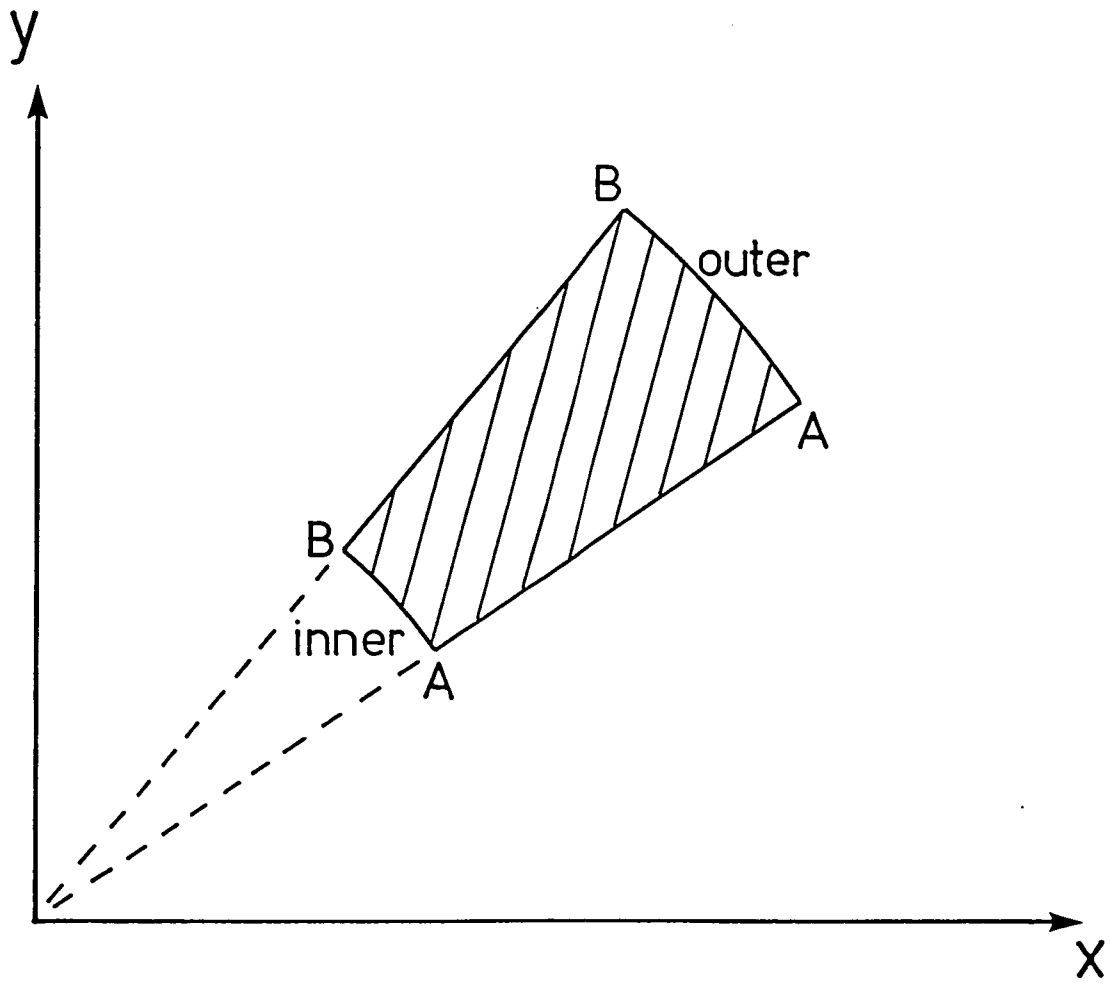

Figure E.2 Conventions for corner corrections

(d & e are measured projected
onto a plane normal to axis
of reflector)

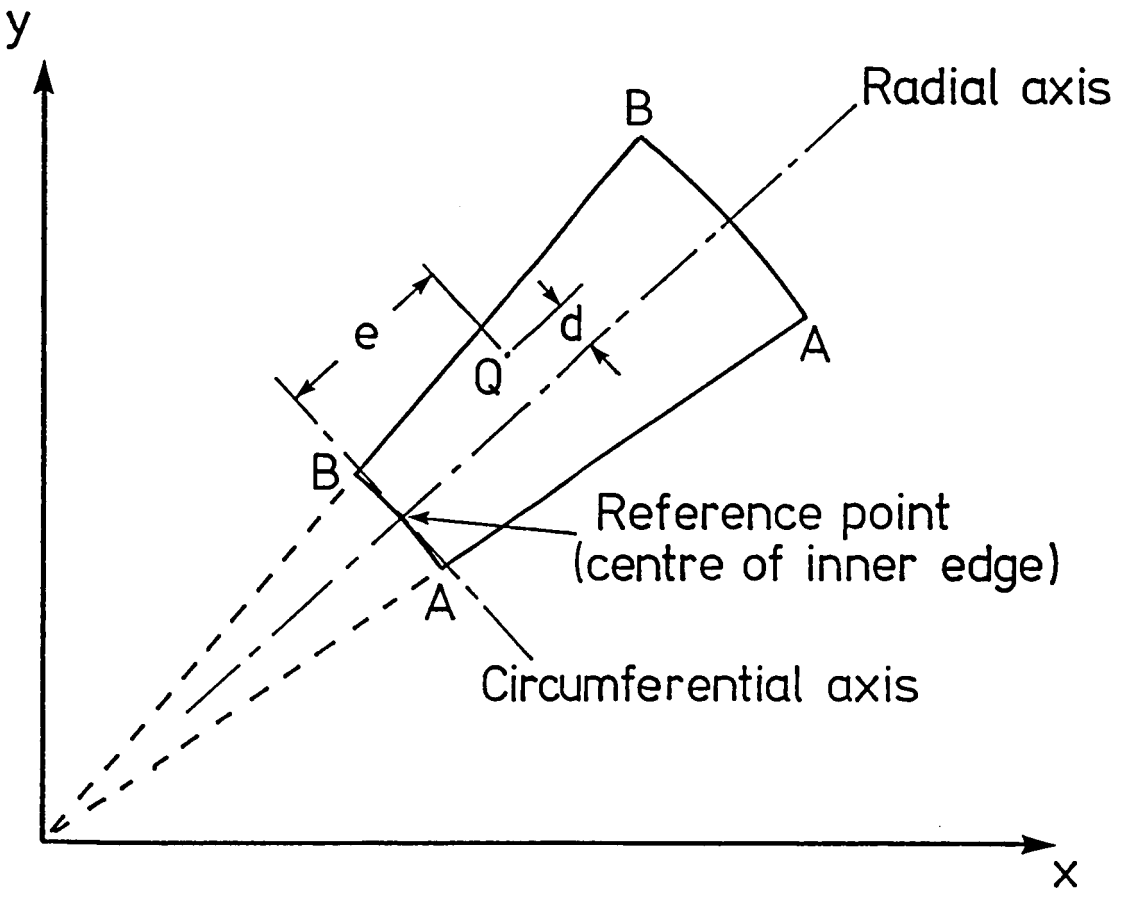

Figure E.3 Geometry for evaluation of resolved corrections

G. SUBREFLECTOR POSITION ADJUSTMENTS

Minor defocusing of a dual-reflector antenna can be corrected by adjustment to the position of either the primary feed or the subreflector. However, due to the magnification properties of dual-reflector feed systems, the antenna performance is almost invariably more sensitive to movement of the subreflector. Furthermore, the subreflector, being more remote from the main structure of the antenna, is more likely to be in error. Thus defocusing is interpreted as arising from subreflector position error.

Subreflector position adjustments are presented in the form of movements in three orthogonal co-ordinates, x, y and z, orientated as illustrated in Figure G.1, such that the z-axis points away from the reflector in the direction of the main beam and the x-axis runs parallel to the axis of the elevation positioner. The arrows in Figure G.1 show the directions of positive x, y and z adjustments so that if a negative adjustment is recommended, its direction must be opposite to that indicated by the arrow.

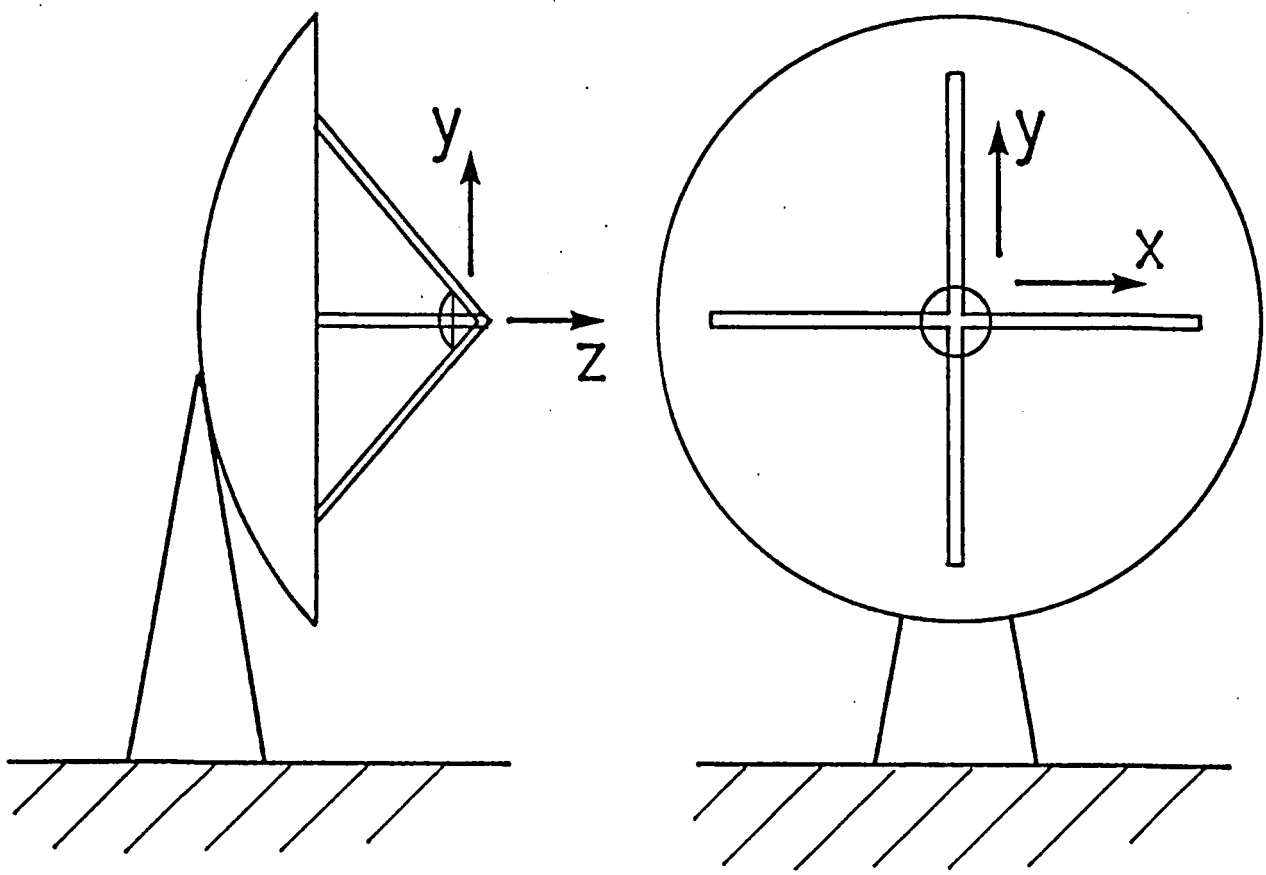

Figure G.1 Coordinate system for subreflector position adjustment

H. FAR FIELD RADIATION PATTERNS

Far-field radiation patterns are presented either in the form of single pattern cuts through the main beam, in the azimuth and elevation principal planes, or as a two-dimensional false-colour display with the main beam at the centre. The colour table used in the two-dimensional presentation shows the regions of most intense radiation as peak red whilst those areas of very low intensity appear as peak blue.

Elevation plane pattern cuts lie in the plane normal to the elevation positioner axis. The elevation scale is measured with respect to the source, a positive angle corresponding to the antenna pointing above the source. These patterns are simply those obtained by rotating the antenna about the elevation axis.

The azimuth pattern cuts lie in the x-z plane, that is the plane containing the elevation axis and the direction of the main beam. These patterns differ very slightly from those which would be obtained by rotating the antenna in azimuth. The difference arises because the two types of azimuth pattern cut lie in slightly different planes which coincide only at the peak of the beam. However, the difference is almost invariably negligible over the angular range shown. The angular scale on the graph indicates the true antenna azimuth offset from the source *(i.e. not the angle measured in the x-z plane)*. The positive direction corresponds to a clockwise rotation of the antenna when viewed from above.

I. GAIN LOSSES

The holographic technique allows several antenna gain loss factors to be identified. These are non-uniform illumination, feed-system misalignment and reflector surface errors. The last two of these are usually the most difficult to obtain by other means. Any practical antenna will possess additional loss mechanisms such as spillover, blockage, ohmic losses etc.. These additional factors are often known accurately from theoretical analysis and can be combined with data obtained from the holographic test to derive the overall gain of the antenna.

In the case of dual-reflector antennas, the loss factor for reflector surface errors embodies imperfections of both the main reflector and the subreflector.

J. ANALYSIS OF REFLECTOR PERFORMANCE WITH FREQUENCY

The purpose of this analysis is to estimate how the reflector (or reflector/subreflector combination) might be expected to perform as a function of frequency.

Three curves are commonly included on the gain/frequency graph. The first of these shows the theoretical gain, as a function of frequency, assuming 100% aperture efficiency. This graph appears as a straight line. The second curve is derived by subtracting the loss due to reflector surface errors, all other loss factors being omitted. For the purpose of calculating the loss due to surface errors, the feed pattern is assumed to be the same as that used in the test.

The third curve, where shown, illustrates the predicted gain variation after panel adjustment. It should be stressed that this prediction serves only to indicate what is theoretically possible. The performance improvement realised will depend on the accuracy with which the panel corrections can be implemented. Furthermore, day to day variations in the antenna due to changing environmental conditions, and longer term ageing of the antenna structure, may make an increased level of performance difficult to maintain.

Gain curves are plotted only up to about the frequency at which maximum gain occurs. Beyond this point, the gain falls off extremely rapidly and becomes much more sensitive to minor changes of reflector shape. Thus, in practice, difficulties may be encountered in attempting to operate the antenna beyond the turnover frequency.